จุฬาลงกรณ์มหาวิทยาลัย
ทุนวิจัย
กองทุนรัชดาภิเษกสมโภช

รายงานวิจัย

Preparation of Mo-SBA 15 and Ti – SBA-15 via Sol – gel Process using Silatrane as Precursor and Their Preliminarily Activity Study

โดย

Sujitra Wongkasemjit

กุมภาพันธ์ 2555

ACKNOWLEDGEMENT

The author would like to express her sincere appreciation to the Ratchadaphisek Somphot Endowment Fund, Chulalongkorn University, for financial support on this research work.

Project Title: "Preparation of Mo-SBA15 and Ti-SBA-15 via Sol-gel Process using Silatrane as Precursor and Their Preliminarily Activity Study"

Name of the Investigator: Associate Professor Sujitra Wongkasemjit

Year: April, 2010-March, 2011

Abstract

In this work, the preparation of Mo-SBA15 and Ti-SBA-15 via sol-gel process using silatrane as precursor and their preliminarily activity study are focused. Functionalized M-SBA-15 (M = Ti and Mo) mesoporous silica catalysts are synthesized through the simple room temperature sol-gel process. SAXS, TEM, and FESEM confirm well-ordered 2D mesoporous hexagonal structures of M-SBA-15 (M = Ti and Mo). Diffuse reflectance UV-visible spectroscopy (DRUV) shows that Ti^{4+} and Mo^{6+} are incorporated into the framework through displacement of Si^{4+} to loadings of 7 mol% Ti and 1 mol% Mo, respectively, without perturbation of the ordered mesoporous structure of the parent SBA-15. N_2 adsorption/desorption measurements yield high surface areas (670–729 m^2/g), with large pore diameters (5.4–6.8 nm) and volumes (0.83–1.04 cm^3/g). The catalytic activity of metal loaded SBA-15 (Ti- and Mo-SBA-15) towards the epoxidation of styrene monomer with H_2O_2 employed as the oxidant is investigated as a function of temperature, time, catalyst loading, ratio of styrene/H_2O_2, and amount of catalyst used. The only products of this reaction are styrene oxide, and benzaldehyde. The selectivity of styrene oxide are 34.2% and 39.9%, at a styrene conversion of 25.8% and 7.7% over the 7 mol% Ti and 1 mol% Mo loaded in SBA-15 catalyst, respectively. The catalytic performance of the sol-gel catalysts is shown to be superior to conventional materials produced by incipient wetness impregnation method under identical reaction conditions.

ชื่อโครงการ "การสังเคราะห์ Mo-SBA15 และ Ti-SBA-15 โดยผ่านกระบวนการโซล-เจล และใช้ไซลาเทรนเป็นสารตั้งต้น และศึกษาความว่องไวของสารในขั้นต้น"

ชื่อผู้วิจัย รองศาสตราจารย์ ดร. สุจิตรา วงศ์เกษมจิตต์

เดือนและปีที่ทำวิจัยเสร็จ มีนาคม 2554

บทคัดย่อ

งานวิจัยนี้ได้มุ่งเป้าไปที่การสังเคราะห์ไทเทเนียม SBA-15 และ โมลิบดินัม SBA-15 โดยผ่านกระบวนการโซล-เจล และใช้ไซลาเทรนเป็นสารตั้งต้น และศึกษาความว่องไวของสารในขั้นต้น ผลวิเคราะห์จาก SAXS และ TEM/FESEM ยืนยันว่า ไทเทเนียม SBA-15 และ โมลิบดินัม SBA-15 ที่สังเคราะห์ได้มีการจัดเรียงโครงสร้างแบบหกเหลี่ยมที่เป็นระเบียบในสองมิติสอดคล้องกับสมมาตร *p6mm* การวิวิเคราะห์ตัวอย่างที่เป็นของแข็งโดยรังสียูวีแสดงให้เห็นว่า ไทเทเนียม และ โมลิบดินัม ได้เข้าไปอยู่ในโครงสร้างของ SBA-15 ในปริมาณ 7 และ 1 โมลเปอร์เซนต์ ตามลำดับ โดยไม่ทำลายโครงสร้างของตัวรองรับ SBA-15 ตัวเร่งปฏิกิริยาที่สังเคราะห์ได้มีพื้นที่ผิวสูง (670–729 ตารางเมตรต่อกรัม), ขนาดรูพรุนใหญ่ (5.4–6.8 อังสตรอม), และ ปริมาตรรูพรุนสูง (0.83–1.04 ลูกบาศก์เซนติเมตรต่อกรัม) นอกจากนี้ ได้ทำการศึกษาผลของ อุณหภูมิ, เวลา, ปริมาณโลหะในตัวเร่งปฏิกิริยา, อัตราส่วนของสไตรีนต่อไฮโดรเจนเปอร์ออกไซด์ และ ปริมาณตัวเร่งปฏิกิริยาที่ใช้ ของตัวเร่งปฏิกิริยา ไทเทเนียม SBA-15 และ โมลิบดินัม SBA-15 ที่มีต่อปฏิกิริยาอีพอกซิเดชั่นของสไตรีนด้วยไฮโดรเจนเปอร์ออกไซด์ ซึ่งผลิตภัณฑ์ที่ได้จากปฏิกิริยานี้ มีเพียงสไตรีนออกไซด์ และเบนซาลดีไฮด์เท่านั้น ความสามารถในการเลือกจำเพาะของ สไตรีนออกไซด์ เป็น 34.2% และ 39.9% ที่ความสามารถในการเปลี่ยนสไตรีน เป็น 25.8% และ 7.7% สำหรับ ตัวเร่งปฏิกิริยาที่มีไทเทเนียม และโมลิบดินัมปริมาณ 7 และ 1 โมลเปอร์เซนต์ ที่ใส่เข้าไปในโครงสร้างของ SBA-15 ตามลำดับ ประสิทธิภาพของตัวเร่งปฏิกิริยาที่สังเคราะห์ด้วยกระบวนการโซล-เจลแสดงผลที่ดีกว่าที่สังเคราะห์ด้วยวิธีการกระจายตัวบนพื้นผิวภายใต้สภาวะเดียวกัน

TABLE OF CONTENTS

	PAGE
Title Page	i
Acknowledgement	ii
Abstract (English)	iii
Abstract (Thai)	iv
Table of Contents	v
List of Tables	viii
List of Figures	ix
List of Schemes	xiii
CHAPTER I INTRODUCTION	1
CHAPTER II THEORETICAL BACKGROUND AND LITERATURE SURVEY	2
2.1 Introduction to Metal Alkoxide	2
2.2 Synthesis of Metal Alkoxides	2
2.3 Sol –Gel Processing	5
2.4 Sol-Gel Process in Surfactant-Templated Silica	6
2.5 Literature Review	7
CHAPTER III A NOVEL ROOM TEMPERATURE SYNTHESIS OF MESOPOROUS SBA-15 FROM SILATRANE	11
Abstract	11
Introduction	11
Experimental	13
Silatrane Synthesis	13
SBA-15 Synthesis	13
Mesopore Ordering	14
Nanostructure	15
Physical Parameters	16
Results and Discussion	16

PAGE

As-synthesized SBA-15 mesoporous material 16
With hydrothermal treatment 18
Without hydrothermal treatment 25
Conclusions 26
Acknowledgements 27
References 27
CHAPTER IV ROOM TEMPERATURE SYNTHESIS OF Ti-SBA-15 FROM SILATRANE AND TITANIUM-GLYCOLATE AND ITS CATALYTIC PERFORMANCE TOWARDS STYRENE EPOXIDATION 30
Abstract 30
Introduction 31
Experimental 32
Materials 32
Ti-SBA-15 sol-gel synthesis 32
Ti-SBA-15 impregnation synthesis 33
Characterization 33
Catalytic activity of Ti-SBA-15 34
Results and Discussion 34
Ti-SBA-15 catalyst crystal chemistry 34
Effect of Ti loading 35
Effect of acidity 39
Effect of temperature 39
Effect of aging time 40
Catalytic activity of Ti-SBA-15 towards styrene epoxidation 41
Conclusions 43
Acknowledgements 44
References 44
CHAPTER V ROOM TEMPERATURE SYNTHESIS OF Mo-SBA-15 VIA SOL-GEL PROCESS AND ITS CATALYTIC

PAGE

ACTIVITY IN STYRENE OXIDATION 47
Abstract 47
Introduction 47
Experimental 48
Materials 49
Mo-SBA-15 sol-gel synthesis 49
Impregnation synthesis 49
Characterization 50
Catalytic activity 50
Results and Discussion 51
Mesostructure and Crystal Chemistry 51
Catalytic activity study of Mo-SBA-15 56
Conclusions 59
Acknowledgements 60
References 60
CHAPTER VI CONCLUSIONS AND RECOMMENDATIONS 62
APPENDIX PUBLICATION PAPERS 62
"A novel room temperature synthesis of mesoporous SBA-15 from silatrane", Journal of Porous Materials, 18 (2011) 167-175 63
"Room temperature synthesis of Ti-SBA-15 from silatrane and titanium-glycolate and its catalytic performance towards styrene epoxidation", Journal of Sol-Gel Science and Technology, 57 (2011), 221-228 73

LIST OF TABLES

TABLE		PAGE
3.1	Properties of SBA-15 as a function of the synthesis route	21
4.1	BET and SAXS analyses of Ti-SBA-15 as a function of amount of Ti loading	38
4.2	BET and SAXS analyses of Ti-SBA-15 as a function of acidity	39
4.3	BET and SAXS analyses of Ti-SBA-15 as a function of Temperature	40
4.4	BET and SAXS analyses of Ti-SBA-15 as a function of aging time	41
4.5	Comparison of catalysts for epoxidation of styrene	42
5.1	Physical and crystallographic properties of Mo-SBA-15 Samples as a function of Mo loading	53
5.2	Epoxidation of styrene monomer with H_2O_2 over Mo-SBA-15 as a function of Mo loading	56
5.3	Epoxidation of styrene monomer with H_2O_2 over Mo-SBA-15 as a function of reaction time	58
5.4	Epoxidation of styrene monomer with H_2O_2 over Mo-SBA-15 as a function of reaction temperature	58
5.5	Epoxidation of styrene monomer with H_2O_2 over Mo-SBA-15 as a function of styrene:H_2O_2 ratio	58
5.6	Epoxidation of styrene monomer with H_2O_2 over Mo-SBA-15 as a function of catalyst used	59

LIST OF FIGURES

FIGURE		PAGE
3.1	Simplified room temperature synthesis of SBS-15 (Route 1) compared to conventional microwave- assisted hydrothermal method (Route 2)	15
3.2	The SAXS pattern of the as-synthesized SBA-15 (A), after calcinations at 550 °C (B) and after calcinations at 850 °C (C). These materials show two strong scattering maxima that are indexed in accord with *p6mm* (hexagonal) symmetry	17
3.3	The TG-DTG peak analyzed in air of SBA-15 after calcinations at 550 °C for 6 h	18
3.4	(a) The SAXS pattern the SBA-15 materials show two strong scattering maxima that are indexed in accordance with *p6mm* symmetry. The relative positions of these maxima are distinct for those mesoporous structures prepared with the assistance of microwave homogenization. (b) The {10} ≡ {11} reflections are anisotropic and show that the upper limit of the crystallographic repeat in the 2D mesopore order is quite sharp (~190Å) but with a long tail of shorter periodicity down to ~167Å. (c) The {30} ≡ {33} scattering that provides a measure of pore diameter shows the channels are slightly larger when microwave treatment is used, as compared to direct hydrothermal synthesis, in agreement with gas absorption measurements (see Table 3.1)	19
3.5	(a) Idealized morphology of the two-dimensional arrangement of silica tubes in SBA-15 and conforming to *p6mm* symmetry. In reality, the tubes are sinuous and extend over a range of diameters which destroys	

FIGURE		PAGE
	long range hexagonal symmetry. (b) Projection along the mesoporous tubes emphasizing the equivalence of {10} ≡ {11} planes and d-spacings that define the underlying crystallographic repeat, while {30} ≡ {33} correspond to a first approximation to the observed channel diameters	20
3.6	FESEM (left-hand side) and TEM (right-hand side) images of SBA-15 prepared hydrothermally at 120°C/1 h with microwave assistance. (a) & (b) At lower magnifications the twisted bundles of silica tubes are seen to co-exist with less crystalline and aperiodic material. (c) (d) When viewed along the pseudo-hexagonal projection it evident that channels not uniform in shape or content. (e) & (f) In <10> FESEM clearly shows cavitation along the channels. While this is not evident in TEM, the regular periodicity the 2D mesopore order is evident	20
3.7	(a) A well-ordered fragment of SBS-15 project in pseudo-*p6mm* projection. (b) The frequency image obtained by fast Fourier transformation (FFT) of the region within the circle yields shows angles that departure from 60^{o} demonstrating that this material fragment better corresponds to *p*2 oblique symmetry. By imposing *p6mm* symmetry and calculating the back Fourier transform the inserted processed image in (a) is generated that yields an average pore diameter of 46 Å	22
3.8	Nitrogen adsorption-desorption isotherms and corresponding pore size distributions for SBA-15 prepared with a microwave -assisted hydrothermal route at (a)120°C /1 h, (b) 100°C /2 h, and (c) directly at RT by stirring. The pore size range is slightly narrower for the latter (FWHM ~ 18 Å) as compared	

FIGURE **PAGE**

	to the former (FWHM ~ 25 Å)	23
3.9	Approximate <10> FESEM (a) and TEM (b) images micrographs of SBA-15 prepared hydrothermally with microwave-assisted method at 100°C/2 h	24
3.10	Approximate <10> FESEM (a) and hexagonal TEM (b) images of SBA-15 prepared at RT without hydrothermal treatment	25
4.1	SAXS patterns of (A) pure silica SBA-15 and Ti-incorporated samples of Ti-SBA-15 containing different amount of Ti loadings; (B) Ti-SBA-15 materials prepared at different acid concentrations; (C) Ti-SBA-15 synthesized at different temperatures; (D) Ti-SBA-15 synthesized at different aging times	36
4.2	TEM images of 7 mol% Ti-SBA-15, in which a) in the direction perpendicular to the pore axis and b) in the direction parallel to the pore axis	37
4.3	N_2 adsorption/desorption isotherms (A) and pore size distributions (B) of Ti-SBA-15 containing different amount of Ti loadings	37
4.4	Diffuse reflectance UV-visible spectra of the synthesized Ti-SBA-15: (A) at different amounts of Ti loadings; (B) at various acid concentrations; (C) at different temperatures; and (D) at different aging times	38
4.5	(A) Effect of reaction time on the styrene oxidation using 0.1 g of catalyst, containing 7.0 mol% titanium content, at 80 °C; (B) Effect of reaction temperature on the styrene oxidation using 0.1 g of catalyst, containing 7 mol% titanium content, for 4 h; (D) Effect of amount of catalyst, containing 7.0 mol% titanium content, at 80 °C for 4 h	43
5.1	SAXS patterns of pure silica SBA-15 and Mo-SBA-15	

FIGURE **PAGE**

	containing different Mo loadings	52
5.2	TEM images of Mo-SBA-15 containing 1.0 mol% Mo (A) in the direction perpendicular to the pore axis and (B) in the direction parallel to the pore axis	52
5.3	Diffuse reflectance UV-visible spectra of Mo-SBA-15	54
5.4	N_2 adsorption/desorption isotherms (A) and pore size distributions (B) of Mo-SBA-1	55

LIST OF SCHEMES

SCHEME		PAGE
2.1	The preparation of silatrane complexes by Wongkasemjit's method	4
2.2	The preparation of titanium glycolate complex (Phonthammachai *et al.*, 2003)	4

CHAPTER I

INTRODUCTION

Mesoporous materials are those with pore in the range of 20–500Å in diameter. They have huge surface areas, providing a vast number of sites where sorption process can occur. These materials have numerous applications in catalysis, separation, and many other fields (Estermann *et al.*, 1991; Hoang *et al.*, 2005; Trong-On *et al.*, 2001; Kubo *et al.*, 2007). Synthesis of these materials is of considerable interest and is constantly being developed to introduce different properties.

Since the discovery of the so-called M41S (Kresge *et al.*, 1992; Beck *et al.*, 1992) silicas, much research work has been concentrated on this new class of mesoporous materials. Originally, this family has been classified into thee subgroups: a hexagonal (MCM-41), a cubic (MCM-48), and a lamellar phase (MCM-50) (Sayari *et al.*, 1996; Vinu *et al.*, 2003). Among the mesoporous silicas, SBA family has been attracted much attention because of thicker walls, better hydrothermal stability and larger pore size than M41S. It is well known that SBA-15 material is analogous to the hexagonal assemblage of cylindrical micelles in the amphiphilic surfactant. The synthesis of SBA-15 mesoporous silicas is achieved by the use of surfactant micelles as structure directing agents in a sol-gel process. Amphiphillic surfactants, poly(ethylene glycol)-block-poly(propylene glycol)-block-poly(ethylene glycol), self assemble into cylindrical micelles, which are encapsulated by an inorganic material. Calcination, a thermal processing technique is then used to remove the organic surfactant, leaving a hexagonal arrangement of mesopores (Goltner *et al.*, 1997; Wanka *et al.*, 1994; Chu *et al.*, 1996). Many researchers almost used tetraethoxysilane (TEOS) as a silica source, however, for this research work, we introduced another source of silica from metal alkoxides precursor.

During the last 9 years, Wongkasemjit and coworkers (2001–2009) synthesized moisture stable metal alkoxides, namely silatrane, alumatrane, cerium glycolate, zirconium glycolate, titanium glycolate, tin glycolate and molybdenum

glycolate, directly from inexpensively corresponding metal oxide using ethylene glycol solvent via the "Oxide One Pot Synthesis (OOPS)" process (Phiriyawirut *et al.*, 2003; Charoenpinijkarn *et al.*, 2001). The reaction gives highly pure metal alkoxides. Both synthesized silatrane and alumatrane have been successfully used as precursors for synthesis of microporous and mesoporous zeolites via sol-gel process such as, LTA (Sathupanya *et al.*, 2002), ANA, GIS (Sathupanya *et al.*, 2003), MFI (Phiriyawirut *et al.*, 2003), TS-1 (Phonthammachai *et al.*, 2003) and MCM-41, Ti-MCM-41, Mo-MCM-41 (Thanabodeekij *et al.*, 2005-2006).

In addition, the inclusion of guest molecules in mesoporous materials is one of focused subjects. Some efforts have been made to incorporate metal atoms, such as V, Mo, Cu, Fe, and Ti, into mesoporous silica materials by using silatrane as a precursor. In terms of catalytic activity, metal loaded-SBA-15 tends to have higher activity than pure silica SBA-15. For example, Cu-SBA-15 showed higher activity and selectivity for hydroxylation of phenol than the pure SBA-15 (Wang *et al.*, 2005), Ti-substituted SBA-15 (Chen *et al.*, 2004), Fe-SBA-15 (Zhang *et al.*, 2007), also showed better catalytic activity for styrene oxidation than pure SBA-15. Therefore, many scientists have developed techniques to incorporate metal into the frameworks, such as a physical-vapor-infiltration, a wet-impregnation, and a sol-gel process. Among them, direct synthesis via sol-gel method has been effectively used by many groups. Wongkasemjit and coworkers have successfully synthesized various types of mesoporous materials using this method, for example, Fe-SBA-1, Ti-SBA-1, cubic mesoporous silica (TanglumLeart *et al.*, 2008-2009), Fe-MCM-41 hexagonal mesoporous silica (Thitsartarn *et al.*, 2008), titanium loaded TS-1 zeolite (Phonthammachai *et al.*, 2006).

Thus, the major aims of this work are to study a novel synthesis route to produce the remarkably high quality SBA-15, and metal loaded SBA-15 viz. Ti-SBA-15 and Mo-SBA-15 by silatrane precursor and using poly(ethylene glycol)-block-poly(propylene glycol)-block-poly(ethylene glycol) as a structure directing agent. The catalytic activities of the synthesized SBA-15 and metal loaded SBA-15 are also focused in this research.

CHAPTER II

THEORETICAL BACKGROUND AND LITERATURE SURVEY

2.1 Introduction to Metal Alkoxide

Metal alkoxides exhibit great differences in physical properties, depending primarily on the position of the metal in the periodic table, and secondarily on the alkyl group. Many alkoxides are strongly associated by intermolecular forces (Bradley *et al.*, 1960; Wardlaw *et al.*, 1956), depending on size and shape of the alkyl groups. Many metal methoxides are non-distillable solids because the small methyl group has little screening effect on the metal atom. With a larger number of methyl groups and smaller atomic radius of the metal, methoxides become sublimable and even distillable.

Metal alkoxides are used for a great variety of purposes (Harwood *et al.*, 1963), especially, adding a metal into an organic solution for a homogeneously catalyzed reaction. They are mainly used in catalysis with partial or complete hydrolysis, alcoholysis, transesterification and sol-gel application. The most outstanding property of metal alkoxides is the ease of hydrolysis. This is specially used for sol-gel application (Klein *et al.*, 1981; Dislich *et al.*, 1971; Heistand *et al.*, 1986; Lacourse *et al.*, 1986).

2.2 Synthesis of Metal Alkoxides

The metal alkoxide precursors for catalyst synthesis are of interest in this work. Apparently, the synthesis of new metal alkoxides possessing unique structures and properties is of great significance for the investigation of sol-gel process as well as the evolution of metal alkoxide chemistry. However, there are a few drawbacks of metal alkoxides that make it difficult to study their structures and properties thoroughly, such as, the extreme moisture sensitivity and the tendency to form

mixtures of structurally complex species upon hydrolysis. Many scientists thus tried to improve the properties of metal alkoxides (Grainsford *et al.*, 1995; Wang *et al.*, 1999).

Laine *et al.* (1991) investigated a straightforward and low-cost synthesis of metal alkoxide precursor. The synthetic method used inexpensive metal oxide precursor to react with ethylene glycol in one step called "Oxide One Pot Synthesis Process (OOPS)" to successfully produce a group I metal alkoxide (Laine, 1995; Blohowiak, 1992).

Wongkasemjit *et al.* (2001) also synthesized silatrane using SiO_2 and triethanolamine/triisopropanolamines (Scheme 2.1). The precursor exhibited outstanding high stability not only in alcohol, but also in water.

$$SiO_2 + N(CH_2CHCH_3OH)_3 + H_2NCH_2(CH_2NHCH_2)_2CH_2NH_2 + HOCH_2CH_2OH$$

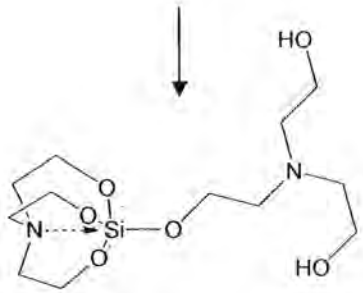

Scheme 2.1 The preparation of silatrane complexes by Wongkasemjit's method.

Not only atrane complexes, but also many metal glycolates were synthesized, especially, Ti, Zr, Ce, Sn and Mo (Ksapbutr *et al.*, 2001; Phontammachai *et al.*, 2003; Junin *et al.*, 2004; Sadtayanon *et al.*, 2004).

$$TiO_2 + 2HOCH_2CH_2OH \xrightarrow[200\ ^\circ C]{TETA} \text{Ti-glycolate complex} + 2H_2O$$

Scheme 2.2 The preparation of titanium glycolate complex (Phonthammachai *et al.*, 2003)

These precursors obtained are highly pure and suitable for studying optimal conditions of the sol-gel process for high surface porous metal oxides suitably used as a catalyst or a catalyst support.

2.3 Sol –Gel Processing

Sol-gel technique has been extensively used to prepare amorphous and crystalline materials. In general, the sol-gel process of metal oxides/alkoxides is the synthesis of an inorganic network at low temperature. This technique involves the transition characterized by a relatively rapid change from a liquid (solution or colloidal solution) into a solid (gel-like state).

Metal alkoxides are a member of metal organic compounds containing an organic ligand attaching to a metal or metalloid atom. Metal alkoxides are popular precursors for the sol-gel process because they react readily with water via hydrolysis reaction to form metal hydroxide, as shown in the following reaction.

$$Si(OR)_4 + H_2O \rightarrow HO\text{-}Si(OR)_3 + ROH \qquad (2.1)$$

where R represents an alkyl ligand (then OR is an alkoxy group), and ROH is an alcohol. Depending on the amounts of water and catalyst in the system, hydrolysis may go to completion, meaning that all of the OR groups are replaced by OH), or partially occur, $Si(OR)_{4n}(OH)_n$. Moreover, the molar ratio of H_2O:$Si(OR)_4$ should be at least 2:1 to approach complete hydrolysis of the alkoxide (Nicolaon and Teichner, 1968).

At its simplest level, sol-gel chemistry with metal alkoxides can be described in terms of two main reactions:

Hydrolysis: $\quad -M\text{-}OR + H_2O \rightarrow -M\text{-}OH + R\text{-}OH \qquad (2.2)$

Condensation: $\quad -M\text{-}OH + XO\text{-}M\text{-} \rightarrow -M\text{-}O\text{-}M + XOH \qquad (2.3)$

where X can be either H or R (an alkyl group).

The most important characteristic of the sol-gel preparation of catalytic materials is its ease to control the reaction rate, leading to the following advantages:

(i) The ability to maintain high purity (because of purity of starting materials);

(ii) The ability to change physical characteristics, such as pore size distribution and pore volume;

(iii) The ability to vary compositional homogeneity at a molecular level;

(iv) The ability to prepare samples at low temperatures;

(v) The ability to introduce several components in a single step;

(vi) The ability to produce samples in different physical forms.

The M-O-M network product is formed by polycondensation reactions, as shown in Reaction 2.3 in which alcohol and water are produced as by-products. Further extent of the condensation of the sol results in the formation of gel. There are many parameters affecting gel properties, such as temperature, pH, type of precursor, and solvent. Varying the temperature is the most effective when it can alter the relative rate of competing reactions. Solvent can change the nature of an alkoxide precursor though solvent exchange or directly affect the condensation reaction. It is also possible to prepare gel without solvent as long as another mean, such as ultrasound irradiation, is used to homogenize. Furthermore, pH of the solution, which can be changed by the addition of either acid or base catalyst, is also the most important parameter in obtaining gel because the rate and content of the hydrolysis reaction are influenced by the change in pH (Aelion *et al.*, 1950).

2.4 Sol-Gel Process in Surfactant-Templated Silica

Mesoporous silica can be synthesized in either the alkaline route (Beck, 1992) or the acid route (Huo *et al.*, 1994) both using amphiphiles as templates. In the acid route, the silica source is silicon alkoxides. The acid catalysis speeds up the hydrolysis

versus the condensation rate and promotes mostly condensation at the ends of silica polymers to form linear silicate ions (Sanchez *et al.*, 1994). On the other hand, the alkaline catalysis favors both hydrolysis and condensation. Thus, the alkaline route leads to a highly condensed and compact structure, and the acid route leads to a more fuzzy and soft network (Sanchez *et al.*, 1994). The acid route is popular for studying its rich morphology, whereas the alkaline route usually provides more stable and ordered materials because silica are highly condensed.

The second important difference is in how the interaction surfactant and silicate are organized. The isoelectric point of silicate is around pH = 2, below which the silicate carries a positive charge, whereas in the alkaline route the silicate is negatively charged. So in the alkaline route, surfactant and silicates organize by the strong S^+I^- electrostatic interaction. In the acid route (with pH <2), the silica species in solution are positively charged as $\equiv SiOH_2^+$ (denoted as I^+). The surfactant (S^+)-silica interaction becomes $S^+X^-I^+$ as mediated by the counterion X^- (Ozin *et al.*, 1997). This micelle-counterion interaction is in thermodynamic equilibrium. For the complex factors one needs to consider are: ion exchange equilibrium of X^- on micellar surface, surface-enhanced concentration of I^+, and proton-catalyzed silica condensation near micellar surface.

The steps in the synthesis can be roughly separated into two parts: the self-assembly of surfactant inorganic system and the inorganic polymerization of silica (Ogawa *et al.*, 1994, Yang *et al.*, 1997). The uncondensed silicate ions serve as the counterions in the early stage of surfactant self-assembly. This occurs quickly. The silica condensation rate is, however, slower, and extent of condensation is pH- and temperature-dependent (Renzo *et al.*, 1999).

2.5 Literature Review

Zhao *et al.* reported that the use of TEOS as silica source and amphiphilic triblock copolymers to direct the organization of polymerizing silica species have resulted in the preparation of well-ordered hexagonal mesoporous silica structure

(SBA-15) with uniform pore size up to approx. 300 Å. The SBA-15 material is synthesized in acidic media produces highly ordered, two-dimensional hexagonal (space group *p6mm*) silica-block copolymer mesophases. Calcination at 500 °C gives porous structures with large interlattice *d* spacings of 74.5 to 320 Å, pore sizes from 46–300 Å, pore volume fraction up to 0.85 and silica wall thicknesses of 31–64 Å. SBA-15 can be readily prepared over a wide range of uniform pore sizes and pore wall thicknesses, using a variety of poly(alkylene oxide) triblock copolymers such as poly(ethylene oxide)-poly(propylene oxide)-poly(ethylene oxide) (PEO-PPO-PEO) and by the addition of cosolvent organic molecule such as 1,3,5-trimethylbenzene (TMB). SBA-15 is formed in acidic condition with HCl, HBr, HI, HNO_3, H_2SO_4 or H_3PO_4 acids, above the isoelectric point of silica (pH 2), no precipitation or formation of silica gel occurs. At neutral (pH 7), only disordered or amorphous silica is obtained (Zhao *et al.*, 1998). Lin *et al.* also found that when the pH is adjusted to 5, fast silica condensation rate leads to the formation of irregular particles rather than crystals (Lin *et al.*, 2008).

Zhao *et al.* also found that the pore size of hexagonal mesoporous SBA-15 can be increased to more than 300 Å by increasing the hydrophobic volume of the self-assemble aggregates. This can be achieved by changing the copolymer composition or block sizes, or by adding cosolvent organic molecule such as TMB (Zhao *et al.*, 1998).

Generally, a hydrothermal treatment time of 11–72 h at 100 °C was needed to yield well-ordered mesoporous structures of high surface area (690 m^2/g), uniform pore diameter (47 Å) and volume (0.56 cm^3/g). Subsequently, Newalkar *et al.* introduced microwave-assisted syntheses to shorten reaction time (2 h) while obtaining materials of similar quality to those prepared in the autoclave. The microwave method proves superior as volumetric heating favors homogeneous nucleation, and fast dissolution and supersaturation of precipitated gels promotes shorter crystallization times (Park *et al.*, 1998; Komarneni *et al.*, 1994).

For titanium-substituted SBA-15, Zhang *et al.* (2002) successfully prepared Ti-SBA-15 using TMOS and titanium isopropoxide as silicon and titanium sources, respectively. Since the hydrolysis of titanium alkoxide is fairly instantaneous, whereas

the hydrolysis of silicon precursor much slower, certain amount of fluoride (F/Si = 0.03–0.05) was added to accelerate the hydrolysis of TMOS; and pH value was adjusted to below 1.0 to obtain high quality of Ti-SBA-15.

Chen *et al.* (2004) successfully synthesized Ti-SBA-15 under acidity hydrothermal conditions using titanium trichloride ($TiCl_3$) and TEOS as titanium and silicon sources, respectively. They pre-mixed H_2O_2 with a certain amount of $TiCl_3$ before adding into the gel-solution to improve the ordered structure of the Ti-SBA-15. At the maximum Si/Ti ratios, only the samples prepared in the presence of H_2O_2 could maintain their ordered structure. In addition, the products synthesized by adding H_2O_2 tended to have higher surface area, larger pore size and pore volume than those synthesized without adding H_2O_2.

In order to synthesize Ti-containing SBA-15, almost all researchers used either titanium isopropoxide or $TiCl_3$ as titanium source. Both compounds are expensive, moisture unstable and relatively high reactivity. Wongkasemjit and coworkers (2003–2006) successfully prepared titanium glycolate using inexpensive and widely available titanium oxide (TiO_2) and ethylene glycol as starting materials via the OOPS process. The resulting moisture stable titanium glycolate could be effectively used to synthesize many types of materials, such as high surface area anatase TiO_2 (Phonthammachai *et al.*, 2003), sillenite ($Bi_{12}TiO_{20}$) (Thanabodeekit *et al.*, 2005), titanium loaded TS-1 zeolite (Phonthammachai *et al.*, 2006), and highly ordered mesoporous Ti-SBA-1 (TanglumLert *et al.*, 2008).

Li *et al.*, (2005) reported that the Fe-SBA-15 could be successfully synthesized using a simple direct hydrothermal method under weak acid condition in the presence of fluoride, using TMOS and iron nitrate ($Fe(NO_3)_3.9H_2O$) as silicon and iron precursors, triblock copolymer surfactant $EO_{20}PO_{70}EO_{20}$ as a template. They found that when the pH value of the solution was lower than 2.0, the highly isolated framework iron species (Fe^{3+}) were obtained. Besides, adding more iron precursor could improve the order of the mesostructure because of the salt effect. Moreover, different iron species were produced by changing the pH value of the solution, and, for

all of the calcined samples, the iron ions exhibited tetrahedral coordination in the silica framework with Fe/Si molar ratio below 0.0022 at pH 1.5.

Melero *et al.* (2007) have reported the preperation of molybdenum-containing SBA-15 using co-condenstion technique under acidic condition using non-ionic surfactant as a template, TEOS and ammonium molybdate tetrahydrate $[(NH_4)_6[Mo_7O_{24}]\cdot 4H_2O]$ as silica and molybdenum sources. They prehydrolized molybdenum precursor for at least 3 h to depolymerize heptamolybdate species to form monomeric soluble moybdenum(VI) species before adding silica and molybdenum precursor into the template solution. After stirring at 40 °C for 20 h the mixture was aged at 100 °C for 24 h and further calcined. The resultant product from this method showed good mesoscopic ordering, narrow pore size distribution and high dispersion of molybdenum species.

Wongkasemjit *et al.* (2009) have been successful to use molybdenum glycolate to prepare Mo-SBA-1 in dilute acidic condition at room temperature using silatrane as a silica source and C_{16}TMAB as a template. The mesoporous Mo-SBA-1 obtained from this method maintained a well-order mesostructure and high surface area. The amount of molybdenum that could be incorporated into the SBA-1 framework was relatively high (up to 5%mol) without any extraframe work.

CHAPTER III

A NOVEL ROOM TEMPERATURE SYNTHESIS OF MESOPOROUS SBA-15 FROM SILATRANE

Abstract

Well-ordered and stable two dimensional mesoporous silica, SBA-15, were synthesized at room temperature (RT) from a silatrane precursor and a non-ionic triblock copolymer ($EO_{20}PO_{70}EO_{20}$) as the structure directing agent. Using a combination of small angle X-ray scattering, electron microscopy and nitrogen gas absorption-desorption isotherms, the RT product was found to be equivalent to SBA-15 prepared using more elaborative microwave-assisted hydrothermal methods. Both synthesis routes yielded large surface areas (486–613 m^2/g), pore diameters (45–67 Å) and channel volumes (0.6–0.8 cm^3/g). All materials condensed as sinuous bundles of silica tubes, in a morphology that approximates *p6mm* symmetry, but where long range order was absent. In addition, a portion of the products consisted of fine crystalline mosaics or were aperiodic. The simplicity of the room temperature synthesis route may provide an inexpensive and energy-saving process for the large scale production of thermally stable SBA-15 as a catalyst support.

Introduction

Mesoporous materials have been of wide scientific and technological interest since the discovery of the M41S family in the 1990s by the Mobil research group[1-2]. Among the mesoporous silicas, the SBA group has attracted attention by virtue of their thicker walls, greater hydrothermal stability and larger pore size as compared to the M41S materials. In particular, well-ordered hexagonal SBA-15 possesses high specific surface areas (characteristically 600–1000 m^2/g), large pore sizes (45–300 Å) and excellent hydrothermal stability (up to 850 °C). These superb properties, place SBA-15 in demand for catalytic, adsorption and separation applications that require high

temperature or operate in corrosive environments[3-10]. Mesoporous silicas are typically synthesized by sol-gel processes where structure-directing amphiphillic surfactants, such as poly(ethylene glycol)-block-poly(propylene glycol)-block-poly(ethylene glycol), self assemble as micelles which are encapsulated by an inorganic silica precursor[11]. Calcination at 500–600 °C oxidizes the surfactant, leaving thee- or two-dimensional mesoporous arrangements of cavities or channels[12-16].

SBA-15 is a 2D mesoporous material first prepared hydrothermally under acidic conditions (pH 1–2) using tetraethyl orthosilicate (TEOS) as the silica source and triblock copolymers to direct the organization of the polymerizing silica species[6-7]. Generally, a hydrothermal treatment time of 11–72 h at 100 °C was needed to yield well-ordered mesoporous structures of high surface area (690 m^2/g), uniform pore diameter (47 Å) and volume (0.56 cm^3/g). Subsequently, Newalkar *et al.*[17] introduced microwave-assisted syntheses to shorten reaction time (2 h) while obtaining materials of similar quality to those prepared in the autoclave. The microwave method proves superior as volumetric heating favors homogeneous nucleation, and fast dissolution and supersaturation of precipitated gels promotes shorter crystallization times[18-30].

Previous work has shown that controlling hydrolysis and condensation is key to preparing well-ordered mesoporous material though sol-gel processing[31]. While TEOS is a common silica source, it is highly susceptible to hydrolysis, and the rapid separation of amorphous silica impedes mesopore formation. Therefore, it is advantageous to use precursors of reduced hydrolytic activity such as silatrane, an organosilicate resistant towards hydrolysis that is stable in air for several weeks. Additionally, silatrane is an inexpensive silica precursor, which can be conveniently synthesized directly from fumed silicon dioxide and triethanolamine in ethylene glycol[32-33]. These starting materials are commercially available and low-priced. Silatrane is a proven silica precursor for the sol-gel synthesis of many microporous[34-37] and mesoporous[38-42] zeolites. In this paper, we describe a simple room temperature route for the preparation of SBA-15 using silatrane under acidic conditions, where a triblock copolymer (pluronic P123) was employed as the structure-directing agent. The demonstration of room temperature synthesis shows that large scale production of SBA-15 can be economical and energy efficient.

Experimental

Silatrane Synthesis

The silatrane precursor was synthesized from fumed silica (99.8%, Sigma-Aldrich, St. Louis, MO) solubilized in triethanolamine (TEA) (Carlo Erba, Milan, Italy), with ethylene glycol (EG) (J.T. Baker, Philipsburg, NJ) employed as the solvent, and acetronitrile (Labscan, Bangkok, Thailand) used for silatrane purification. Following the method of Wongkasemjit *et al.*[43] 0.125 mol TEA was refluxed with 0.1 mol silicon dioxide in ethylene glycol (100 mL) at 200 °C under nitrogen for 10 h in an oil bath. Excess ethylene glycol was removed under vacuum at 110 °C to obtain a crude brown solid that was washed with acetronitrile to remove TEA and EG residues. The white silatrane product was vacuum dried overnight then examined by Fourier-transform infrared (FT-IR) absorption spectrometery (Bruker Optics EQUINOX55, Karlsruhe, Germany) at a resolution of 2 cm^{-1}, and thermogravimetric analysis (DuPont 2950, Twin Lakes, WI) at a heating rate of 10 °C/min from room temperature to 750 °C in a nitrogen atmosphere.

The FT-IR bands observed were 3000–3700 cm^{-1} (w, νO–H), 2860–2986 cm^{-1} (s, νC–H), 1244–1275 cm^{-1} (m, νC–N), 1170–1117 cm^{-1} (bs, νSi–O), 1093 cm^{-1} (s, νSi–O–C), 1073 cm^{-1} (s, νC–O), 1049 cm^{-1} (s, νSi–O), 1021 cm^{-1} (s, νC–O), 785 and 729 cm^{-1} (s, νSi–O–C), and 579 cm^{-1} (w, νN-Si). TGA showed one sharp mass loss at 390 °C and gave a 19% ceramic yield of $N(CH_2CH_2O)_3Si–OCH_2CH_2–N(CH_2CH_2OH)_2$.

SBA-15 Synthesis

Mesoporous SBA-15 was synthesized from silatrane with poly(ethylene glycol)-block-poly(propylene glycol)-block-poly(ethylene glycol) ($EO_{20}PO_{70}EO_{20}$) (P123) (Sigma-Aldrich) employed as the template, and hydrochloric acid (Labscan Asia) as the catalyst in accord with the procedure of Stucky *et al*[6-7]. A solution of $EO_{20}PO_{70}EO_{20}$:HCl:silatrane:H_2O = 2:60:4.25:12 (mass ratio) was prepared by

dissolving 4 g of $EO_{20}PO_{70}EO_{20}$ polymer in 80 g of 2 M HCl (part A) and 8.8 g of silatrane in 20 g of H_2O (part B) with stirring continued for 1 h to ensure complete dissolution. For Route 1 synthesis, the solution of part B was then poured into part A, stirred at room temperature (RT) for 24 h, the product was recovered by filtration, washed with deionized water, and dried overnight under ambient conditions. For Route 2, the RT product was in addition treated in an autoclave placed in a microwave oven at 300W for 1–2 h at 100 or 120 °C. After cooling to RT, the material was filtered, washed and dried as for the Route 1 SBA-15. Both Routes 1 and 2 silicas were calcined at 550 °C in air for 6 h using a tube furnace (Carbolite, CFS 1200, Hope Valley, U.K.) at a heating rate of 1 °C/min to remove the residual organics (Figure 3.1). The microwave assisted product prepared at 120 °C was taken as the baseline material.

Mesopore Ordering

Small-angle X-ray scattering (SAXS) patterns were obtained with a PANalytical PW3830 X-ray instrument using CuKα radiation generated at 50kV and 40 mA. Thin powder samples (0.02 g) were spread uniformLy on adhesive tape and mounted on an aluminium frame (15–20 mm). The scattering patterns were recorded on an image plate and intensities extracted as two dimensional plots against scattering angle (2θ) by integration across approximately 450 pixels/degree 2 theta (Figure 3.2a). As replication of the 2θ zero shift was poor, the relative, rather than absolute positions of the scattering maximum were compared. By using identical sample weights the intensity of the peaks could be directly compared. If the stacking of silica mesotubes is perfectly hexagonal and conforms to *p6mm* plane symmetry than the 2D crystallographic repeat can be indexed as {10} ≡ {11}, while the second order reflections provide a measure of the channel diameter and can be indexed as {30} ≡ {33} (Figure 3.2b). Additional scattering (e.g. {-1-1} or {-2-1}) out to larger d-spacings will be significant only if the coherent hexagonal domain sizes are sufficiently extensive.

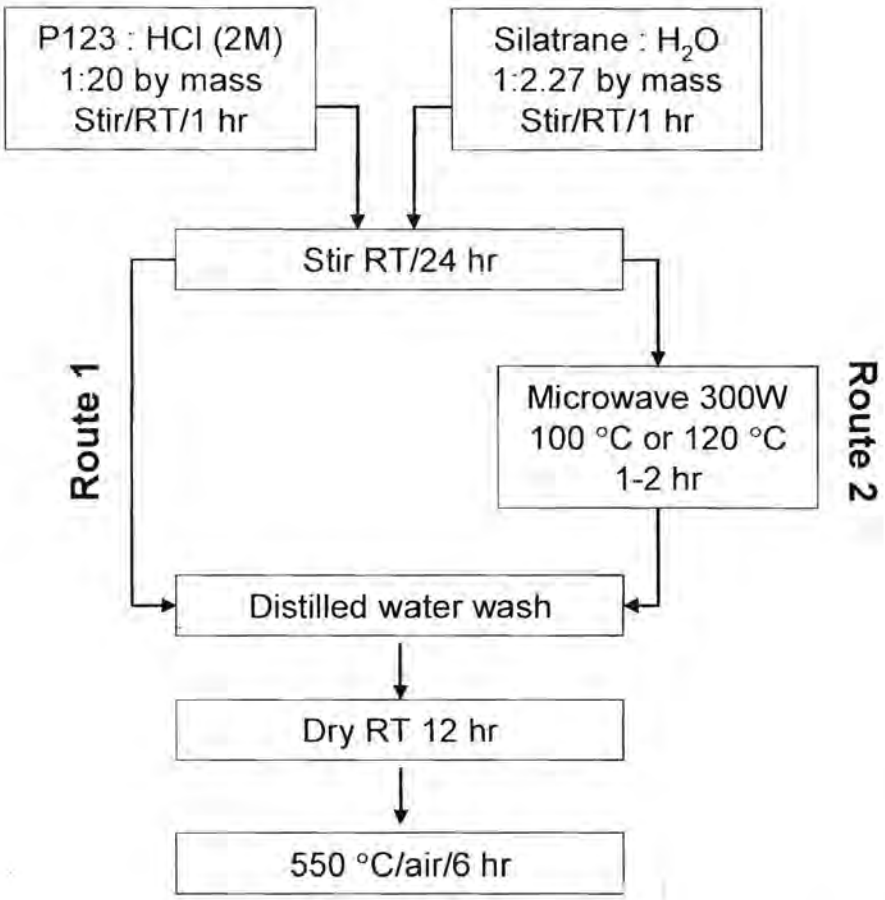

Figure 3.1 Simplified room temperature synthesis of SBS-15 (Route 1) compared to conventional microwave-assisted hydrothermal method (Route 2).

Nanostructure

Field Emission Scanning Electron Microscope (FESEM) images were obtained from powders mounted on double-sided carbon tape using a JEOL JSM-7500F, operating at an accelerating voltage of 0.3–0.5 kV to minimize the effects of charging. Transmission electron microscopy (TEM) was conducted using a JEOL JEM-2100F TEM instrument operated at an accelerating voltage of 200 kV with a large objective aperture. For TEM, the powder was lightly ground under ethanol, sometimes with the introduction of liquid N_2 to enhance fracture and produce thin flakes that were dispersed ultrasonically. Two drops of the suspension were deposited on holey carbon-coated copper grids. The periodicity of SBA-15 projected along the mesotubes

were studied by fast Fourier transformation of TEM images using CRISP[44] to extract interplanar angles, with deviations from 60° indicating an oblique rather than hexagonal metric. The average size of the channels was obtained by assuming *p6mm* symmetry and carrying out a back Fourier transform with the diameter measured directly from the reprocessed image.

Physical Parameters

Nitrogen sorption isotherms were obtained at -196 °C after out gassing at 250 °C for 12 h (Quantasorb JR, Mount Holly, NJ). The surface area and average pore size were determined by the Brunauer–Emmett–Teller (BET) method.

Results and Discussion

As-synthesized SBA-15 mesoporous material

The SAXS pattern for as-synthesized mesoporous silica (SBA-15) prepared with $EO_{20}PO_{70}EO_{20}$ shows two well-resolved peaks (Figure 3.2A) that are indexable as {10} ≡ {11} and {30} ≡ {33} reflections associated with *p6mm* hexagonal symmetry. The intense {10} peak reflects a *d* spacing of 150 Å, corresponding to a unit-cell parameter (a_0 = 173 Å). After calcination in air at 550 °C for 6 h, SAXS (Figure 3.2B) shows that the *p6mm* morphology is preserved. Two peaks are still observed, confirming that hexagonal SBA-15 is thermally stable. A similarly high degree of mesoscopic order is observed for hexagonal SBA-15 even after calcination at 850 °C.

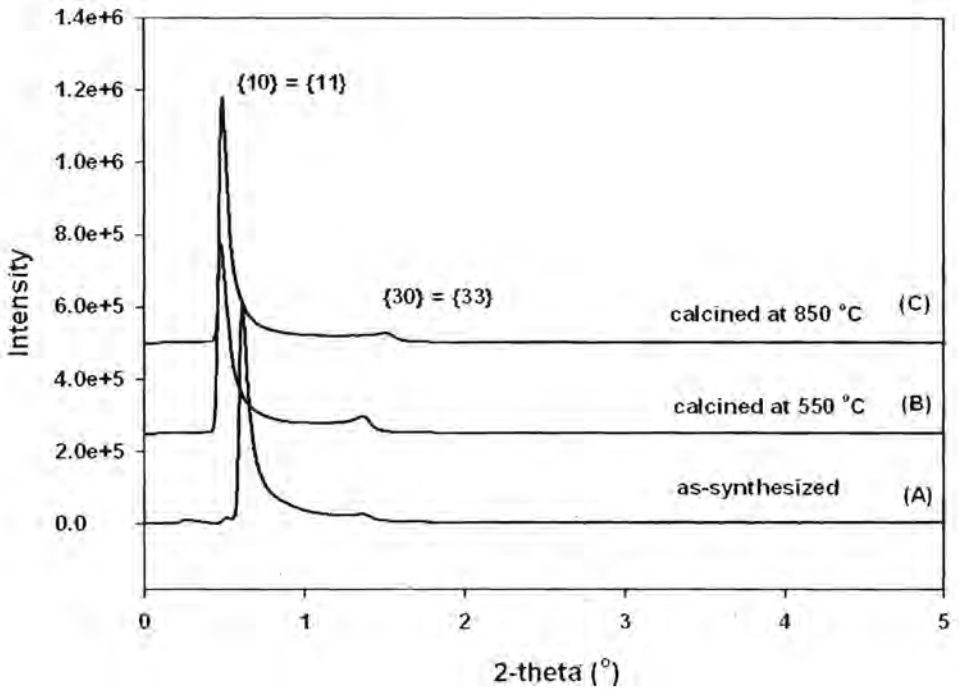

Figure 3.2 The SAXS pattern of the as-synthesized SBA-15 (A), after calcinations at 550 °C (B) and after calcination at 850 °C (C). These materials show two strong scattering maxima that are indexed in accord with *p6mm* (hexagonal) symmetry.

Thermal gravimetric and differential thermal analyses (TGA and DTA) in air of the SBA-15 sample calcined at 550 °C for 6 h and prepared with $EO_{20}PO_{70}EO_{20}$ show total weight losses of 11.02 weight % (Figure 3.3). At 94.6 °C, TGA registers a 2.11 weight % loss because of desorption of water. There is no weight loss at 145 °C which would correspond to the decomposition temperature of the block copolymer[6] indicating that there is no any nitrogen or carbon species left in the mesoporous wall, and confirming that the template has completely been removed.

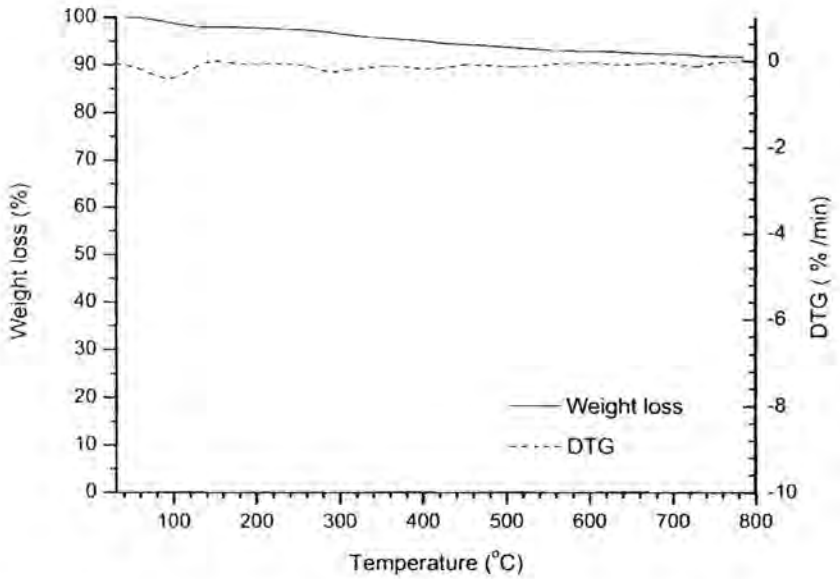

Figure 3.3 The TG-DTG peak analyzed in air of SBA-15 after calcinations at 550 °C for 6 h.

With hydrothermal treatment

A. High temperature microwave-assisted hydrothermal synthesis (120 °C/1 h)

This benchmark material yielded a SAXS pattern with first and second order scattering centered at d-spacings of 182.5 Å (a_o = 210.7 Å) and 65.8 Å (Figure 3.4a). When indexed according to the plane group *p6mm* as {10} ≡ {11} and {30} ≡ {33} (Figure 3.5), the ratio $d_{\{10\} \equiv \{11\}} / d_{\{30\} \equiv \{33\}} = 2.8$, rather than 3, since the overall structure shows significant deviations from the hexagonal metric, and more nearly conforms to oblique *p*2 (Table 3.1). Both scattering maxima are anisotropic such that {10} ≡ {11} shows a sharp upper limit of the d-spacing at ~190 Å, but a long tail towards higher scattering angles down to ~167 Å (Figure 4b), while the {30} ≡ {33} feature is asymmetric in an opposite sense and spans channel diameters from 63–67 Å. Higher order features such as {-1-1} are barely discernable because the coherent hexagonal domains were quite restricted (Figure 3.4b). Microscopy confirmed the absence of longer range periodicity as implied by SAXS. Field Emission scanning electron microscope (FESEM) showed that SBA-15 possesses a sinuous morphology

at the scale of a few hundred nanometers and coexisted with poorly ordered mesopore fragments (Figure 3.6a). In TEM, the mosaic character of even the better ordered fragments was evident (Figure 3.6b). At higher magnifications FESEM suggests that the channels are partially cavitated, rather than open conduits, which would limit mass transport (Figure 3.6c), however the TEM images show the projected absorption contrast and periodicity are insensitive to random channel blockages (Figure 3.6d). In detail, images collected parallel to the pseudo 6-fold rotation axis clearly show variability in both channel diameter and filling (Figure 3.6e), while <10> ≡ <11> projections confirm tubule ordering (Figure 3.6f).

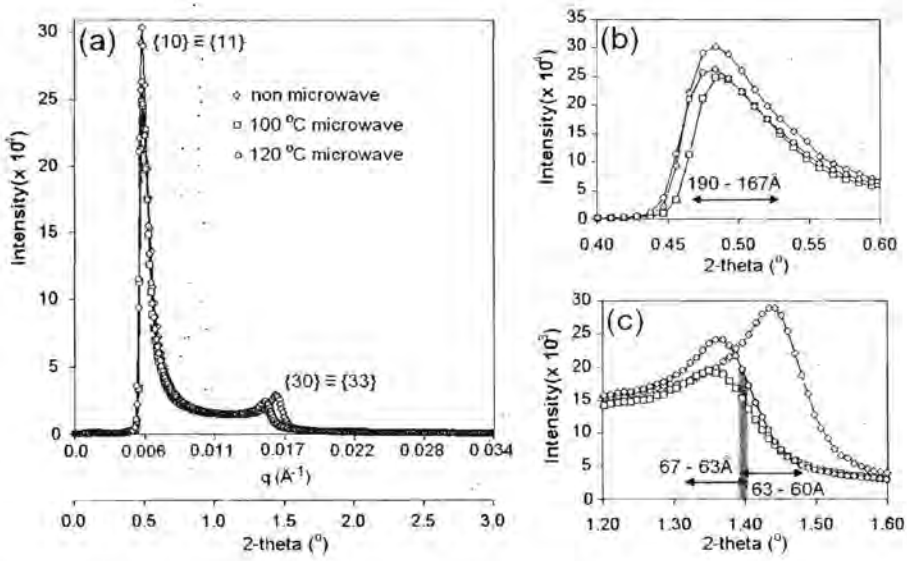

Figure 3.4 (a) The SAXS pattern the SBA-15 materials show two strong scattering maxima that are indexed in accordance with *p6mm* symmetry. The relative positions of these maxima are distinct for those mesoporous structures prepared with the assistance of microwave homogenization. (b) The {10} ≡ {11} reflections are anisotropic and show that the upper limit of the crystallographic repeat in the 2D mesopore order is quite sharp (~190Å) but with a long tail of shorter periodicity down to ~167Å. (c) The {30} ≡ {33} scattering that provides a measure of pore diameter shows the channels are slightly larger when microwave treatment is used, as compared to direct hydrothermal synthesis, in agreement with gas absorption measurements (see Table 3.1).

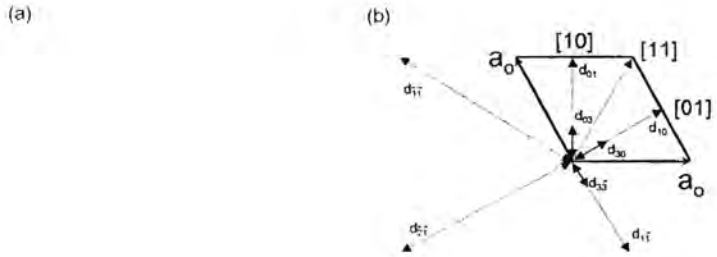

Figure 3.5 (a) Idealized morphology of the two-dimensional arrangement of silica tubes in SBA-15 and conforming to *p6mm* symmetry. In reality, the tubes are sinuous and extend over a range of diameters which destroys long range hexagonal symmetry. (b) Projection along the mesoporous tubes emphasizing the equivalence of {10} ≡ {11} planes and d-spacings that define the underlying crystallographic repeat, while {30} ≡ {33} correspond to a first approximation to the observed channel diameters.

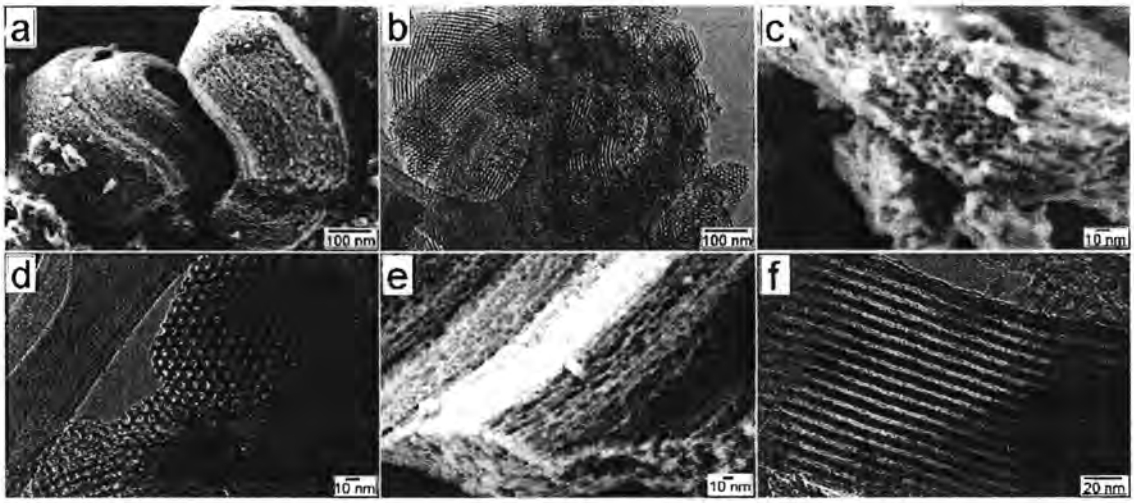

Figure 3.6 FESEM (left-hand side) and TEM (right-hand side) images of SBA-15 prepared hydrothermally at 120°C/1 h with microwave assistance. (a) & (b) At lower magnifications the twisted bundles of silica tubes are seen to co-exist with less crystalline and aperiodic material. (c) (d) When viewed along the pseudo-hexagonal projection it evident that channels not uniform in shape or content. (e) & (f) In <10> FESEM clearly shows cavitation along the channels. While this is not evident in TEM, the regular periodicity the 2D mesopore order is evident.

Fast Fourier transform analysis of 6-fold TEM projections confirmed that departures from *p6mm* symmetry were systemic, with the {10} ≡ {11} interplanar angles deviating from 60° (Figure 3.7a,b). By imposing hexagonal symmetry as the average structure and applying the back Fourier reconstruction, a processed image is recovered from which the pore diameter is directly accessible (Figure 3.7a) and shows an average tunnel diameter of 46 Å. The pore diameters derived from SAXS and TEM image processing, bracket the value obtained by nitrogen adsorption measurements, which gave a diameter of 54 Å (Table 3.1), pore volume of 0.8 cm^3/g and a high surface area (613 m^2/g) (Figure 3.8a). The isotherm was an IUPAC type IV with an H1-type hysteresis loop[5]. However, SBA-15 synthesized from silatrane showed a smaller pore volume (0.8 cm^3/g) and surface area (613 m^2/g) compared to equivalent material synthesized from TEOS (0.99 cm^3/g and 805.9 m^2/g). This is consistent with the SAXS observation that the silatrane source yielded less well-ordered mesopores[6,7,16] . While the TEOS derived SBA-15, X-ray scattering patterns contain upto four peaks indicative of longer range periodicity.

Table 3.1 Properties of SBA-15 as a function of the synthesis route

Synthesis*		Surface Area (m^2/g)	Channel Volume (cm^3/g)	Channel Diameter (Å)			$d_{(10)}/d_{(30)}$
		BET	BET	BET	TEM	SAXS	SAXS
Route 1	Without hydrothermal treatment	486	0.6	50	~45	60-63	3
Route 2	With hydrothermal treatment via microwave assisted method at **100 °C for 2 h.**	572	0.8	55	~45	63-67	2.8
	With hydrothermal treatment via microwave assisted method at **120 °C for 1 h.**	613	0.8	54	~45	63-67	2.8

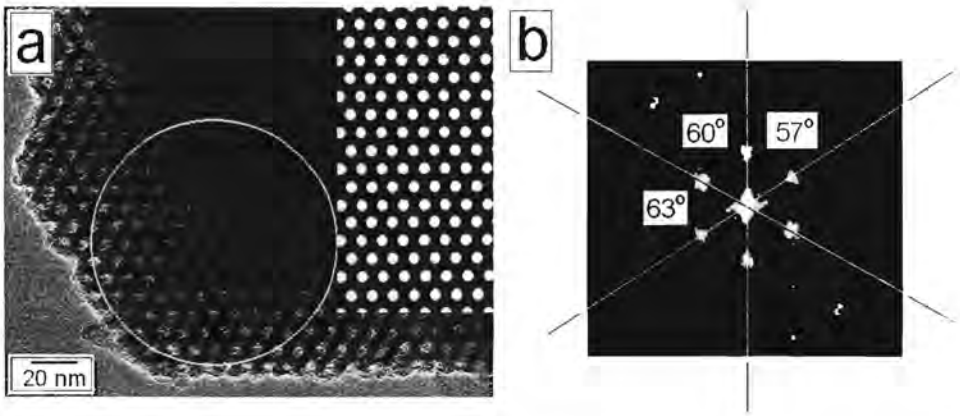

Figure 3.7 (a) A well-ordered fragment of SBS-15 project in pseudo-*p6mm* projection. (b) The frequency image obtained by fast Fourier transformation (FFT) of the region within the circle yields shows angles that departure from 60° demonstrating that this material fragment better corresponds to *p*2 oblique symmetry. By imposing *p6mm* symmetry and calculating the back Fourier transform the inserted processed image in (a) is generated that yields an average pore diameter of 46 Å.

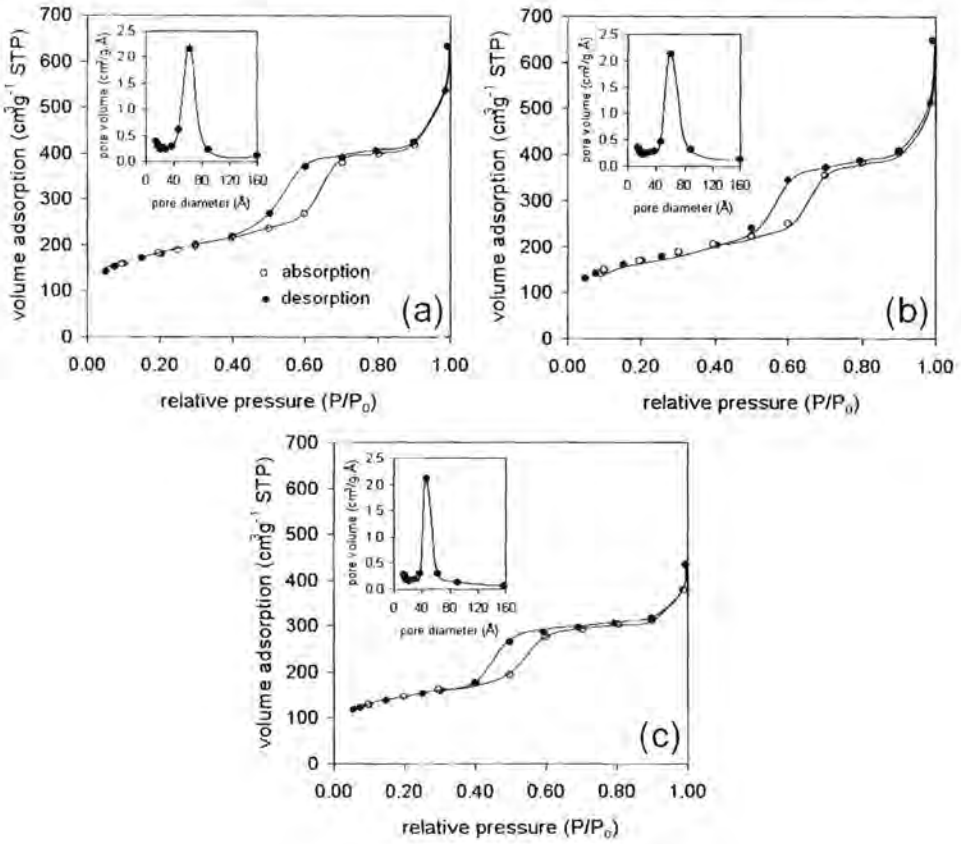

Figure 3.8 Nitrogen adsorption-desorption isotherms and corresponding pore size distributions for SBA-15 prepared with a microwave-assisted hydrothermal route at (a)120°C /1 h, (b) 100°C /2 h, and (c) directly at RT by stirring. The pore size range is slightly narrower for the latter (FWHM ~ 18 Å) as compared to the former (FWHM ~ 25 Å).

B. Low temperature microwave-assisted hydrothermal synthesis (100 °C/2h)

The characteristics of SBA-15 prepared at 100 °C were broadly similar to those of the 120 °C material, with the $d_{\{10\} \equiv \{11\}} / d_{\{30\} \equiv \{33\}} = 2.8$ (Figure 3.5) and a cavitated channel structure (Figure 3.9). The surface area (572 m^2/g) and pore diameter (55 Å) are identical to those obtained at 120 °C / 1 h (Figure 3.8b).

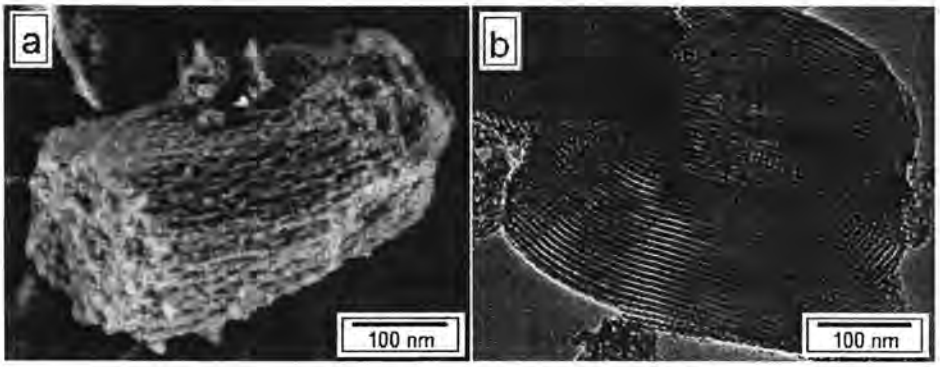

Figure 3.9 Approximate <10> FESEM (a) and TEM (b) images micrographs of SBA-15 prepared hydrothermally with microwave-assisted method at 100°C/2 h.

Generally, the work related to SBA-15 employs a hydrothermal treatment step via autoclave or microwave assisted methods using TEOS as a silica source, and P123 as the template. For example, Su et al[45], studied the orientation of mesochannels using a laser-modified polyimide surface, with TEOS was employed as silica source and P123 as the structure directing agent. The material was hydrothermally treated in an autoclave at 110 °C for 48 h. The orientation of the mesochannels was evaluated by X-ray scattering measurement. One narrow {10} peak of the 2D hexagonal phase appeared. The absence of a {11} peak, which would normally be observed in a hexagonal structure, was consistent with the mesopore channels oriented parallel to the substrate. Okamoto *et al*[46], studied the site-specific synthesis of mixed valence Ti-O-Fe complexes within the pores of ordered mesoporous silica SBA-15 using TEOS and P123. The powder exhibited thee reflections corresponding to {10}, {11} and {20} of a two-dimensional hexagonal pore structure. Newalkar *et al.*[17] reported a microwave-assisted synthesis method to shorten the synthesis time that employed TEOS and P123, that can be reduced the reaction time to 2 h and yield the product similar to that prepared by 48 h conventional autoclave treatment. It is believed the rapid heating to the crystallization temperature by volumetric heating favored homogeneous nucleation, fast supersaturation by the rapid dissolution of precipitated gels, and ultimately a shorter crystallization time.

Zhao *et al*[6-7], used TEOS and P123 to synthesize SBA-15 in acidic conditions as a function of temperature and time. Using an autoclave, it took 48 h to complete the reaction and achieve well-ordered SBA-15 with high surface area (690 m^2/g), uniform pore size of (47 Å) and pore volume (0.56 cm^3/g), these results are similar to the data obtained from the sample from this work.

Without hydrothermal treatment

Direct RT synthesis

The relative positions of the SAXS scattering maxima appear at 182.5 Å and 60.8 Å and conform almost exactly to the hexagonal metric with $d_{\{10\} \equiv \{11\}} / d_{\{30\} \equiv \{33\}} = 3.0$ (Figure 3.4). The spread of crystallographic repetition is unchanged (190 – 167 Å), however the channel diameter is slightly smaller (63 – 60 Å), in agreement with the BET measurements that yielded a surface area (486 m^2/g) and pore diameter (50 Å) (Figure 3.8c), Table 3.1). Micrograph collected near the principal axial projections is indistinguishable from the hydrothermally prepared material (Figure 3.10).

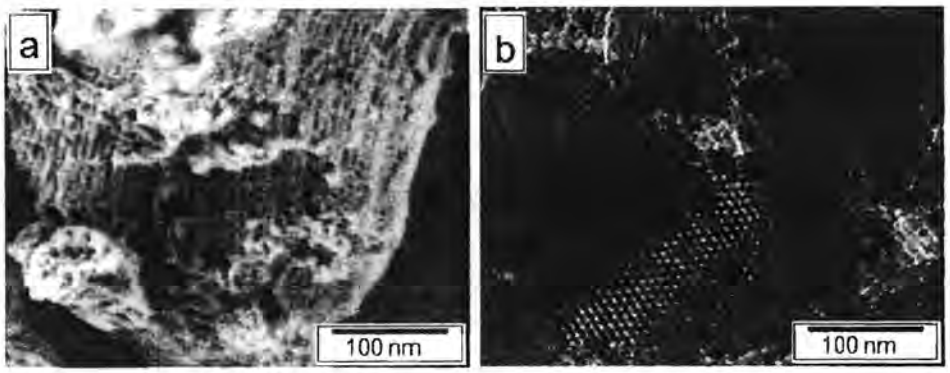

Figure 3.10 Approximate <10> FESEM (a) and hexagonal TEM (b) images of SBA-15 prepared at RT without hydrothermal treatment.

SAXS indicates that SBA-15 prepared at RT are well-ordered 2D mesoporous materials, comparable to those microwave-assisted hydrothermal products, with the latter yielding a marginally superior product in terms of higher BET surface area and mesopore order. When conventional precursors such as TEOS are used, it is believed that the hydrothermal conditions promote the condensation of metal oxide bridges, leading to better ordered structures. However, this benefit is minimal when silatrane is employed, as it is stable towards hydrolysis and can be employed at room temperature. TanglumLert *et al*[48], reported the successful synthesis of well-ordered and stable SBA-1 mesoporous silica via sol-gel process using silatrane as a silica source. The high quality SBA-1 was produced under mild acidic condition, C_nTMAB was used as a template, and the reaction was conducted at room temperature.

As it can be seen from the TEM images, the silica wall thickness between RT and microwave-assisted hydrothermal samples are equally similar, implying that silatrane condensation of Si-O-Si takes place at room temperature. By operating at ambient, this method minimizes process complexity while forming well-ordered SBA-15. The results from SAXS, FESEM and TEM clearly indicate that SBA-15 obtained from the room temperature (without hydrothermal treatment), and microwave-assisted method are comparable, and would facilitate economical and energy saving large scale production

Conclusions

It has been demonstrated that SBA-15 can be successfully synthesized at room temperature using silatrane, an inexpensive and conveniently prepared silica, as the silica precursor. The crystallographic, morphological and physical properties of SBA-15 obtained by this simple process are comparable to mesoporous silica prepared by the more complex microwave-assisted hydrothermal method. This new preparative route may allow inexpensive, energy-saving and efficient production of SBA-15 for a range of catalytic and environmental applications.

Acknowledgements

This research work is financially supported by the Postgraduate Education and Research Program in Petroleum and Petrochemical Technology (ADB) Fund (Thailand) and the Ratchadapisake Sompote Fund, Chulalongkorn University. We thank Mr Tan Teck Siong for assistance in collecting the secondary electron images, and the School of Materials Science & Engineering NTU for partially financial support.

References

1. Kresge, C. T.; Leonowicz, M. E.; Roth, W. J.; Vartuli, J. C.; Beck, J. S. *Nature* **1992**, *359*, 710-712.
2. Beck, J. S.; Vartuli, J. C.; Roth, W. J.; Leonowicz, M. E.; Kresge, C. T.; Schmitt, K. D.; Chu, C. T. W.; Olson, D. H.; Sheppard, E. W.; McCullen, S. B.; Higgins, J. B.; Schlenker, J. L. *J. Am. Chem. Soc.* **1992**, *114*, 10834-10843.
3. Davis M. E. *Chem. Ind.* **1992**, *4*, 137.
4. Estermann M.; McCusker L. B.; Baerlocher C.; Merroche A.; Kessler H. *Nature* **1991**, *352*, 320.
5. Hoang V-T.; Huang Q.; Ei M.; Do T-O.;Kaliaguine S. *Langmuir* **2005**, *21*, 2051-2057
6. Zhao, D.; Feng, J.; Huo, Q.; Melosh, N.; Frerickson, G. H.; Chmelka, B. F.; Stucky, G. D. *Science* **1998**, *279*, 548-552.
7. Zhao, D.; Huo, Q.; Feng, J.; Chmelka, B. F.; Stucky, G. D. *J. Am. Chem. Soc.* **1998**, *120*, 6024-6036.
8. Trong-On, D.; Desplantier-Giscard, D.; Danumah, D.; Kaliaguine, S. *Appl. Catal.*, A **2001**, *222*, 299-357.
9. Kubo S.; Kosuge K.; *Langmuir*, **2007**, *23*, 11761-11768.
10. Coasne B.; Galarneau A.; Renzo D.F.; Pellenq R.J.M. *Langmuir* **2006,** *22,* 11097-11105.
11. Kruk M.; Cao L. *Langmuir* **2007,** *23,* 7247-7254.
12. Goltner C. G.; Antonietti M. *Adv Mater.* **1997**, *9*, 431.

13. Antonietti M.; Goltner C. *Angew. Chem. Int. Ed. Engl.* **1997**, *36*, 910.
14. Wanka G.; Hoffmann H.; Ulbricht W. *Macromolecules* **1994**, *27*, 4145.
15. Chu B.; Zhou, *Surfactant Science Series* **1996**, *60*, 67.
16. Zukal A.; Siklova H.; Cejka J. *Langmuir* **2008,** *24,* 9837-9842.
17. Newalkar B.; Komarneni S.; Katsuki H. *Chem. Commun.* **2000**, 2389-2390.
18. Komarneni S.; Roy R.; Li Q. H. *Mater. Res. Bull.* **1992**, *27*, 1393.
19. Komarneni S.; Li Q. H.; Stefansson K. M.; Roy R. *J. Mater. Res.* **1993**, *8*, 3176.
20. Komarneni S.; Li Q. H.; Roy R. *J. Mater. Chem.* **1994**, *4*, 1903.
21. Komarneni S.; Pidugu R.; Li Q. H.; Roy R. *J. Mater.Res.* **1995**, *10*, 1687.
22. Komarneni S.; Li Q. H.; Roy R. *J. Mater. Res.***1996**, *11*, 1866.
23. Komarneni S.;. Menon V. C. *Mater. Lett.* **1996**, *27*, 313.
24. Chu P.; Dwyer F. G.; Vartuli J. C. *US Pat.* **1988**, 4 778 666.
25. Lohe U.; Bertram R.; Jancke K.; Kurzawski I.; Parlitz B.; Loeffler E.; Scheier E. *J. Chem. Soc., Faraday Trans.* **1995**, *91*, 1163.
26. Girnus I.; Jancke K.; Vetter R.; Richter-Mendau J.; Caro J. *Zeolites* **1995**, *15*, 33.
27. Meng X.; Xu W.; Tang S.; Pang W. *Chin. Chem. Lett.* **1992**, *3*, 69.
28. A. Arafat, J. C. Jansen, A. R. Ebaid and H. Van Bekkum, *Zeolites*, **1993**, *13*, 162.
29. Wu C. G.; Bein T. *Chem. Commun.* **1996**, 925.
30. Park M.; Komarneni S. *Microporous Mesoporous Mater.*, **1998**, *20*, 39.
31. Cabrera S.; Haskouri J. E,; Guillem C.; Latorre J.; Beltran-porter A.; Beltran-porter D.; Marcos M. D.; Amoros P.; *Solid state Sci* **2000**, *2*, 405.
32. Phiriyawirut P.; Magaraphan R.; Jamieson A. M.; Wongkasemjit S. *Material Science and Engineering* **2003**, *A361*, 147-154.
33. Charoenpinijkarn W.; Suwankruhasn M.; Kesapabutr B.; Wongkasemjit S.; Jamieson A. M. *European Polymer Journal* **2001**, *37*, 1441-1448.
34. Sathupanya M.; Gulari E.; Wongkasemjit S. *J. Eur. Ceram. Soc.* **2002**, *22*, 1293–1303.
35. Sathupanya M.; Gulari E.; Wongkasemjit S. *J. Eur. Ceram. Soc.* **2003**, *23*, 2305–2314.
36. Phonthammachai N.; Chairassameewong T.; Gulari E.; Jameison A. M.; Wongkasemjit S. *J. Met. Mater. Min.* **2003**, *12*, 23.

37. Phiriyawirut P.; Jamieson A. M.; Wongkasemjit S. *Microporous Mesoporous Mater*. **2005**, *77*, 203–213.

38. Thanabodeekij N.; TanglumLert W.; Gulari E.; Wongkasemjit S. *Appl. Organomet. Chem.* **2005**, *19*, 1047–1054.

39. Thanabodeekij N.; Sadthayanon S.; Gulari E.; Wongkasemjit S. *Mater. Chem. Phys.* **2006**, *98*, 131–137.

40. S. Mintova J. Cejka, *Stud. Surf. Sci. Catal*. **2007**, *168*, 301-326

41. J. Cejka, S. Mintova, *Catal. Rev*. **2007**, *49*, 457-509

42. Perez-Ramirez J, Chistensen CH, Egeblad K, Chistensen CH, Groen JC, *Chem. Soc. Rev*. **2008**, *37*, 2530-2542

43. Piboonchaisit P.; Wongkasemjit S.; Laine R. *J. Sci. Soc. Thailand* **1999,** *25*, 113.

44. X. Zou, M. Sundberg, M. Larine and S. Hovmoller, "Structure Projection Retrieval by Image Processing of HTEM Images Taken under Non-Optimum Defocus Conditions," *Ultramicroscopy* **1996**, 62, 103-121.

45. Su B.; Lu X.; Lu Q. *Langmuir*, **2008**, *24*, 9695-9699.

46. Okamoto A.; Nakamura R.; Osawa H.; Hashimoto K. *Langmuir*, **2008**, *24*, 7011-7017.

47. Song S. W.; Hidajat K.; Kawi S.*Langmuir*, **2005**, *21*, 9568-9575.

48. TanglumLert W.; Imae T.; White T.J.; Wongkasemjit S. *J. Am. Ceram. Soc.* **2007**, *90*, 3992-3997.

CHAPTER IV

ROOM TEMPERATURE SYNTHESIS OF Ti-SBA-15 FROM SILATRANE AND TITANIUM-GLYCOLATE AND ITS CATALYTIC PERFORMANCE TOWARDS STYRENE EPOXIDATION

Abstract

A novel room temperature sol-gel synthesis of Ti-SBA-15 is described using moisture stable silatrane and titanium-glycolate precursors, and a non-ionic triblock copolymer ($EO_{20}PO_{70}EO_{20}$) as the structure directing agent. Catalyst performance was optimized by systematically investigating the influence of acidity, reaction time and temperature, and titanium loading. Small angle X-ray scattering (SAXS) and transmission electron microscopy (TEM) showed well-ordered 2D mesoporous hexagonal structures, while N_2 adsorption/desorption measurements yielded high surface areas (up to 670 m^2/g), with large pore diameters (5.79 nm) and volumes (0.83 cm^3/g). Diffuse reflectance UV-visible spectroscopy (DRUV) was found that tetravalent titanium as $Ti^{4+}O_4$ tetrahedra were incorporated in the framework though displacement of $Si^{4+}O_4$ after calcination (550 °C/6 h) to loadings of 7mol% Ti without perturbation of the ordered mesoporous structure, or decoration by extra-framework anatase containing $Ti^{4+}O_6$ octahedra. The catalytic activity and selectivity of styrene epoxidation using hydrogen peroxide (H_2O_2) showed that the conversion of styrene increases significantly at higher titanium contents. The only products of this reaction were styrene oxide and benzaldehyde, with selectivity of 34.2% and 65.8%, respectively, at a styrene conversion of 25.8% over the 7mol% Ti-SBA-15 catalyst. Beyond this titanium loading, anatase is deposited on the framework and catalytic activity degrades. The performance of the new catalyst is also shown to be superior to conventional materials produced by incipient wetness impregnation where Ti resides on the surface of SBA-15, giving a styrene conversion of 11.9% under identical reaction conditions.

Introduction

Since the discovery of the large and uniform hexagonal channel motifs, high specific surface area, and excellent hydrothermal stability of SBA-15 silica molecular sieve by Zhao *et al.*[1,2], using nonionic triblock copolymers as templates, much effort has been devoted to enhancing the syntheses and functionality of these materials because of their potential as catalysts, adsorbents for large organic molecules, and guest-host chemical supports[3,4]. However, pure silica porous materials are poor catalysts due to weak acidity and redox potential[5,6]. To overcome these limitations, heteroatoms are incorporated into the framework to the create active sites, and many transition metals promote beneficial catalytic responses[7-10].

The introduction of Ti-substituted molecular sieves has added a new dimension to the application of silica based meso-frameworks for catalytic oxidation, and Ti-SBA-15 has proven to be a versatile catalyst for the selective oxidation with peroxide enhancement to produce fine chemicals and pharmaceuticals. To be effective, Ti should be incorporated crystallochemically in tetrahedral oxygen co-ordination (TiO_4) by isomorphic $Si^{4+} \leftrightarrow Ti^{4+}$ substitution, rather than as co-existing catalytically inactive anatase with $Ti^{4+}O_6$ octahedra[11]. Several attempts have been made to introduce titanium into the mesoporous silica framework of SBA-15[12-18] by direct synthesis or post-synthesis treatment[9,16,19-23]. The principle limitation of the post-synthesis method is that metal oxides are deposited on external surfaces of the catalyst which blocks the channels and prevents the reactant molecules accessing many reactive sites in the matrix[23]. Zhang *et al.*[14] reported the successful incorporation of Ti into SBA-15 though a fluoride mediated reaction that accelerated the hydrolysis of a silica precursor. However, the expensive starting materials have limited its use. Newalkar *et al.*[16] reported the microwave-assisted hydrothermal synthesis of Ti-SBA-15 using TEOS and $TiCl_4$ as silica and titanium sources.

Wongkasemjit *et al.*[24-26] successfully prepared silatrane and titanium glycolate using inexpensive and widely available silica and titanium oxide as starting materials, respectively. The resulting moisture stable silatrane and titanium glycolate can be effectively used to synthesize many technological materials[27-31]. Commercially

available silica and titanium sources are highly susceptible to hydrolysis, resulting in the rapid separation of amorphous silica that impedes mesopore formation. Therefore, it is advantageous to use precursors of reduced hydrolytic activity. Moreover, silatrane has also been proven successful for the synthesis of SBA-15 mesoporous silica at room temperature[32]. In the present study, this approach is extended to the synthesis of highly ordered Ti-SBA-15 from silatrane and titanium glycolate precursors, where the acidity, reaction temperature, reaction time, and Ti loading were optimized systematically. The catalysts were characterized using several complimentary techniques, including SAXS, DRUV, TEM, and N_2 adsorption. The catalytic activity of Ti-SBA-15 towards the epoxidation of styrene monomers with H_2O_2 employed as the oxidant was investigated as a function of temperature, time, and catalyst loading. To establish a baseline for comparison, titanium glycolate was impregnated on a SBA-15 framework by the incipient wetness impregnation method[33].

Experimental Section

Materials

Fumed silica (SiO_2, 99.8%) (Sigma-Aldrich, St. Louis, MO), titanium dioxide (TiO_2) (Carlo Erba, Milan, Italy), triethanolamine (TEA) (Carlo Erba, Milan, Italy), tetraethylenetriamine (TETA) (Facai, Bangkok, Thailand), ethylene glycol (EG) (J.T. Baker, Philipsburg, NJ), acetronitrile (Labscan, Bangkok, Thailand), poly(ethylene glycol)-block-poly(propylene glycol)-block-poly(ethylene glycol) ($EO_{20}PO_{70}EO_{20}$) (Sigma-Aldrich, Singapore), hydrochloric acid (HCl) (Labscan, Asia) were used without further purification or treatment.

Ti-SBA-15 sol-gel synthesis

Ti-SBA-15 materials were synthesized from silatrane and titanium-glycolate. The non-ionic triblock copolymer surfactant $EO_{20}PO_{70}EO_{20}$ was used as the structure-directing agent and 2 M HCl was the acid catalyst. The preparation of Ti-SBA-15 with

various n_{Ti}/n_{Si} molar ratios followed the method of Samran *et al.*[32]. A solution of $EO_{20}PO_{70}EO_{20}$:HCl:silatrane:H_2O = 2:60:4.25:12 (mass ratio) was prepared by dissolving 4 g of $EO_{20}PO_{70}EO_{20}$ polymer in 80 g of 2 M HCl (part A) and 8.8 g of silatrane, synthesized according to ref. 25-26, in 20 g of H_2O (part B) with continuously stirring for 1 h to ensure complete dissolution. The solution of part B was then poured into part A. The required amount of titanium glycolate[24] was added into the homogenous solution with stirring. The resulting gel was aged at room temperature (RT) for 24 h and the product recovered by filtration, washed with deionized water, and dried overnight at ambient. Silicas were calcined at 550 °C in air for 6 h using a tube furnace (Carbolite, CFS 1200, Hope Valley, U.K.) at a heating rate of 0.5 °C/min to remove the residual organics. The catalysts were designated as *(x)* mol% Ti-SBA-15 where *x* denotes the percentage of the n_{Ti}/n_{Si} ratio. Titanium-free mesoporous SBA-15 was synthesized using the same procedure ($EO_{20}PO_{70}EO_{20}$:HCl:silatrane:H_2O = 2:60:4.25:12 (mass ratio)) in the absence of titanium glycolate. The reaction conditions for synthesis of Ti-SBA-15 were studied as a function of Ti loading, acidity, reaction time, and reaction temperature.

Ti-SBA-15 impregnation synthesis

Incipient wetness impregnation was used to deposit Ti metal on the SBA-15 support [38], using 7 and 10 mol% titanium glycolate. The precursor was dissolved in water and dropped onto the catalyst supports. Drying was carried out at 100 °C for 12 h, followed by calcination (550 °C/6 h) in a Carbolite furnace (CFS 1200) at a heating rate of 0.5 °C/min.

Characterization

SAXS patterns were obtained with a PANalytical PW3830 X-ray instrument using CuKα (λ_{av}=0.154 nm) radiation generated at 50kV and 40 mA, over the 2θ range 0.5–10°, step size of 0.01° and dwell time of 10 seconds per step. TEM was conducted

using a JEOL JEM-2100F TEM instrument operated at an accelerating voltage of 200 kV with a large objective aperture. Nitrogen adsoption and desorption isotherms were measured at -196 °C after outgassing at 250 °C for 12 h under vacuum (Quantasorb JR, Mount Holly, NJ). The specific surface area was determined by the Brunauer–Emmett–Teller (BET) method. The pore size distributions were obtained from the adsorption and desorption branches of the nitrogen isotherms by the Barrett-Joyner-Halenda method. DRUV spectra were recorded from 190–600 nm with a Shimadzu UV-2550 spectrophotometer from catalyst powders loaded in a teflon cell and using $BaSO_4$ as a reference.

Catalytic activity of Ti-SBA-15

The catalytic activity of Ti-SBA-15 towards epoxidation of styrene was established by combining 5 mmol of styrene, 5 mmol of 30% H_2O_2, 5 mL of acetronitrile and a required amount of Ti-SBA-15 (0.0500–0.2000 g) in a glass flask. The suspension was stirred and heated to a fixed time (1–6 h) and temperature (70–90 °C) in an oil bath. Chemical analyses were carried out with a gas chomatograph (GC) equipped with a capillary column (DB-Wax, 30 m x 0.25 mm) and flame ionization detector (FID). The conversion of styrene was calculated based upon the amount of styrene monomer consumed.

Results and Discussion

Ti-SBA-15 catalyst crystal chemistry

Zhao *et al.*[1] synthesized good quality SBA-15 of high surface area (690 m^2/g) using TEOS as the silica precursor that was aged (35 °C/20 h) prior to hydrothermal reaction (100 °C/48 h). Recently, Samran *et al.*[32] reported a novel method to prepare SBA-15 from silatrane at room temperature via a sol-gel process using a nonionic triblock copolymer as the template to avoid the need for hydrothermal treatment. Following this approach, high quality Ti-SBA-15, of large surface area (592–670

m^2/g), pore volume (0.83 cm^3/g) and pore size (5.7 nm), was readily synthesized. Generally, the SAXS pattern of SBA-15 shows scattering attributable to {10} and {30} planes of a 2D hexagonal meso-channel arrangement. These characteristic lines were also observed in Ti-SBA-15. Moreover, the nature of Ti^{4+} as substitutional TiO_4 units or extra-framework TiO_6 polyhedra could be differentiated by DRUV. Catalysts showed strong adsorption, around 220 nm, typical of the ligand-to-metal charge transfer transition in the tetrahedrally coordinated TiO_4 or $HOTiO_3$ species. This band arises from dπ-pπ charge transfer between the Ti and O atoms associated with Ti-O-Si bonds and became more intense with increasing Ti content. An additional band at 330 nm for higher Ti contents is attributed to extra-framework titanium (probably anatase), suggesting there is an upper limit for Ti displacement of Si in the SBA-15 framework[34].

Effect of Ti loading

The SAXS patterns of calcined Ti-SBA-15 with 1-10 mol% Ti loading all show intense {10} ≡ {11} and {30} ≡ {33} reflections associated with *p6mm* plane symmetry[32] indicative of well ordered mesopores (Figure 4.1A). As Ti loading increased SBA-15 was not perturbed, due to the mild synthesis conditions and extraordinarily high purity and moisture stability of the silatrane precursor. TEM of the Ti-SBA-15 (7 mol% Ti loading) directly confirmed the long range periodicity of the mesopores[2] (Figure 4.2). N_2 adsorption/desorption isotherms and pore size distribution patterns provide quantitative assessments of the porosity (Figure 4.3). All catalysts yielded a type IV isotherm (IUPAC classification), with a H1 type hysteresis loop characteristic of a large diameter mesoporous solid with narrow pore size distribution[2]. The well-defined step at a relatively high pressure of 0.5–0.7 corresponds to capillary condensation of N_2, within uniform pores (> 5 nm diameter) and surface area (up to 670 m^2/g) (Table 4.1). The BET surface area and pore size slightly decrease with increasing Ti loading. DRUV spectra of Ti-SBA-15 all show an absorption band centered at ~ 220 nm, with the intensity increasing with Ti loading (Figure 4.4A), that is attributed to charge transfer transition associated with isolated $Ti^{4+}O_4$ coordination.

However, at the 10%mol Ti loading, the 330 nm band appears from extra-framework anatase $Ti^{4+}O_6$.

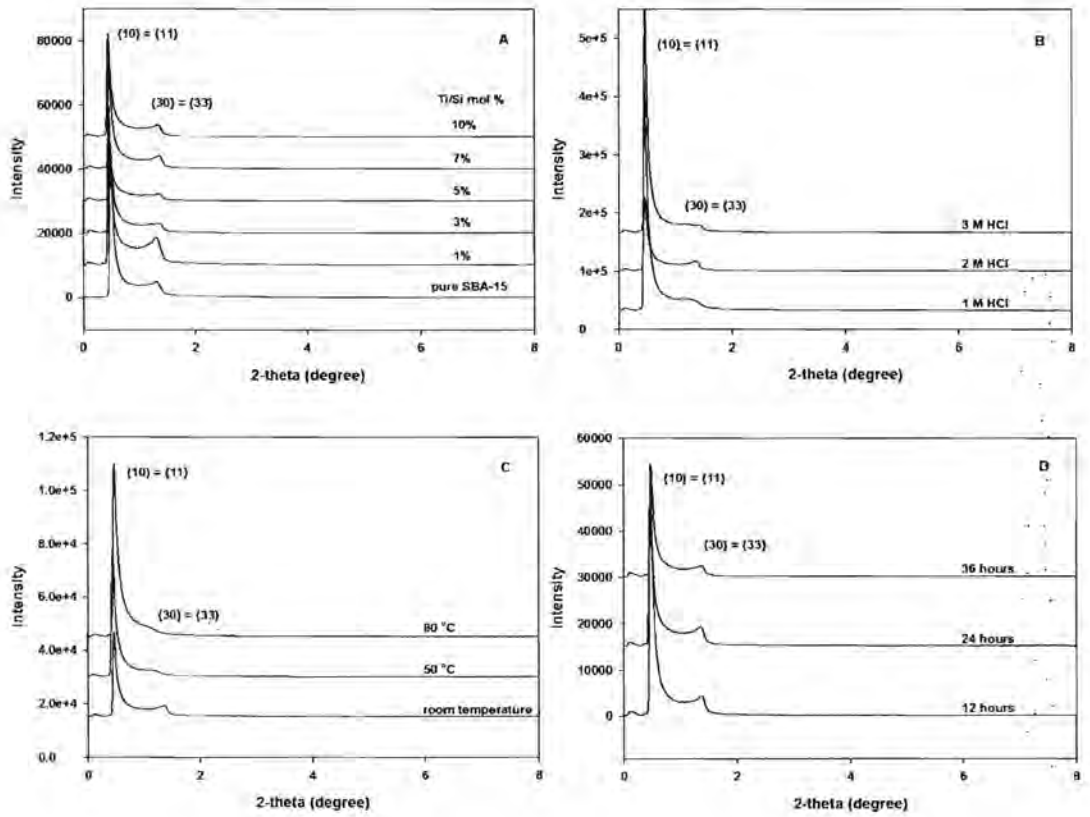

Figure 4.1 SAXS patterns of (A) pure silica SBA-15 and Ti-incorporated samples of Ti-SBA-15 containing different amount of Ti loadings; (B) Ti-SBA-15 materials prepared at different acid concentrations; (C) Ti-SBA-15 synthesized at different temperatures; (D) Ti-SBA-15 synthesized at different aging times.

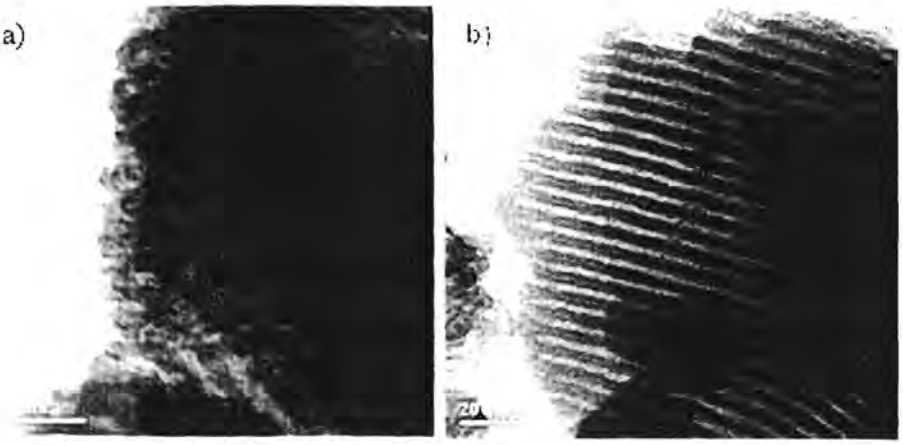

Figure 4.2 TEM images of 7 mol% Ti-SBA-15, in which a) in the direction perpendicular to the pore axis and b) in the direction parallel to the pore axis.

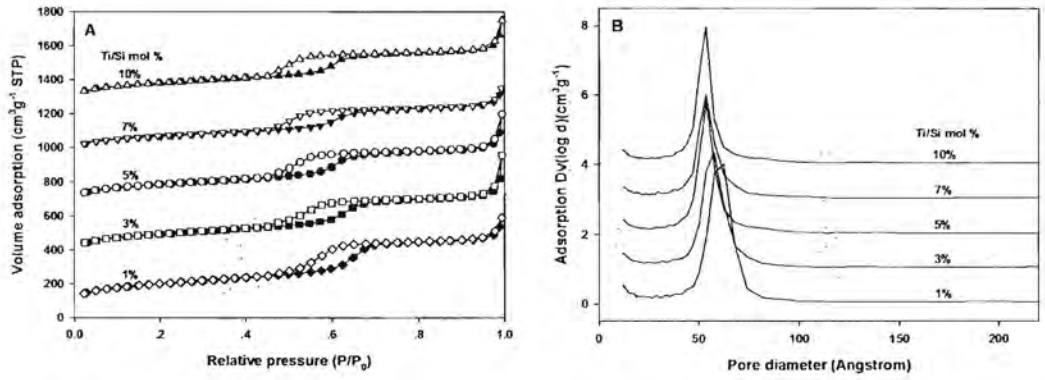

Figure 4.3 N_2 adsorption/desorption isotherms (A) and pore size distributions (B) of Ti-SBA-15 containing different amount of Ti loadings.

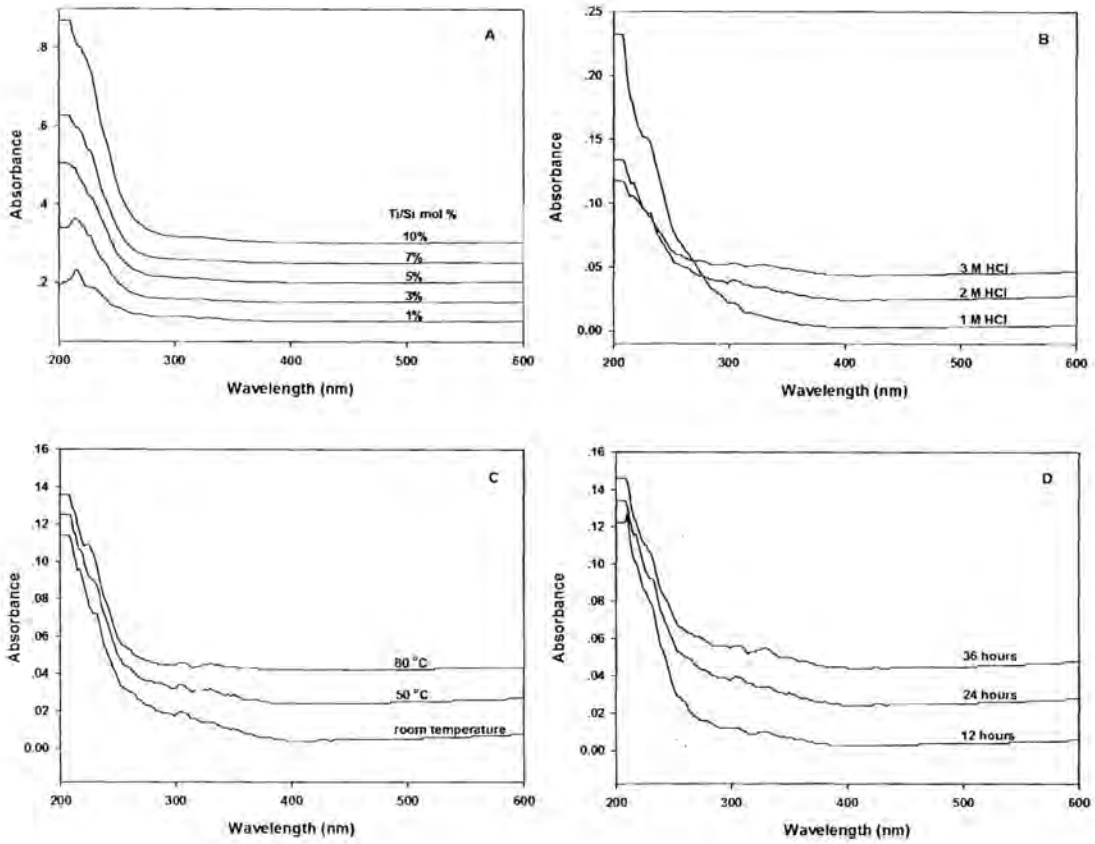

Figure 4.4 Diffuse reflectance UV-visible spectra of the synthesized Ti-SBA-15: (A) at different amounts of Ti loadings; (B) at various acid concentrations; (C) at different temperatures; and (D) at different aging times.

Table 4.1 BET and SAXS analyses of Ti-SBA-15 as a function of amount of Ti loading

Loaded Ti (%)	Surface area (m^2/g)	Pore Volume (cm^3/g)	Channel diameter (nm)	
	BET	BET	BET	SAXS
1	670	0.83	5.79	6.8
3	643	0.81	5.77	6.7
5	618	0.76	5.40	6.5
7	592	0.67	5.39	6.5
10	597	0.71	5.37	6.4

Effect of acidity

The SAXS patterns of Ti-SBA-15 materials prepared at different acidity are shown in Figure 4.1B, all exhibit a clear {10} reflection indicating uniform pore diameter, but the {30} reflection is broad when the acidity is reduced to 1M, suggesting that interpore order correlation is limited. Additionally, DRUV showed strong absorption at 220 nm for the 1M HCl sample as direct evidence for Ti^{4+} incorporated into the mesoporous silica framework (Figure 4.4B). It can be concluded that lower acidity favored framework incorporation of Ti which disrupts long range order in SBA-15 in agreement with Vinu *et al.*[12], who reported that lowering the acidity decreases the hydrolysis rate of the titanium precursors to match that of silica precursors. This may enhance the interaction between the Ti-OH and Si-OH species in the gel resulting in more complete Ti incorporation. At the highest acid concentration (3M HCl), DRUV yielded weak absorption at 220 nm, due to the ready dissociation of Ti-O-Si bonds[13]. While a change in acid concentration does not notably affect the surface area, pore volume and pore size (Table 4.2), the use of 2 M HCl is considered optimal because it maintained the well ordered structure of the mesopores and showed high Ti incorporation.

Table 4.2 BET and SAXS analyses of Ti-SBA-15 as a function of acidity

Acidity (M)	Surface area (m^2/g)	Pore Volume (cm^3/g)	Channel diameter (nm)	
	BET	BET	BET	SAXS
1 M	582	0.78	5.63	-
2 M	597	0.71	5.37	6.4
3 M	606	0.74	5.38	6.2

Effect of temperature

Temperature affects liquid crystal formation[30] (Table 4.3). In the present case, increasing the reaction temperature from ambient to 80 °C for Ti-SBA-15 catalyst (10mol% Ti loading/2M HCl/24 h) showed {10} periodicity remained intact while

{30} was absent (Figure 4.1C). BET confirmed the increase in pore size with reaction temperature (Table 4.3), while DRUV showed that at 80 °C, $Ti^{4+}O_6$ disappeared because the Ti^{4+} species preferentially displaced Si^{4+} in the framework of SBA-15 (Figure 4.4C). However, 2D order was compromised at the higher temperature, and therefore room temperature proved most suitable for the synthesis of Ti-SBA-15. Zhao *et al.*[2] reported that higher temperatures resulted in larger pore sizes possibly due to the PEO blocks becoming more hydrophobic that increased hydrophobic domain volumes, and lead to wider channels with accelerated Ti^{4+} incorporation into the SBA-15 framework but simultaneously limited long range order.

Table 4.3 BET and SAXS analyses of Ti-SBA-15 as a function of temperature

Temperature (°C)	Surface area (m^2/g)	Pore Volume (cm^3/g)	Channel diameter (nm)	
	BET	BET	BET	SAXS
RT	597	0.71	5.37	6.4
50	596	0.72	5.68	-
80	626	0.95	6.60	-

Effect of aging time

Aging time is an important parameter because in alkoxide-derived gels, the condensation reaction between surface functional groups continues beyond the gel point. During aging, there are changes in the textural and physical properties of the gel, and from 12 to 36 h (10mol% Ti loading/2 M HCl / RT) SAXS revealed that whilst the narrow {10} reflection is preserved, the {30} reflection broadens with aging time due to disruption of long-range hexagonal periodicity[30] (Figure 4.1D). DRUV spectra indicate that with longer aging extra framework anatase $Ti^{4+}O_6$ appears (Figure 4.4D), while N_2 adsorption isotherms found the surface area, pore volume and pore size all decreased (Table 4.4). It is believed that long reaction times, beyond equilibrium, cause the condensation reaction to reverse, resulting in mesopore deterioration[35].

Table 4.4 BET and SAXS analyses of Ti-SBA-15 as a function of aging time

Time (h)	Surface area (m^2/g)	Pore Volume (cm^3/g)	Channel diameter (nm)	
	BET	BET	BET	SAXS
12	637	0.79	5.68	6.4
24	597	0.71	5.37	6.4
36	609	0.71	5.39	-

Catalytic activity of Ti-SBA-15 towards styrene epoxidation

Styrene oxide and benzaldehyde were the principle products of styrene epoxidation with H_2O_2 over Ti-SBA-15. All titanium loaded catalysts demonstrated considerably higher styrene conversion than pure SBA-15 (Table 4.5). Raising the Ti content to 7 mol% increased the conversion of styrene remarkably (from 2.9% to 25.8%) with the selectivities for styrene oxide and benzaldehyde of 34.2% and 65.8%, respectively. Additionally, Ti-SBA-15 prepared by the sol-gel synthesis showed significantly higher conversion of styrene (25.8%) than an equivalent catalyst (in terms of Ti content) synthesized by the impregnation method (11.9%). When Ti content exceeds 7 mol% conversion efficiency decreases (from 25.8% to 12.4%), in agreement with DRUV that found the $Ti^{4+}O_4$ content was maximized in this catalyst beyond which $Ti^{4+}O_6$ extra-framework titanium appears as anatase which is less active. Combined with the diffraction and microscopy results, it is confirmed that Ti^{4+} incorporated within the SBA-15 framework is most active. This conclusion is consistent with Zhang *et al.*[14] and Ji *et al.*[36], who reported that the titanium species in the SBA-15 framework are the active sites for styrene oxidation reaction. Moreover, the selectivity of styrene oxide decreased while selectivity of benzaldehyde increased with titanium loading consistent with the study of Yu *et al.*[37] who reported that an increase of the Ti content in the mesoporous catalysts decreases epoxide selectivity and H_2O_2 efficiency due to a decrease of isolated Ti atoms in the SBA-framework.

Table 4.5 Comparison of catalysts for epoxidation of styrene			
Catalyst (%)	**Styrene conversion (%)**	**Selectivity (%)**	
		Styrene oxide	**Benzaldehyde**
0% Ti (sol-gel)	2.9	46.6	53.4
3% Ti (sol-gel)	14.4	42.1	57.9
5% Ti (sol-gel)	13.9	36.8	63.2
7% Ti (sol-gel)	25.8	34.2	65.8
10% Ti (sol-gel)	12.4	30.1	69.9
7% Ti (impreg.)	11.9	45.7	54.3
10% Ti (impreg.)	10.2	29.2	70.8

Figure 4.5A shows that over 7 mol% Ti-SBA-15 styrene conversion increases with time whereas selectivity decreases, which may attributed to the secondary oxidation of styrene oxide[33]. The reaction is initially rapid due to the abundance of H_2O_2[36], reaches a maximum after 4 h, then remains constant for up to 6 h. The conversion of styrene slightly increased by raising the temperature from 70 to 90 °C (Figure 4.5B) consistent with the study of Laha *et al.*[38], but the selectivity of Ti-SBA-15 toward styrene oxide was highest at 80 °C. The selectivity of benzaldehyde also increased with increasing the reaction temperature, meaning that the higher temperature favors further oxidation of styrene oxide[11]. The effect of catalyst concentration is shown in Figure 4.5C, with styrene conversion increasing from 11.2% to 25.8% as the mass of catalyst was adjusted from 0.05 g to 0.10 g, beyond which the rate was essentially constant. The initial improvement in performance with catalyst loading is due to an increase of active Ti sites in the system that facilitates styrene conversion[38].

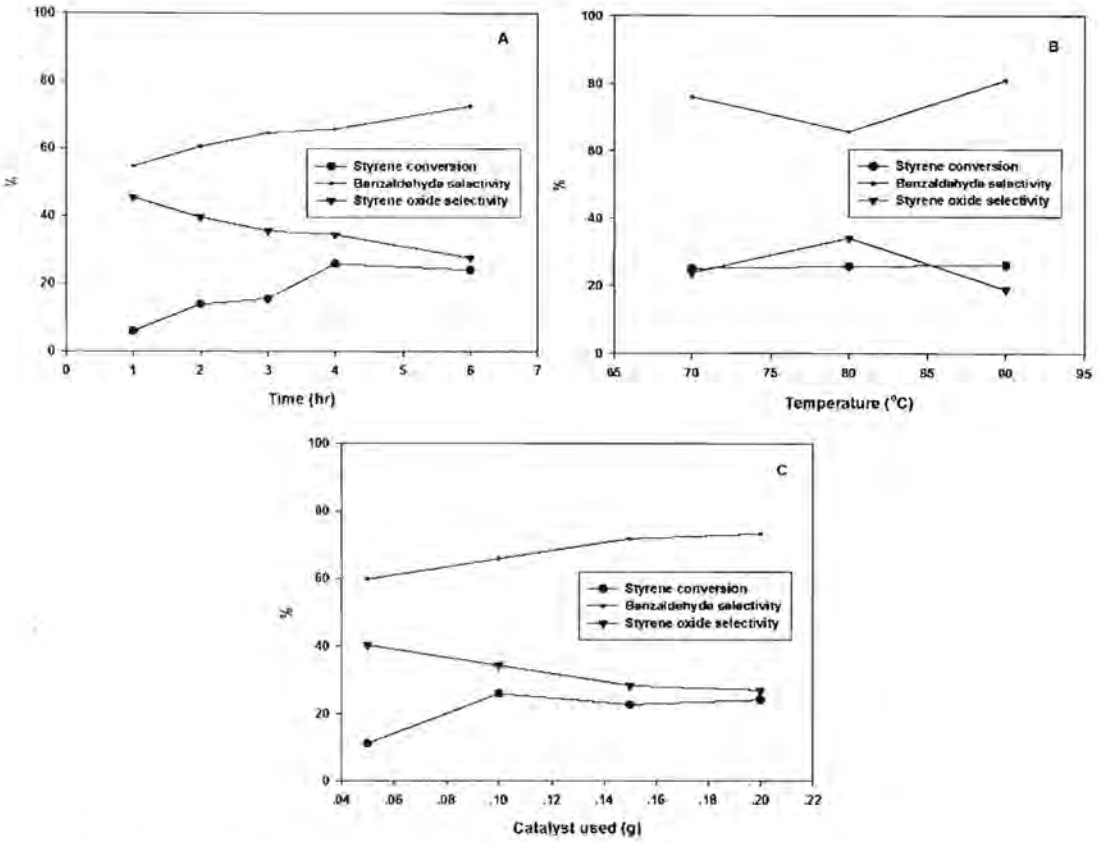

Figure 4.5 (A) Effect of reaction time on the styrene oxidation using 0.1 g of catalyst, containing 7.0 mol% titanium content, at 80 °C; (B) Effect of reaction temperature on the styrene oxidation using 0.1 g of catalyst, containing 7 mol% titanium content, for 4 h; (D) Effect of amount of catalyst, containing 7.0 mol% titanium content, at 80 °C for 4 h.

Conclusions

Ti-SBA-15 was successfully synthesized via a sol-gel process using silatrane as the silica precursor, titanium glycolate as a titanium source, and nonionic triblock copolymer as a template. The method is straightforward and can be conducted at room temperature without the need for hydrothermal treatment as conventionally required. Systematic variations of acidity, aging temperature, aging time, and Ti loading lead to an optimized Ti-SBA-15 product. Crystallochemical incorporation of titanium by $Ti^{4+}O_4$ substitution for $Si^{4+}O_4$ in the mesopores proves superior to impregnation or

decoration with anatase ($Ti^{4+}O_6$). Tetrahedral Ti^{4+} coordination is maintained to a loading of 7 mol% titanium. Ti-SBA-15 materials show relatively high activity in the epoxidation reaction of styrene monomers due to the presence of $Ti^{4+}O_4$ in the SBA-15 framework. For the optimized catalyst (7 mol% Ti loading/2 M HCl/24 h/RT), the epoxidation reaction of styrene was most effective at 80 °C/4 h, using 0.05 g catalyst with the only products being styrene oxide and benzaldehyde. The selectivity of styrene oxide and benzaldehyde reached 34.2% and 65.8% at a styrene conversion of 25.8%. This research demonstrates that Ti-SBA-15 heterocatalyst can be synthesized by a low cost and energy efficient process that will allow scale-up for possible industrially application.

Acknowledgements

This research work is financially supported by the Postgraduate Education and Research Program in Petroleum and Petrochemical Technology (ADB) Fund (Thailand), the Ratchadapisake Sompote Fund, Chulalongkorn University, and the Thailand Research Fund (TRF). The SAXS patterns were collected by Mr. An Tao and Ms. Li Henan at the School of Materials Science and Engineering, Nanyang Technological University.

References

1. Zhao, D.; Feng, J.; Huo, Q.; Melosh, N.; Frerickson, G. H.; Chmelka, B. F.; Stucky, G. D. *Science* **1998**, *279*, 548-552.
2. Zhao, D.; Huo, Q.; Feng, J.; Chmelka, B. F.; Stucky, G. D. *J. Am. Chem. Soc.* **1998**, *120*, 6024-6036.
3. Sayari, A. *Chem Mater.* **1996**, *8*, 1840.
4. Corma, A. *Chem. Rev.* **1997**, *97*, 2373.
5. Soler-Illia Galo, J. De A.A.; Sanchez, C.; Lebeau, B.; Patarin, J. *Chem. Rev.* **2002**, *102*, 4093.

6. Taguchi, A.; Schuth, F. *Micropor. Mesopor. Mater.* **2005**, *77*, 1.
7. He, N.; Bao, S.; Xu, Q. *Appl. Catal.: A* **1998**, *169*, 29.
8. Corma, A.; Fornes V.; Navarro, M.T.; Perez-Pariente, J. *J. Catal.* **1994**,*148*, 569.
9. Vinu, A.; Murugesan, V.; Bohlmann, W.; Hartmann, M. *J. Phys. Chem. B* **2004,** *108,* 11496.
10. Vinu, A.; Murugesan, V.; Tangermann, O.; Hartmann, M. *Chem. Mater.* **2004**, *16*, 3056.
11. Wu, P.; Tatsumi, T. *Chem. Mater.* **2002**, *14*, 1657-1664.
12. Vinu, A.; Srinivasu, P.; Miyahara, M.; Ariga, K. *J. Phys. Chem. B* **2006**, *110*, 801-806.
13. Chen, Y.; Huang, Y.; Xiu, J.; Han, X.; Bao, X. *Appl. Catal. A: Gen.* **2004**, *273*, 185.
14. Zhang, W. H.; Lu, J.; Han, B.; Li, M.; Xiu, J.; Ying, P.; Li, C. *Chem. Mater.* **2002**, *14*, 3413.
15. Wu, S.; Han, Y.; Zou, Y. C.; Song, J. W.; Zhao, L.; Di, Y.; Liu, S. Z.; Xiao, F. S. *Chem. Mater.* **2004**, *16*, 486.
16. Newalkar, B. L.; Olanrewaju, J.; Komarneni, S. *Chem. Mater.* **2001**, *13*, 552.
17. Berube, F.; Kleitz, F.; Kaliaguine, S. *J. Phys. Chem. C* **2008**, *112*, 14403.
18. Berube, F.; Kleitz, F.; Kaliaguine, S. *J. Mater. Sci.* **2009**, *44*, 6727.
19. Luan, Z. H.; Hartmann, M.; Zhao, D. Y.; Zhou, W. Z.; Kevan, L. *Chem. Mater.* **1999**, *11*, 1621.
20. Luan, Z. H.; Bae. J. Y.; Kevan, L. *Chem. Mater.* **2000**, *12*, 3202.
21. Morey, M. S.; O'Brien, S.; Schwarz, S.; Stucky, G. D. *Chem. Mater.* **2000**, *12*, 898.
22. Yue, Y. H.; Gedeon, A.; Bonardet, J. L.; Melosh, N.; D'Espinose, J. B.; Fraissard, J. *Chem. Commun.* **1999**, 1967.
23. Murugavel, R.; Roesky, H. W. *Angew. Chem., Int. Ed. Engl.* **1997**, *36*, 477.
24. Phonthammachai, N.; Chairassameewong, T.; Gulari, E.; Jamieson, A.M.; Wongkasemjit, S. *Met. Mater. Min.* **2002**, *12*, 23-28.
25. Phiriyawirut, P.; Magaraphan, R.; Jamieson, A. M.; Wongkasemjit, S. *Material Science and Engineering A* **2003**, *361*, 147-154.

26. Charoenpinijkarn, W.; Suwankruhasn, M.; Kesapabutr, B.; Wongkasemjit, S.; Jamieson, A. M. *European Polymer Journal* **2001**, *37*, 1441-1448.
27. Phonthammachai, N.; Chairassameewong, T.; Gulari, E.; Jemieson, A.M.; Wongksemjit, S. *Microporous and Mesoporous Material* **2003**, *66*, 261-271.
28. TanglumLert, W.; Imae, T.; White, T. J.; Wongkasemjit, S. *Materials Letters* **2008**, *62*, 4545-4548.
29. Sathupanya, M.; Gulari, E.; Wongkasemjit, S. *J. Eur. Ceram. Soc.* **2003**, *23*, 2305–2314.
30. Phiriyawirut, P.; Jamieson, A. M.; Wongkasemjit, S. *Microporous Mesoporous Mater.* **2005**, *77*, 203–213.
31. Thanabodeekij, N.; Sadthayanon, S.; Gulari, E.; Wongkasemjit, S. *Mater. Chem. Phys.* **2006**, *98*, 131–137.
32. Samran, B.; White, T.J.; Wongkasemjit, S. *Journal of Porous Materials* **2010** DOI. 10.1007/s10934-010-9367-3
33. TanglumLert, W.; Imae, T.; White, T. J.; Wongkasemjit, S. *Cat. Comm.* **2009**, *10*, 1070-1073.
34. Wang, Y.; Zhang, Q.; Shishido, T.; Takehira, K. *J. Catal.* **2002**, *209*,186-196.
35. Yilmaz, VT.; Topcu, Y.; Karadag A. *Thermchimica Acta* **2002**, *383*, 129-133.
36. Ji, D.; Zhao, R.; Lv, G.; Qian, G.; Yan, L.; Suo, J. *Applied Catalysis A : General* **2005**, *281*, 39-45
37. Yu, J.; Feng, Z.; Xu, L.; Li, M.; Xin, Q.; Liu, Z.; Li, C. *Chem. Mater.* **2001**, *13*, 994.
38. Laha, S.C.; Kumar, R. *J. of catal.* **2001**, *204*, 64-70.

CHAPTER V

ROOM TEMPERATURE SYNTHESIS OF Mo-SBA-15 VIA SOL-GEL PROCESS AND ITS CATALYTIC ACTIVITY IN STYRENE OXIDATION

Abstract

A series of molybdenum-substituted mesoporous SBA-15 (Mo-SBA-15) silicas with various Mo/Si mole ratios were synthesized at room temperature by a sol-gel process from moisture stable silatrane and molybdenum glycolate as metal sources, and a non-ionic triblock copolymer ($EO_{20}PO_{70}EO_{20}$) as a template. Small angle X-ray scattering (SAXS), transmission electron microscopy (TEM) and field emission scanning electron microscopy (FESEM) revealed a highly ordered *p6mm* hexagonal mesoporous structure. Diffuse reflectance UV-visible spectroscopy (DRUV) indicated that the incorporation of Mo^{6+} into the SBA-15 framework was optimal at 1.0 mol% molybdenum, beyond which extra-framework MoO_3 forms. N_2 adsorption/desorption measurements showed high surface areas (up to 729 m^2/g), with large pore diameters (6.8 nm) and volumes (1.04 cm^3/g). Mo-SBA-15 showed high catalytic activity for the epoxidation of styrene monomer with hydrogen peroxide (H_2O_2). The products of this reaction were styrene oxide and benzaldehyde.

Introduction

Since researchers from the Mobil Research and Development Corporation reported the M41S family of mesoporous silicas[1-2], much effort has been devoted to simplify the synthesis and expand to application of mesoporous molecular sieves. In particular, SBA-15 prepared using a non-ionic triblock copolymer as template is of interest due to its narrow pore size distribution[3] that leads to uniform hexagonal arrangement of channels (5–30 nm). A large internal surface area (600–1000 m^2/g) creates a large number of dispersed catalytically active centers, while the thick framework walls (~3–7 nm) possess a hydrothermal stability exceeding that of thinner-

walled MCM-41 materials[1-3]. However, pure silica SBA-15 is poorly catalytic due to the lack of lattice defect, limited redox properties, basicity and acidity. These limitations can be overcome by introducing guest species into the SBA-15 framework to improve the catalytic activity[4].

Zhao *et al.*[3] synthesized SBA-15 directly in acidic conditions from tetraethylorthosilicate (TEOS) and $EO_{20}PO_{70}EO_{20}$ as a template by hydrothermal treatment (100 °C/48 h). Recently, Samran et al.[5] reported the room temperature sol-gel synthesis of SBA-15 using a silatrane precursor, and $EO_{20}PO_{70}EO_{20}$ as the structure directing agent. In both the direct method and sol-gel process, SBA-15 formed via $(S^0H^+)(X^-I^+)$ entities where S, X and I are the non-ionic surfactant, halide anion and protonated Si-OH, respectively[3,6].

Among various metal dopants, molybdenum-bearing catalysts show high activity for many reactions, such as propene metathesis[7-8], propene oxidation[9-11] and methanol oxidation[12]. The most widely used methods for preparing Mo-SBA-15 are post-synthesis impregnation[13] and direct synthesis[14]. For example, Mo-SBA-15 was prepared hydrothermally (100 °C/24 h) by Melero *et al.*[15] using tetraethylorthosilicate (TEOS) and ammonium molybdate tetrahydrate ($(NH_4)_6(Mo_7O_{24}).4H_2O$) as the silica and molybdenum sources. In this paper, we report a simple and effective sol-gel route to directly incorporate molybdenum into the SBA-15 framework from moisture stable silatrane and molybdenum glycolate precursors, the reaction proceeds at room temperature rather than hydrothermally. The incorporation of molybdenum was characterized by small angle X-ray scattering (SAXS), transmission electron microscopy (TEM), field emission scanning electron microscopy (FESEM), diffuse reflectance UV-visible spectroscopy (DRUV), and N_2 adsorption. The catalytic activity of Mo-SBA-15 towards epoxidation of styrene monomer with H_2O_2 employed as the oxidant, was studied as a function of temperature, time, catalyst loading, Mo content and styrene:H_2O_2 ratio. The performance of catalysts synthesized via impregnation and sol-gel methods was compared.

Experimental

Materials

Fumed silica (SiO_2, 99.8%) (Sigma-Aldrich, St. Louis, MO), triethanolamine (TEA) (Carlo Erba, Milan, Italy), ethylene glycol (EG) (J.T. Baker, Philipsburg, NJ), acetronitrile (Labscan, Bangkok, Thailand), molybdenum (VI) oxide (Fluka, Asia), poly(ethylene glycol)-block-poly(propylene glycol)-block-poly(ethylene glycol) ($EO_{20}PO_{70}EO_{20}$) (Sigma-Aldrich, Singapore), hydrochloric acid (HCl) (Labscan, Asia), hydrogen peroxide (H_2O_2) (Labscan, Asia), and styrene monomer (Labscan, Asia) were used without further purification.

Mo-SBA-15 sol-gel synthesis

Mo-SBA-15 was synthesized from silatrane and molybdenum glycolate as the silica and molybdenum sources, $EO_{20}PO_{70}EO_{20}$ as the structure-directing agent, and 2 M HCl was the acid catalyst. Different n_{Mo}/n_{Si} molar ratios were introduced according to the method of Samran *et al.*[5]. A solution of $EO_{20}PO_{70}EO_{20}$:HCl:silatrane:H_2O = 2:60:4.25:12 (mass ratio) was prepared by dissolving 4 g of $EO_{20}PO_{70}EO_{20}$ polymer in 80 g of 2 M HCl (part A) and 8.8 g of silatrane[16-17] in 20 g of H_2O (part B) with continuous stirring for 1 h to ensure complete dissolution. The solution of part B was then poured into part A. The required amount of molybdenum glycolate[18] was added to the homogenous solution with stirring. The resulting gel was aged at room temperature (RT) for 24 h and the product recovered by filtration, washed with deionized water, and dried at ambient overnight. This resin was calcined (550 °C/air/6 h) in a tube furnace (Carbolite, CFS 1200, Hope Valley, U.K.) at a heating rate of 0.5 °C/min to remove residual organics. The catalysts were designated as *(x)* mol% Mo-SBA-15 where *x* denotes the n_{Mo}/n_{Si} percentage used during synthesis. Molybdenum-free SBA-15 was synthesized using the same procedure ($EO_{20}PO_{70}EO_{20}$:HCl:silatrane:H_2O = 2:60:4.25:12) in the absence of molybdenum glycolate.

Impregnation synthesis

The incipient wetness impregnation method was used to deposit molybdenum on the SBA-15 support, using 1.0 and 1.25 mol% molybdenum glycolate. The precursor was dissolved in water and dropped onto the catalyst supports. Drying (100 °C/12 h) was followed by calcination (550 °C/6 h) at a heating rate of 0.5 °C/min.

Characterization

The products were characterized by powder X-ray diffraction (XRD) with a PANalytical PW3830 instrument using CuKα (λ_{av} = 0.154 nm) radiation generated at 50kV and 40 mA, over the 2θ range 0.5–10°, step size of 0.01° and dwell time of 10 seconds per step. Transmission electron microscopy (TEM) was conducted using a Hitachi H-7100FA machine operating at 125 kV with a large objective aperture. Field emission scanning electron microscopy (FESEM) was used to collect secondary electron images from powders mounted on double-sided carbon tape using a Zeiss Ultra plus, operating at 0.3–0.5 kV to minimize charging. Nitrogen adsoption and desorption isotherms were measured at -196 °C after outgassing at 250 °C for 12 h under vacuum (Quantasorb JR, Mount Holly, NJ) to determine the Brunauer–Emmett–Teller (BET) specific surface area. The pore size distributions were obtained from the adsorption and desorption branches of the nitrogen isotherms by the Barrett-Joyner-Halenda method. Diffuse reflectance UV-visible (DRUV) spectroscopic measurements were recorded on a Shimadzu UV-2550 spectrophotometer fitted with an ISR-2200 integrating sphere attachment and recorded from 190–600 nm and using $BaSO_4$ as a reference.

Catalytic activity

The epoxidation of styrene was measured from data collected in a batch reactor. The catalyst (0.05–0.20 g), styrene (5 mmol), hydrogen peroxide (2.5–10 mmol of 30 wt% aqueous solution) and acetronitrile (5 mL) were introduced to a glass flask with closed cap (30 mL). The reactant mixture was stirred and heated for a fixed

time (6–48 h) and temperature (60–80 °C) in an oil bath. The products were identified and quantified by gas chomatography (GC) employing a capillary column (DB-Wax, 30 m x 0.25 mm) and flame ionization detector (FID). The conversion of styrene was calculated based upon the quantity of styrene monomer consumed.

Results and Discussion

Mesostructure and Crystal Chemistry

Pure SBA-15 and Mo-SBA-15 (0.25–1.25 mol% Mo) synthesized via sol-gel processing and calcined at 550°C gave the SAXS patterns shown in Figure 5.1. In all cases the two well-resolved scattering maxima at 2θ of 0.45° and 1.35° could be indexed to the {10} ≡ {11} and {30} ≡ {33} reflections, respectively. These scattering peaks are characteristic of *p6mm* symmetry and similar to pure silica SBA-15[5]. This hexagonal motif was observed for all Mo-SBA-15 materials indicating that mesopore order was sustained after the introduction of molybdenum into the framework, due to the mild synthesis conditions employed and the extraordinarily high purity and moisture resistance of the silatrane precursor. The d-spacing (d_{10}) and the hexagonal translational parameter (a_0), increased significantly at 1.0 mol% Mo (Table 5.1). This may arise because the Mo-O bond length in either tetrahedral or octahedral coordination is longer than Si-O[19], indicative of Mo substitution, the increase in d_{10} and a_0 compared to the pure SBA-15 could confirm the incorporation of molybdenum species into the framework of SBA-15. As d_{10} and a_0 decrease for Mo content > 1.0 mol% an upper limit for framework incorporation is supposed under these synthetic conditions. The shift of d-spacings to smaller angles with increasing in Mo loading is analogous to other metal-substituted mesoporous materials[20]. Transmission electron micrograph (Figure 5.2) showed well aligned channel, confirming the long range ordered hexagonal structure of the synthesized materials.

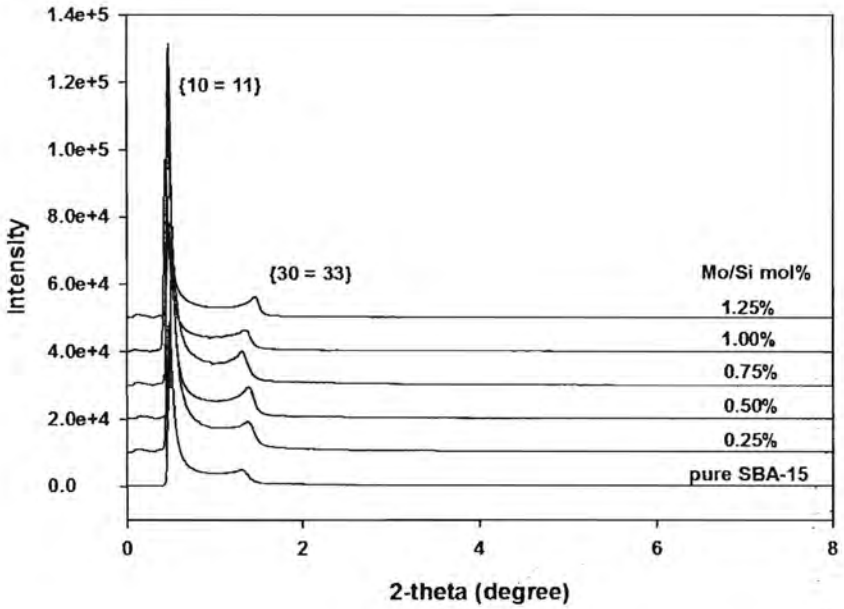

Figure 5.1 SAXS patterns of pure silica SBA-15 and Mo-SBA-15 containing different Mo loadings

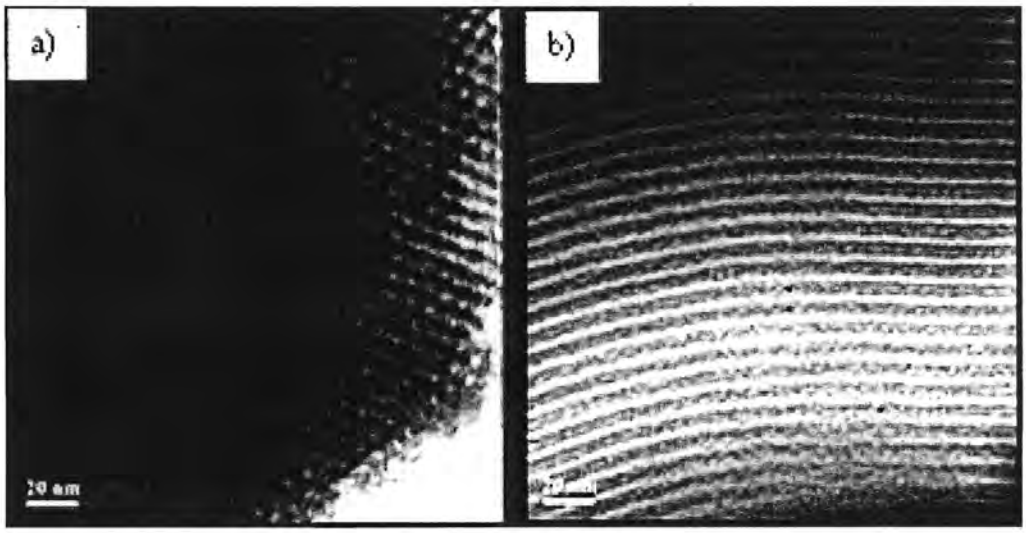

Figure 5.2 TEM images of Mo-SBA-15 containing 1.0 mol% Mo (A) in the direction perpendicular to the pore axis and (B) in the direction parallel to the pore axis

Table 5.1 Physical and crystallographic properties of Mo-SBA-15 samples as a function of Mo loading

Sample	Physical properties				Crystallographic properties	
Loaded Mo (mol%)	Surface area (m^2/g)	Pore volume (cm^3/g)	Channel diameter (nm)		d_{10}(nm)	a_0(nm)
	BET	BET	BET	SAXS	SAXS	SAXS
Pure SBA-15	570	0.72	5.03	6.0-6.3	18.2	21.0
0.25	607	0.77	5.38	6.2-6.5	18.6	21.5
0.50	687	0.81	5.77	6.1-6.4	17.1	19.7
0.75	729	1.04	6.76	6.5-6.8	18.6	21.5
1.00	708	0.76	5.38	6.3-6.6	20.7	23.9
1.25	409	0.47	4.62	5.8-6.1	18.6	21.5

Diffuse reflectance UV-vis (DRUV) spectrometry was used to extract coordination sphere and bonding information for calcined Mo-SBA-15 (0.25–1.25 mol% Mo) with all materials showing strong adsorption from 220–250 nm and at 290 nm (Figure 5.3). According to Cotton *et al.*[21], these bands are expected for ligand-metal charge transfer in oxomolybdates (O^{2-}-Mo^{6+}) with the position of the electronic transitions depending on ligand field symmetry surrounding the Mo center; tetrahedral Mo^{6+} (T_d) will show a higher energy transition than octahedral (O_h)[22]. Therefore, the 220–250 nm absorption is attributed to isolated tetrahedral Mo^{6+} species of mono- and dioxo molybdenum species, indicating that the MoO^{4-} species incorporated into the framework via Mo-O-Si bridge, due to the transition of an oxygen $2p\pi$ electron into the empty d-orbital of the molybdenum, consistent with Jezlorowski *et al.*[23]. The band at 290 nm refers to the electronic transitions of Mo-O-Mo bonds from molybdenum oligomer species[15]. The absorption tail at ~340–400 nm in the 1.25 mol% Mo sample

suggests extra-framework trioxide MoO_3, that contains octahedral Mo^{6+} species (O_h ($t_{2u}, t_{1g} \rightarrow t_{2g}$))[24-25]. These results provide further confirmation that the upper limit of framework molybdenum incorporation in SBA-15 is < 1.0 mol%.

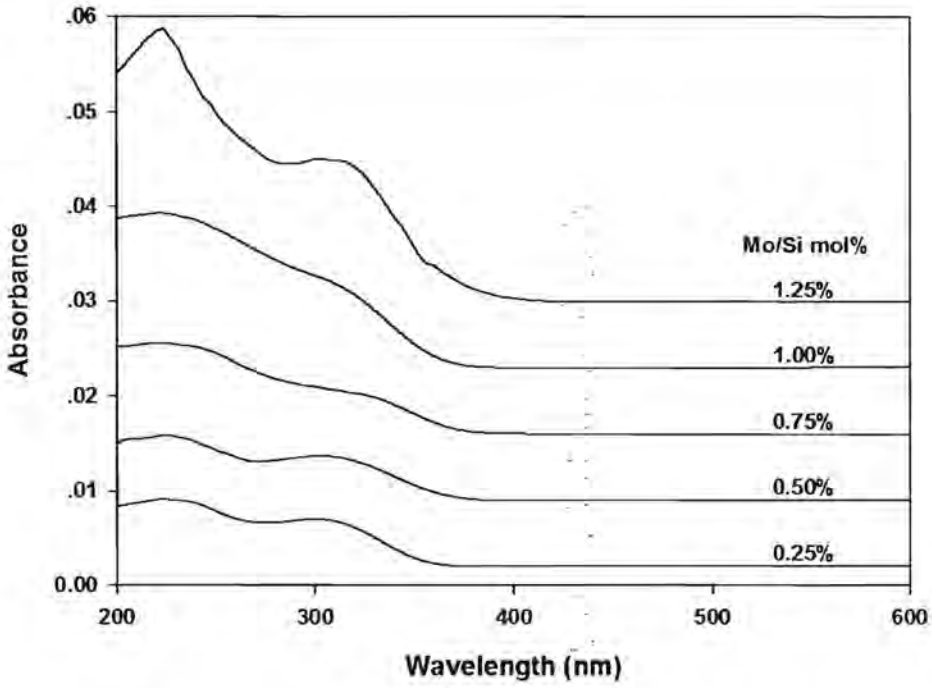

Figure 5.3 Diffuse reflectance UV-visible spectra of Mo-SBA-15

N_2 adsorption/desorption isotherms; all sample yield type IV isotherms (IUPAC classification) and exhibit broad H1 type hysteresis loops, typical of large-pore mesoporous solids. The corresponding pore size distribution curves derived from the desorption branch of the calcined Mo-SBA-15 are presented in Figure 5.4. The well-defined step at a relatively high pressure of 0.5–0.7 corresponds to capillary condensation of N_2 within uniform pores (> 5 nm diameter) and high surface area (up to 729 m^2/g) (Table 5.1). The synthesized Mo-SBA-15 catalysts exhibited large surface areas (607–729 m^2/g) and pore volumes (0.72–1.04 cm^3/g). However, the incorporation of molybdenum into the framework of SBA-15 to high molybdenum loadings (1.25 mol% Mo) has significant effect on the BET, pore volume, pore diameter and especially so for surface area, and could indicate the formation of extra-framework MoO_3 within the pores as suggested by DRUV.

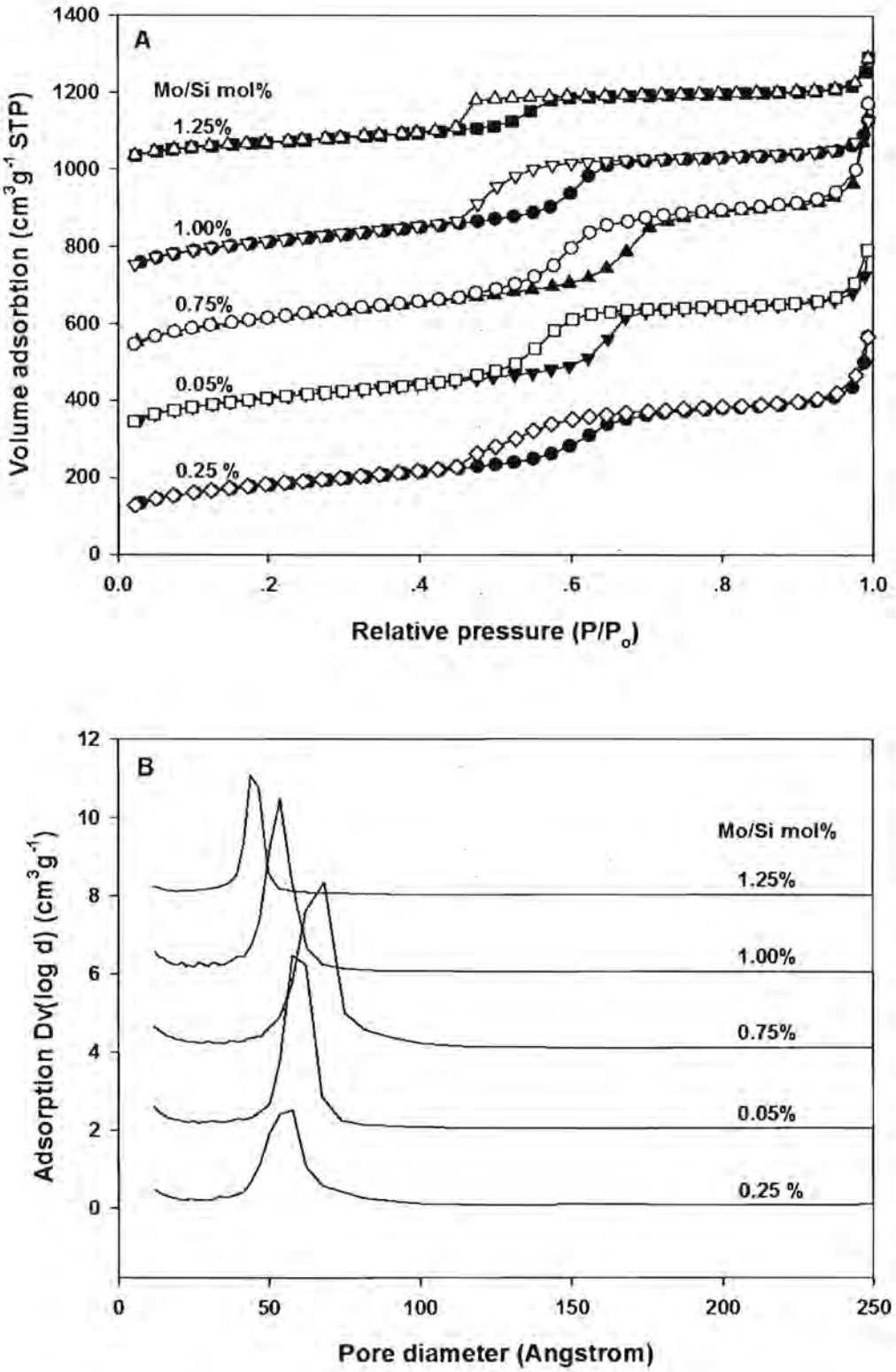

Figure 5.4 N_2 adsorption/desorption isotherms (A) and pore size distributions (B) of Mo-SBA-1

Catalytic activity study of Mo-SBA-15

Catalytic activity towards epoxidation of styrene using H_2O_2 as an oxidant was tested in a batch-type reactor. At the end of the reaction the catalyst was separated by filtration and the products analyzed by gas chomatography (Table 5.2). A blank reaction performed over pure SBA-15 under identical conditions showed no catalytic activity. Hydrogen peroxide alone was also unable to oxidize styrene in the absence of mesoporous silica, whereas all Mo-SBA-15 samples were efficient catalysts. Styrene conversion increased with molybdenum content up to 1.0 mol% to a maximum of 6.3% with the selectivities for benzaldehyde and styrene oxide 70.9% and 29.1%, respectively. However, at 1.25 mol% Mo loading, conversion efficiency and selectivity of styrene oxide significantly decreased, consistent with extra-framework MoO_3 causing channel blockage that restricts the diffusion of styrene to the tetrahedral molybdenum framework species where oxidation is likely to take place[19].

Table 5.2 Epoxidation of styrene monomer with H_2O_2 over Mo-SBA-15 as a function of Mo loading

Loaded Mo (mol %)	Styrene conversion (%)	Selectivity (%)	
		Benzaldehyde	Styrene oxide
Styrene and H_2O_2*	-	-	-
Pure SBA-15	-	-	-
0.25% Mo	5.7	75.1	24.9
0.50% Mo	5.5	65.2	34.8
0.75% Mo	5.8	77.6	27.6
1.00% Mo	6.3	70.9	29.1
1.25% Mo	4.4	81.0	19.0
1.00% Mo (impreg.)	4.7	77.9	22.1
1.25% Mo (impreg.)	4.2	80.9	19.1

*The reaction was conducted in the absence of mesoporous silica.

Reaction condition: catalyst 0.05 g/70 °C/24 h/styrene:H_2O_2 = 1:1

To provide a baseline for comparison, molybdenum was impregnated onto the SBA-15 framework and its catalytic activity studied. The impregnated material containing 1.0 mol% Mo showed lower styrene conversion (4.7%) than the equivalent catalyst obtained from sol-gel processing (6.3%); the poor dispersion and mesopore plugs of metal oxides appear responsible for the relatively poor catalytic activity of the former[26]. Additionally, the impregnated samples deliver lower styrene oxide selectivity (22.1%) than the catalyst prepared via sol-gel process (29.1%). This result agrees with Rana *et al.*[27] who reported that Mo-MCM-41 synthesized hydrothermally showed a higher activity for the oxidation of cyclohexane and gave a more stable cyclohexanol product, in comparison to the impregnated catalyst. This was attributed to the tetrahedral coordination of active molybdenum in the silica framework. The effect of reaction time was investigated in thee stages from 6 to 48 h (Table 5.3) and showed that at 48 h, styrene conversion increases significantly to 22.6% while styrene oxide selectivity substantially decreases to 7.5% with a corresponding increase in benzaldehyde selectivity of 92.5%. Benzaldehyde is produced during nucleophilic attack of styrene oxide by H_2O_2 followed by cleavage of the intermediate hydroxyl-hydroperoxistyrene[28]. As temperature increased from 60° to 80 °C, styrene conversion was enhanced to 42.1% at 80 °C (Table 5.4), but selectivity of benzaldehyde increased at the cost of the styrene oxide, indicating that benzaldehyde forms mainly via further oxidation of styrene oxide, and that the higher temperature favors the oxidation of styrene oxide [19]. In contrast, the product obtained from the reaction temperature of 60 °C was only benzaldehyde which could be formed from a radical mechanism though direct oxidative cleavage of the styrene side chain double bond[28]. The styrene conversion was greatly enhanced (9.1%) when the mole ratios of styrene: H_2O_2 are 1:1.5 (Table 5.5). With increasing styrene/H_2O_2 mole ratio, styrene conversion increased considerably due to improved H_2O_2 utilization, beyond which, no further was observed. The effect of catalyst loading in the batch reactor is shown in Table 5.6. Styrene conversion reached 6.3% when 0.05g of catalyst was used and did not significantly change when compared with 0.10g and 0.15g. The maximum styrene oxide selectivity (39.9%) with reasonable styrene conversion (7.7%) was observed at 0.10g catalyst. Hence, the optimum catalyst used was 0.10g.

Table 5.3 Epoxidation of styrene monomer with H_2O_2 over Mo-SBA-15 as a function of reaction time

Time (h)	Styrene conversion (%)	Selectivity (%)	
		Benzaldehyde	Styrene oxide
6	4.2	72.3	27.7
24	6.3	70.9	29.1
48	22.6	92.5	7.5

Reaction condition: 0.05 g of 1.0 mol% Mo/styrene:H_2O_2 = 1:1

Table 5.4 Epoxidation of styrene monomer with H_2O_2 over Mo-SBA-15 as a function of reaction temperature

Temperature (°C)	Styrene conversion (%)	Selectivity (%)	
		Benzaldehyde	Styrene oxide
60	5.4	>99	-
70	6.3	70.9	29.1
80	42.1	84.5	15.5

Reaction condition: 0.05 g of 1.0 mol% Mo/styrene:H_2O_2 = 1:1

Table 5.5 Epoxidation of styrene monomer with H_2O_2 over Mo-SBA-15 as a function of styrene:H_2O_2 ratio

Ratio of styrene:H_2O_2	Styrene conversion (%)	Selectivity (%)	
		Benzaldehyde	Styrene oxide
1:0.5	7.5	72.7	27.3
1:1.0	6.3	70.9	29.1
1:1.5	9.1	72.7	27.3
1:2.0	5.5	69.1	30.8

Reaction condition: 0.05 g of 1.0 mol% Mo/70 °C/24 h

Table 5.6 Epoxidation of styrene monomer with H_2O_2 over Mo-SBA-15 as a function of catalyst used

Catalyst used (g)	Styrene conversion (%)	Selectivity (%)	
		Benzaldehyde	Styrene oxide
0.05	6.3	70.9	29.1
0.10	7.7	60.1	39.9
0.15	6.5	74.5	25.5

Reaction condition: 1.0 mol% Mo/70 °C/24 h/styrene:H_2O_2 = 1:1

Conclusions

Mo-SBA-15 was synthesized via a sol-gel process using silatrane as the silica precursor, molybdenum glycolate as the molybdenum source, and a nonionic triblock copolymer ($EO_{20}PO_{70}EO_{20}$) as template. This room temperature synthesis is simple and avoids hydrothermal treatment as conventionally required. The catalysts maintained a *p6mm* hexagonal mesostructure, high surface area (729 m^2/g), large pore diameter (6.8 nm) and volume (1.04 cm^3/g). The optimal framework molybdenum loading into SBA-15 without separation of extra-framework MoO_3 while maintaining tetrahedral coordination is 1.0 mol%. In addition, these Mo-SBA-15 materials show relatively high catalytic activity for the epoxidation of styrene monomer with hydrogen peroxide due to the presence of molybdenum species in the SBA-15 framework. The product obtained from sol-gel synthesis provides superior catalytic activity compared to the impregnation method. The optimal condition for epoxidation of styrene over Mo-SBA-15 is 70°C for 24 h, using 0.10 g catalyst containing 1.0 mol% Mo, and a 1:1 mol ratio of styrene:H_2O_2. The only products obtained are styrene oxide and benzaldehyde. The selectivity of styrene oxide and benzaldehyde reached 39.9% and 60.1% at a styrene conversion of 7.7%, and demonstrates that Mo-SBA-15 heterocatalyst can be synthesized by an inexpensive and energy saving process for a range of catalytic applications.

Acknowledgements

This research work is financially supported by the Postgraduate Education and Research Program in Petroleum and Petrochemical Technology (ADB) Fund (Thailand), the Ratchadapisake Sompote Fund, Chulalongkorn University, and the Thailand Research Fund (TRF). The SAXS patterns were collected by Mr. An Tao and Ms. Li Henan at the School of Materials Science and Engineering, Nanyang Technological University. Dr. Frank Brink of the Australian National University collected the secondary electron images.

References

1. Kresge, C. T.; Leonowicz, M. E.; Roth, W. J.; Vartuli, J. C.; Beck, J. S. *Nature* **1992**, *359*, 710-712.
2. Beck, J. S.; Vartuli, J. C.; Roth, W. J.; Leonowicz, M. E.; Kresge, C. T.; Schmitt, K. D.; Chu, C. T. W.; Olson, D. H.; Sheppard, E. W.; McCullen, S. B.; Higgins, J. B.; Schlenker, J. L. *J. Am. Chem. Soc.* **1992**, *114*, 10834-10843.
3. Zhao, D.; Feng, J.; Huo, Q.; Melosh, N.; Frerickson, G. H.; Chmelka, B. F.; Stucky, G. D. *Science* **1998**, *279*, 548-552.
4. Xiao, F.-S. Top. Catal. **2005**, *35*, 9.
5. Samran, B.; White, T.J.; Wongkasemjit, S. *Journal of Porous Materials* **2010** DOI. 10.1007/s10934-010-9367-3
6. Zhao, D.; Huo, Q.; Feng, J.; Chmelka, B. F.; Stucky, G. D. *J. Am. Chem. Soc.* **1998**, *120*, 6024-6036.
7. Ono, T.; Anpo, M.; Kubokawa, Y. *J. Phys. Chem.* **1986**, *90*, 4780.
8. Liu, T-C.; Forissier, M.; Coudurier, G.; Ve´drine, J.C. *J. Chem. Soc. Faraday. Trans.* **1989**, *85*, 1607.
9. Giordano, N.; Meazza, M.; Castellan, A.; Bart. J.C.J.; Ragaini, V. *J. Catal* **1977**, *50*, 342.
10. Ressler, T.; Wienold, J.; Jentoft, R.E.; Girgsdies, F. *Eur. J. Inorg. Chem.* **2003**, *2*, 301.
11. Kotov, St.V.; Balbolov, E. *J. Mol. Catal. A* **2001**, *176*, 41–48.

12. Louis, C.; Tatibouet, J.-M.; Che, M. J. Catal. **1988,** *109*, 354.
13. Yang, Q.; Cope´ret, C.; Li, C., Basset, J.M. *New. J. Chem.* **2003**, *27*, 319–323.
14. Zhang, W.; Wangt, J.; Tanev, P.T.; Pinnavaia, T. *Chem. Commun.* **1996**, *69*, 79–980.
15. Melero, J.A.; Iglesias, J.; Arsuaga, J.M.; Sainz-Pardo, J.; de Frutos, P.; Blazquez, S. *J. Applied Catalysis A : General* **2007,** *331*, 84–94.
16. Phiriyawirut, P.; Magaraphan, R.; Jamieson, A. M.; Wongkasemjit, S. *Material Science and Engineering A* **2003**, *361*, 147-154.
17. Charoenpinijkarn, W.; Suwankruhasn, M.; Kesapabutr, B.; Wongkasemjit, S.; Jamieson, A. M. *European Polymer Journal* **2001**, *37*, 1441-1448.
18. Wongkasemjit, S.; Tamuang, S.; TanglumLert, W.; Imae, T. *Materials Chemistry and Physics* **2009**, *117*, 301-306.
19. Ji, D.; Zhao, R.; Lv, G.; Qian, G.; Yan, L.; Suo, J. *Applied Catalysis A : General* **2005**, *281*, 39-45
20. Lui, C.; Chen, C.; Leu, J.; Lin, Y. *J. Sol-Gel Sci Techn* **2007**, *43*, 47-51.
21. Cotton, F.A.; Wilkinson, G. *Advance Inorganic Chemistry, 4th ed., John Wiley & Sons, New York,* **1980**.
22. Weber, R.S. *J. Catal.* **1995**, *151*, 470-474.
23. Jezlorowski, H.; Knozinger, H. *J. Phy. Chem.* **1979**, *83*, 1166-1173.
24. Higashimoto, S.; Hu, Y.; Tsumura, R.; Iino, K.; Matsuoka, M.; Yamashita, H.; Shul, Y.; Che, M.; Anpo, M. *J. Catal.* **2005**, *235*, 272-278.
25. Che, S.; Sakamoto, H.; Yoshitake, H.; Terasaki, O.; Tatsumi, T. *J. Phys. Chem. B* **2001**, *105*, 10565-10572.
26. Zhang, L.; Hua, Z.; Dong X.; Li, L.; Chen, H.; Shi, J. *Journal of molecular catalysis A: Chemical* **2007**, *268*, 155-162.
27. Rana, R.K.; Viswsabathan, B. *Catal. Lett.* **1998**, *52*, 25-29.
28. Hulea, V.; Dumitriu, E. *Applied Catalysis A : General* **2004**, *277*, 99-106.

CHAPTER VI

CONCLUSIONS AND RECOMMENDATIONS

Conclusions

The metal substituted SBA-15 mesoporous materials (Ti- and Mo-SBA-15) were successfully synthesized through the simple room temperature sol-gel process. DRUV results provide evidence that there is the upper limit of metal incorporation into SBA-15 framework. The SBA-15 framework can accommodate up to 7 mol% Ti and 1 mol% Mo without perturbing mesopore order. The catalysts maintained a *p6mm* hexagonal mesostructure, high surface areas (670–729 m^2/g), large pore diameters (5.4–6.8 nm), and volumes (0.83–1.04 cm^3/g).

Crystallochemical incorporation of Ti^{4+} and Mo^{6+} substitution for Si^{4+} in the mesopores via sol-gel process proves superior catalytic performance to post-synthesis method by incipient wet impregnation under identical reaction condition. These materials were used as a catalyst in the catalytic activity of styrene epoxidation with H_2O_2. All Ti- and Mo-SBA-15 demonstrate good activity and selectivity in this reaction. The only products obtained are styrene oxide and benzaldehyde. The selectivity of styrene oxide reached 34.2 and 39.9% at a styrene conversion of 25.8% and 7.7% for 7 mol% Ti-SBA-15 and 1 mol% Mo-SBA-15, respectively. This research demonstrates that M-SBA-15 (M = Ti and Mo) heterocatalysts can be synthesized by a low cost and energy efficient process that will allow to scale-up for possible industrially application.

Recommendations

The incorporation of two or three types of metals into SBA-15 framework should be studied to explore the potential in synergistic effect. Upscale of SBA-15 synthesis should be studied to explore the possibility to bring it to the industry.

APPENDIX

PUBLICATION PAPERS

1. "A novel room temperature synthesis of mesoporous SBA-15 from silatrane", Journal of Porous Materials, 18 (2011) 167-175.

2. "Room temperature synthesis of Ti-SBA-15 from silatrane and titanium-glycolate and its catalytic performance towards styrene epoxidation", Journal of Sol-Gel Science and Technology, 57 (2011), 221-228.

J Porous Mater (2011) 18:167–175
DOI 10.1007/s10934-010-9367-3

A novel room temperature synthesis of mesoporous SBA-15 from silatrane

Busaraporn Samran · Timothy J. White · Sujitra Wongkasemjit

Published online: 3 March 2010

Abstract Well-ordered and stable two dimensional mesoporous silica, SBA-15, was synthesized at room temperature (RT) from a silatrane precursor and a non-ionic triblock copolymer ($EO_{20}PO_{70}EO_{20}$) as the structure-directing agent. Using a combination of small angle X-ray scattering, electron microscopy, and nitrogen gas absorption–desorption isotherms, the RT product was found to be equivalent to SBA-15 prepared using more elaborative microwave-assisted hydrothermal methods. Both synthesis routes yielded large surface areas (486–613 m^2/g), pore diameters (45–67 Å) and channel volumes (0.6–0.8 cm^3/g). All materials condensed as sinuous bundles of silica tubes in a morphology that approximates *p6mm* symmetry, but where long range order was absent. In addition, portions of the products consisted of fine crystalline mosaics or were aperiodic. The simplicity of the room temperature synthesis route may create an inexpensive and energy-saving process for the large scale production of thermally stable SBA-15 as a catalyst support.

Keywords Silatrane · SBA-15 · Synthesis · Non-ionic triblock copolymer

B. Samran · S. Wongkasemjit
The Petroleum and Petrochemical College, Chulalongkorn University, Bangkok 10330, Thailand

B. Samran · S. Wongkasemjit (✉)
Center of Excellence for Petroleum, Petrochemicals, and Advanced Materials, Chulalongkorn University, Bangkok 10330, Thailand
e-mail: dsujitra@chula.ac.th

T. J. White (✉)
School of Materials Science and Engineering, Nanyang Technological University, Nanyang Avenue 639798, Singapore
e-mail: tjwhite@ntu.edu.sg

1 Introduction

Mesoporous materials have been of wide scientific and technological interest since the discovery of the M41S family in the 1990s by the Mobil research group [1, 2]. Among the mesoporous silicas, the SBA group has attracted attention by virtue of their thicker walls, greater hydrothermal stability, and larger pore size as compared to the M41S materials. In particular, well-ordered hexagonal SBA-15 possesses high specific surface areas (characteristically 600–1,000 m^2/g), large pore sizes (45–300 Å) and excellent hydrothermal stability (up to 850 °C). These superb properties place SBA-15 in demand for catalytic, adsorption, and separation applications that require high temperature or operate in corrosive environments [3–10]. Mesoporous silicas are typically synthesized by sol–gel processes where structure-directing amphiphillic surfactants, such as poly(ethylene glycol)-block-poly(propylene glycol)-block-poly(ethylene glycol), self assemble as micelles that are encapsulated by an inorganic silica precursor [11]. Calcination at 500–600 °C oxidizes the surfactant, leaving three- or two-dimensional mesoporous arrangements of cavities or channels [12–16].

SBA-15 is a 2D mesoporous material first prepared hydrothermally under acidic conditions (pH 1–2) using tetraethyl orthosilicate (TEOS) as the silica source and triblock copolymers to direct the organization of the polymerizing silica species [6, 7]. Generally, a hydrothermal treatment time of 11–72 h at 100 °C was needed to yield well-ordered mesoporous structures of high surface area (690 m^2/g), uniform pore diameter (47 Å) and volume (0.56 cm^3/g). Subsequently, Newalkar et al. [17] introduced microwave-assisted synthesis to shorten the reaction time (2 h) while obtaining materials of similar quality to those prepared in an autoclave. The microwave method

proves superior as volumatrix heating favors homogeneous nucleation, and fast dissolution and supersaturation of precipitated gels promotes shorter crystallization times [18–30].

Previous work has shown that controlling the hydrolysis and condensation is key to preparing well-ordered mesoporous material through sol–gel processing [31]. While TEOS is a common silica source, it is highly susceptible to hydrolysis; and the rapid separation of amorphous silica impedes mesopore formation. Therefore, it is advantageous to use precursors of reduced hydrolytic activity such as silatrane, which is an organosilicate resistant to hydrolysis and is stable in air for several weeks. Additionally, silatrane is an inexpensive silica precursor, which can be conveniently synthesized directly from fumed silicon dioxide and triethanolamine in ethylene glycol [32, 33]. These starting materials are commercially available and are low-priced. Silatrane is a proven silica precursor for the sol–gel synthesis of many microporous [34–37] and mesoporous [38–42] zeolites. In this paper, we describe a simple room temperature route for the preparation of SBA-15 using silatrane under acidic conditions, where a triblock copolymer (pluronic P123) was employed as the structure-directing agent. The demonstration of the room temperature synthesis shows that large scale production of SBA-15 can be economical and energy efficient.

2 Experimental section

2.1 Silatrane synthesis

The silatrane precursor was synthesized from fumed silica (99.8%, Sigma–Aldrich, St. Louis, MO) solubilized in triethanolamine (TEA; Carlo Erba, Milan, Italy), with ethylene glycol (EG; J.T. Baker, Philipsburg, NJ) employed as the solvent, and acetronitrile (Labscan, Bangkok, Thailand) used for silatrane purification. Following the method of Wongkasemjit et al. [43], 0.125 mol TEA was refluxed with 0.1 mol silicon dioxide in ethylene glycol (100 mL) at 200 °C under nitrogen for 10 h in an oil bath. Excess ethylene glycol was removed under vacuum at 110 °C to obtain a crude brown solid that was washed with acetronitrile to remove any TEA and EG residues. The white silatrane product was vacuum dried overnight, then examined by Fourier transform infrared (FT-IR) absorption spectrometery (Bruker Optics EQUINOX55, Karlsruhe, Germany) at a resolution of 2 cm^{-1}, and by thermogravimatric analysis (DuPont 2950, Twin Lakes, WI) at a heating rate of 10 °C min^{-1} from room temperature to 750 °C in a nitrogen atmosphere.

The FT-IR bands observed were 3,000–3,700 cm^{-1} (w, νO–H), 2,860–2,986 cm^{-1} (s, νC–H), 1,244–1,275 cm^{-1} (m, νC–N), 1,170–1,117 cm^{-1} (bs, νSi–O), 1,093 cm^{-1} (s, νSi–O–C), 1,073 cm^{-1} (s, νC–O), 1,049 cm^{-1} (s, νSi–O), 1,021 cm^{-1} (s, νC–O), 785 and 729 cm^{-1} (s, νSi–O–C), and 579 cm^{-1} (w, νN-Si). TGA showed one sharp mass loss at 390 °C and gave a 19% ceramic yield of $N(CH_2CH_2O)_3Si{-}OCH_2CH_2{-}N(CH_2CH_2OH)_2$.

2.2 SBA-15 synthesis

Mesoporous SBA-15 was synthesized from silatrane with poly(ethylene glycol)-block-poly(propylene glycol)-block-poly(ethylene glycol) ($EO_{20}PO_{70}EO_{20}$) (P123) (Sigma–Aldrich) employed as the template, and hydrochloric acid (Labscan Asia) as the catalyst in accordance with the procedure of Stucky et al. [6, 7]. A solution of $EO_{20}PO_{70}EO_{20}$:HCl:silatrane:H_2O equal to 2.60:4.25:12 (mass ratio) was prepared by dissolving 4 g of $EO_{20}PO_{70}EO_{20}$ polymer in 80 g of 2 M HCl (part A) and 8.8 g of silatrane in 20 g of H_2O (part B) while stirring continuously for 1 h to ensure complete dissolution. For the Route 1 synthesis, the solution from part B was then poured into part A and stirred at room temperature (RT) for 24 h; the product was recovered by filtration, washed with deionized water, and dried overnight under ambient conditions. For the Route 2, the RT product was, in addition, treated in an autoclave placed in a microwave oven at 300 W for 1–2 h at 100 or 120 °C. After cooling, the RT material was filtered, washed, and dried as for the Route 1 SBA-15. Both the Route 1 and Route 2 silicas were calcined at 550 °C in air for 6 h using a tube furnace (Carbolite, CFS 1200, Hope Valley, U.K.) at a heating rate of 1 °C/min to remove the residual organics (Fig. 1). The microwave-assisted product prepared at 120 °C was taken as the baseline material.

2.3 Mesopore ordering

Small-angle X-ray scattering (SAXS) patterns were obtained with a PANalytical PW3830 X-ray instrument using CuKα radiation generated at 50 kV and 40 mA. Thin powder samples (0.02 g) were spread uniformly on adhesive tape and mounted on an aluminum frame (15–20 mm). The scattering patterns were recorded on an image plate and the intensities extracted as two-dimensional plots against scattering angle (2θ) by integration across approximately 450 pixels/degree 2 theta (Fig. 2a). As replication of the 2θ zero shift was poor, the relative, rather than absolute, positions of the scattering maximum were compared. By using identical sample weights, the intensity of the peaks could be directly compared. If the stacking of silica mesotubes is perfectly hexagonal and conforms to *p6mm* plane symmetry, then the 2D crystallographic repeat can be indexed as {10} − {11}, while the second order reflections provide a measure of the channel diameter and

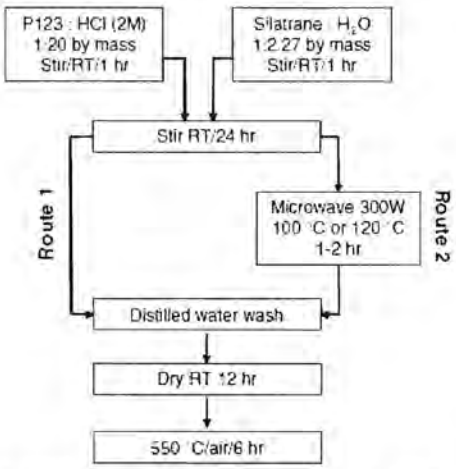

Fig. 1 Simplified room temperature synthesis of SBS-15 (*Route 1*) compared to the conventional microwave assisted hydrothermal method (*Route 2*)

can be indexed as {30} – {33} (Fig. 2b). Additional scattering (e.g. {−1−1} or {−2 1}) out to larger *d*-spacings will be significant only if the coherent hexagonal domain sizes are sufficiently extensive.

2.4 Nanostructure

Field Emission Scanning Electron Microscope (FESEM) images were obtained from powders mounted on double-sided carbon tape using a JEOL JSM-7500F operating at an accelerating voltage of 0.3–0.5 kV to minimize the effects of charging. Transmission electron microscopy (TEM) was conducted using a JEOL JEM-2100F TEM instrument operated at an accelerating voltage of 200 kV with a large objective aperture. For the TEM, the powder was lightly ground under ethanol, sometimes with the introduction of liquid N_2 to enhance fracturing and produce thin flakes that were dispersed ultrasonically. Two drops of the suspension were deposited on holey carbon-coated copper grids. The periodicity of the SBA-15 projected along the mesotubes was studied by fast Fourier transformation of TEM images using CRISP [44] to extract the interplanar angles, with deviations from 60°, indicating an oblique rather than hexagonal matrix. The average size of the channels was obtained by assuming *p6mm* symmetry and carrying out a back Fourier transformation with the diameter measured directly from the reprocessed image.

2.5 Physical parameters

Nitrogen sorption isotherms were obtained at −196 °C after outgassing at 250 °C for 12 h (Quantasorb JR, Mount Holly, NJ). The surface area and average pore size were determined by the Brunauer–Emmett–Teller (BET) method.

3 Results and discussion

3.1 As-synthesized SBA-15 mesoporous material

The SAXS pattern for the as-synthesized mesoporous silica (SBA-15) prepared with $EO_{20}PO_{70}EO_{20}$ shows two well-resolved peaks (Fig. 3a) that are indexable as {10} – {11} and {30} – {33} reflections associated with *p6mm* hexagonal symmetry. The intense {10} peak reflects a *d* spacing of 150 Å, corresponding to a unit-cell parameter (a_0 = 173 Å). After calcination in air at 550 °C for 6 h, the SAXS (Fig. 3b) shows that the *p6mm* morphology is preserved. Two peaks are still observed, confirming that hexagonal SBA-15 is thermally stable. A similarly high degree of mesoscopic order is observed for hexagonal SBA-15 even after calcination at 850 °C.

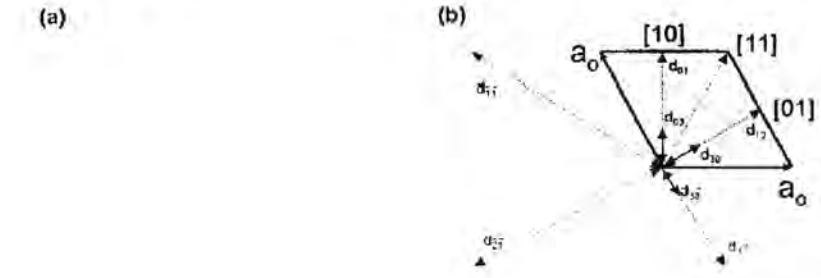

Fig. 2 Idealized morphology (a) of the two dimensional arrangement of silica tubes in SBA-15 conforming to *p6mm* symmetry. In reality, the tubes are sinuous and extend over a range of diameters, destroying long range hexagonal symmetry. Projection along the mesoporous tubes (b) emphasizing the equivalence of {10} – {11} planes and *d* spacings that define the underlying crystallographic repeat, with {30} – {33} corresponding to a first approximation to the observed channel diameters

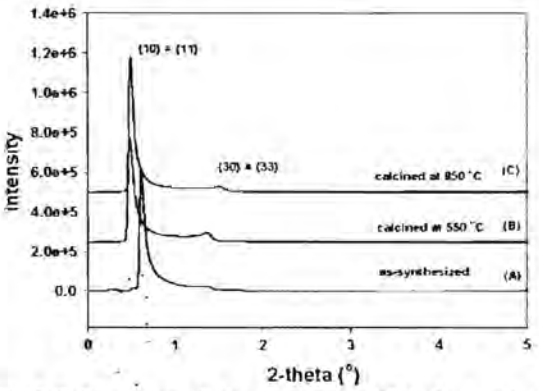

Fig. 3 SAXS pattern of the as-synthesized SBA-15 (*A*), after calcinations at 550 °C (*B*), and after calcination at 850 °C (*C*). These materials show two strong scattering maxima that are indexed in accordance with *p6mm* (*hexagonal*) symmetry

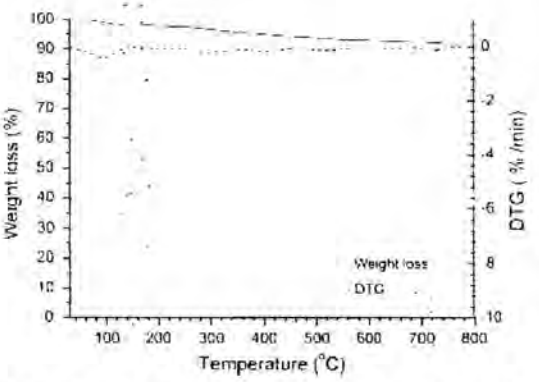

Fig. 4 TG-DTG peak analyzed in air of SBA-15 after calcination at 550 °C for 6 h

Thermogravimatric and differential thermal analyses (TGA and DTA) in air of the SBA-15 sample calcined at 550 °C for 6 h and prepared with $EO_{20}PO_{70}EO_{20}$ show total weight losses of 11.02 weight % (Fig. 1). At 94.6 °C, the TGA registers a 2.11 weight % loss because of the desorption of water. There is no weight loss at 145 °C, which would correspond to the decomposition temperature of the block copolymer [6], indicating that there is no nitrogen or carbon species left in the mesoporous wall, and confirming that the template has been completely removed.

3.1.1 With hydrothermal treatment

3.1.1.1 High temperature microwave-assisted hydrothermal synthesis (120 °C/1 h) This benchmark material yielded a SAXS pattern with first- and second-order scattering centered at *d*-spacings of 182.5 Å (a_0 = 210.7 Å) and 65.8 Å (Fig. 5a). When indexed according to the plane group *p6mm* as {10} − {11} and {30} − {33}, the ratio $d_{\{10\}-\{11\}}/d_{\{30\}-\{33\}}$ equals to 2.8, rather than 3, since the overall structure shows significant deviations from the hexagonal matrix, and more nearly conforms to oblique *p2* (Table 1). Both scattering maxima are anisotropic such that {10} − {11} shows a sharp upper limit of the *d*-spacing at ~ 190 Å, but a long tail towards higher scattering angles down to ~ 167 Å (Fig. 5b), while the {30} − {33} feature is asymmatrix in an opposite sense and spans channel diameters from 63 to 67 Å. Higher order features such as {−1 1} are barely discernable because the coherent hexagonal domains were quite restricted (Fig. 5b). Microscopy confirmed the absence of longer range periodicity as implied by SAXS. Field emission scanning electron microscopy (FESEM) showed that the SBA-15 possessed a sinuous morphology at a scale of a few hundred nanometers coexisting with poorly ordered mesopore fragments (Fig. 6a). In the TEM images, the mosaic character of even the better ordered fragments is evident (Fig. 6b). At higher magnifications the FESEM suggests that the channels are partially cavitated, rather than being open conduits, which would limit mass transport (Fig. 6c); however, the TEM images show that the projected absorption contrast and periodicity are insensitive to random channel blockages (Fig. 6d). In detail, images collected parallel to the pseudo sixfold rotation axis clearly show variability in both channel diameter and filling (Fig. 6e), while the <10> − <11> projections confirm tubule ordering (Fig. 6f).

Fast Fourier transform analysis of the sixfold TEM projections confirmed that departures from *p6mm* symmetry were systemic, with the {10} − {11} interplanar angles deviating from 60° (Fig. 7a, b). By imposing hexagonal symmetry as the average structure and applying the back Fourier reconstruction, a processed image is recovered, from which the pore diameter is directly accessible (Fig. 7a) and shows an average tunnel diameter of 46 Å. The pore diameters derived from SAXS and TEM image processing, support the values obtained by nitrogen adsorption measurements, which gave a diameter of 54 Å (Table 1), a pore volume of 0.8 cm^3/g, and a high surface area (613 m^2/g) (Fig. 8a). The isotherm was IUPAC type IV with an H1-type hysteresis loop [5]. However, the SBA-15 synthesized from silatrane showed a smaller pore volume (0.8 cm^3/g) and surface area (613 m^2/g) compared to equivalent material synthesized from TEOS (0.99 cm^3/g and 805.9 m^2/g). This is consistent with the SAXS observation that the silatrane source yielded less well-ordered mesopores [6, 7, 16]. While for the TEOS derived SBA-15, X-ray scattering patterns contain up to four peaks, indicative of longer range periodicity.

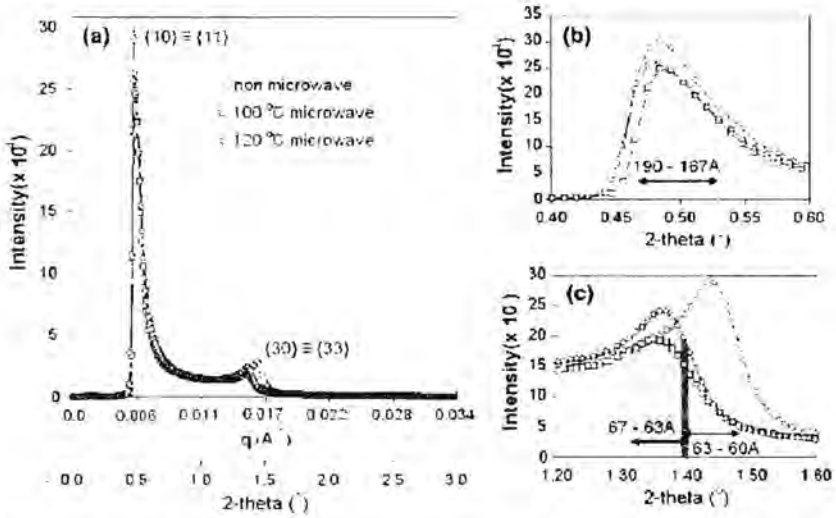

Fig. 5 SAXS pattern (a) of the SBA-15 materials show two strong scattering maxima that are indexed in accord with *p6mm* symmetry. The relative positions of these maxima are distinct for those mesoporous structures prepared with the assistance of microwave homogenization. The (10) ≡ (11) reflections (b) are anisotropic and show that the upper limit of the crystallographic repeat in the 2D mesopore order is quite sharp (~190 Å) but with a long tail of shorter periodicity down to ~167 Å. The (30) ≡ (33) scattering (c) which provides a measure of pore diameter, shows that the channels are slightly larger when microwave treatment is used, as compared to direct hydrothermal synthesis, in agreement with the gas absorption measurements (see Table 1)

Table 1 Properties of SBA-15 as a function of the synthesis route

Synthesis[a]	Surface area (m^2/g) BET	Channel volume (cm^3/g) BET	Channel diameter (Å) BET	TEM	SAXS	$d_{(10)}/d_{(30)}$ SAXS
Route 1						
Without hydrothermal treatment	486	0.6	50	~45	60–63	3
Route 2						
With hydrothermal treatment via microwave assisted method at 100 °C for 2 h	572	0.8	55	~45	63–67	2.8
With hydrothermal treatment via microwave assisted method at 120 °C for 1 h	613	0.8	54	~45	63–67	2.8

[a] All materials calcined at 550 °C to remove the template

3.1.1.2 Low temperature microwave-assisted hydrothermal synthesis (100 °C/2 h). The characteristics of the SBA-15 prepared at 100 °C were broadly similar to those of the 120 °C material, with the $d_{(10)} \equiv (11)/d_{(30)} \equiv (33)$ equal to 2.8 (Fig. 5) and a cavitated channel structure (Fig. 9). The surface area (572 m^2/g) and pore diameter (55 Å) are identical to those obtained at 120 °C/1 h (Fig. 8b).

Generally, the work related to SBA-15 employs a hydrothermal treatment step via autoclave- or microwave-assisted methods using TEOS as a silica source and P123 as the template. For example, Su et al. [45], studied the orientation of mesochannels using a laser-modified polyimide surface with TEOS employed as the silica source and P123 as the structure-directing agent. The material was hydrothermally treated in an autoclave at 110 °C for 48 h. The orientation of the mesochannels was evaluated by X-ray scattering. One narrow {10} peak of the 2D hexagonal phase appeared. The absence of an {11} peak, which would normally be observed in a hexagonal structure, was consistent with the mesopore channels oriented parallel to the substrate. Okamoto et al. [46], studied the site-specific synthesis of mixed valence Ti–O–Fe complexes within the pores of ordered mesoporous silica SBA-15 using TEOS and P123. The powder exhibited three reflections corresponding to {10}, {11}, and {20} of a two-dimensional hexagonal pore structure. Newalkar et al. [17] reported a

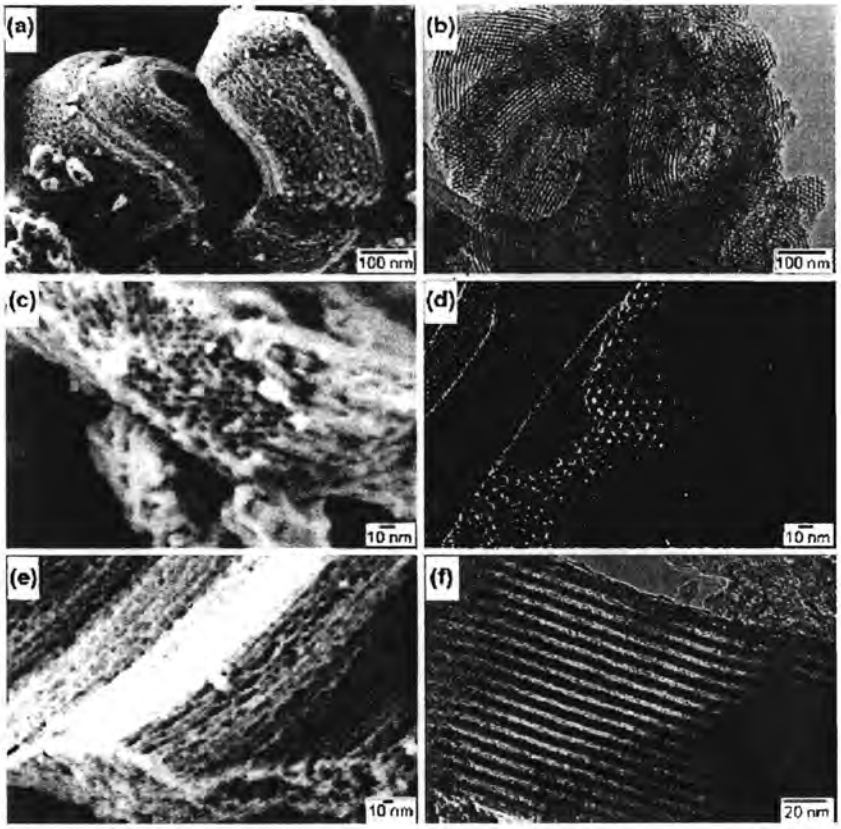

Fig. 6 FESEM (*left side*) and TEM (*right side*) images of SBA-15 prepared hydrothermally at 120 °C for 1 h with microwave assistance. At lower magnifications a, b the twisted bundles of silica tubes are seen to co-exist with less crystalline and aperiodic material. When viewed along the pseudo-hexagonal projection c, d it is evident that the channels are not uniform in shape or content. The <10> FESEM e, f clearly shows cavitation along the channels. While this is not evident in the TEM, regular periodicity of the 2D mesopore order is evident

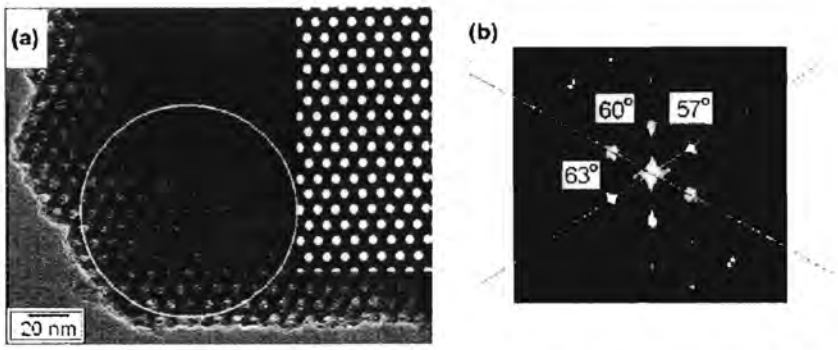

Fig. 7 A well-ordered fragment (a) of SBA-15 in pseudo-*p6mm* projection. The frequency image (b) obtained by fast Fourier transformation (*FFT*) of the region within the *circle* yields shows angles that depart from 60° demonstrating that this material fragment better corresponds to *p2* oblique symmetry. By imposing *p6mm* symmetry and calculating the back Fourier transform, the inserted processed image in (a) is generated that yields an average pore diameter of 46 Å

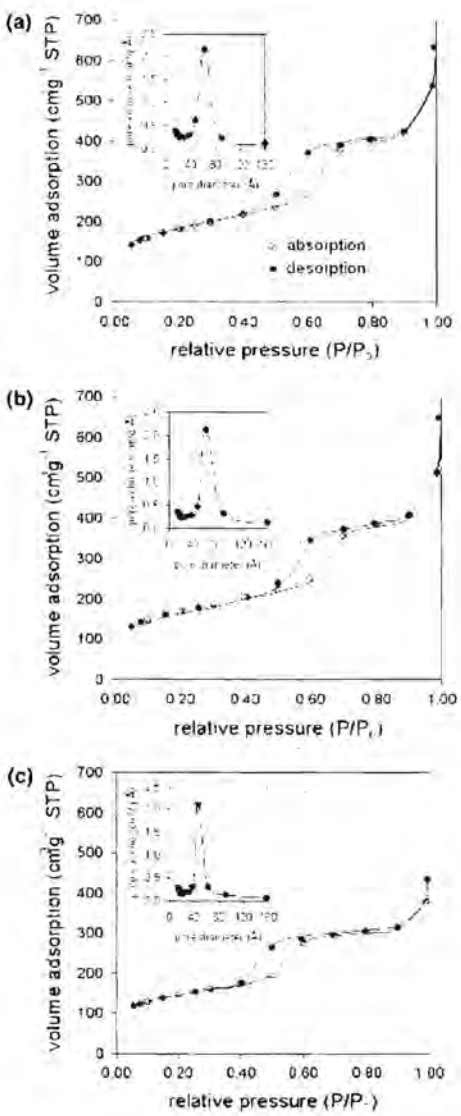

Fig. 8 Nitrogen adsorption desorption isotherms and corresponding pore size distributions for SBA-15 prepared with a microwave-assisted hydrothermal route at a 120 °C for 1 h, b 100 °C for 2 h, and c directly at RT by stirring. The pore size range is slightly narrower for the latter (FWHM ~18 Å) as compared to the former (FWHM ~25 Å)

microwave-assisted synthesis method to shorten the synthesis time that employed TEOS and P123; they found that the reaction time can be reduced to 2 h and that the product yield is similar to that prepared in 48 h by the conventional autoclave treatment. It is believed that the rapid heating to the crystallization temperature by volumetric heating favored homogeneous nucleation, fast supersaturation by the rapid dissolution of precipitated gels, and ultimately a shorter crystallization time.

Zhao et al. [6, 7], used TEOS and P123 to synthesize SBA-15 in acidic conditions as a function of temperature and time. Using an autoclave, it took 48 h to complete the reaction and achieve well-ordered SBA-15 with a high surface area (690 m^2/g), a uniform pore size of 47 Å, and a pore volume of 0.56 cm^3/g; these results are similar to the data obtained from the sample from this present work.

3.1.2 *Without hydrothermal treatment*

3.1.2.1 Direct RT synthesis The relative positions of the SAXS scattering maxima appear at 182.5 and 60.8 Å and conform almost exactly to the hexagonal matrix with $d_{(10)} = 1/\sqrt{3}d_{(30)} = (33)$ equal to 3.0 (Fig. 5). The spread of the crystallographic repetition is unchanged (190–167 Å), however, the channel diameter is slightly smaller (63–60 Å), in agreement with the BET measurements that yielded a surface area of 486 m^2/g and a pore diameter of 50 Å (Fig. 8c, Table 1). Micrographs collected near the principal axial projections are indistinguishable from the hydrothermally prepared material (Fig. 10).

SAXS indicates that the SBA-15 prepared at RT are well-ordered 2D mesoporous materials, comparable to the microwave-assisted hydrothermal products, with the latter yielding a marginally superior product in terms of higher BET surface area and mesopore order. When conventional precursors such as TEOS are used, it is believed that the hydrothermal conditions promote the condensation of metal oxide bridges, leading to better ordered structures. However, this benefit is minimal when silatrane is employed, as it is stable towards hydrolysis and can be employed at room temperature. Tanglumlert et al. [47] reported the successful synthesis of well-ordered and stable SBA-1 mesoporous silica via the sol–gel process using silatrane as a silica source. High quality SBA-1 was produced under mild acidic conditions. C_nTMAB was used as a template, and the reaction was conducted at room temperature.

As can be seen from the TEM images (Fig. 6), the silica wall thickness between the RT and the microwave-assisted hydrothermal samples are similar, implying that silatrane condensation of Si–O–Si takes place at room temperature. By operating at ambient conditions, this method minimizes process complexity while forming well-ordered SBA-15. The results from the SAXS, FESEM, and TEM clearly indicate that the SBA-15 products obtained at room temperature (without hydrothermal treatment) and by the microwave-assisted method are comparable, and would facilitate economical and energy-saving large-scale production.

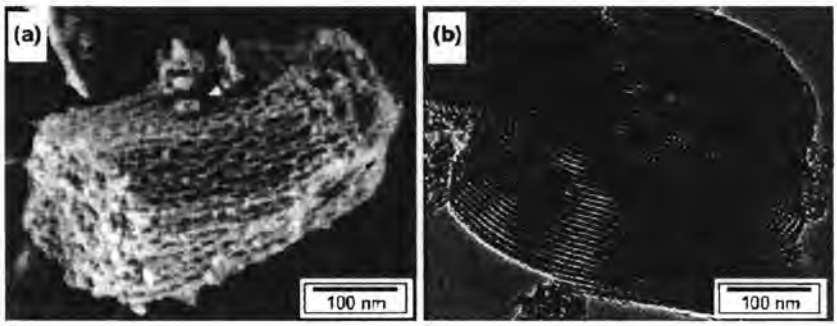

Fig. 9 Approximate <10> FESEM (a) and TEM (b) micrographs of SBA-15 prepared hydrothermally by the microwave-assisted method at 100 °C for 2 h

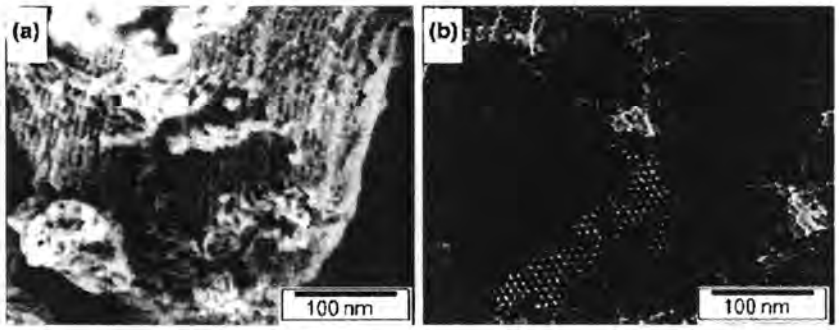

Fig. 10 Approximate <10> FESEM (a) and hexagonal TEM (b) images of SBA-15 prepared at RT without hydrothermal treatment

4 Conclusions

It has been demonstrated that SBA-15 can be successfully synthesized at room temperature using silatrane, an inexpensive and conveniently prepared silica, as the silica precursor. The crystallographic, morphological, and physical properties of the SBA-15 obtained by this simple process are comparable to mesoporous silica prepared by the more complex microwave-assisted hydrothermal method. This new preparative route may allow inexpensive, energy-saving, and efficient production of SBA-15 for a range of catalytic and environmental applications.

Acknowledgments This research is financially supported by the Postgraduate Education and Research Program in Petroleum and Petrochemical Technology (ADB) Fund (Thailand), the Ratchadapisake Sompote Fund, Chulalongkorn University, and, the Thailand Research Fund (TRF). We thank Mr. Tan Teck Siong for assistance in collecting the secondary electron images, and the School of Materials Science & Engineering NTU for the partially financial support. Special thanks go to Mr. Robert Wright for the English proofreading.

References

1. C.T. Kresge, M.E. Leonowicz, W.J. Roth, J.C. Vartuli, J.S. Beck, Nature 359, 710–712 (1992)
2. J.S. Beck, J.C. Vartuli, W.J. Roth, M.E. Leonowicz, C.T. Kresge, K.D. Schmitt, C.T.W. Chu, D.H. Olson, E.W. Sheppard, S.B. McCullen, J.B. Higgins, J.L. Schlenker, Am. Chem. Soc. 114, 10834–10843 (1992)
3. M.E. Davis, Chem. Ind. 4, 137 (1992)
4. M. Estermann, L.B. McCusker, C. Baerlocher, A. Merrouche, H. Kessler, Nature 352, 320 (1991)
5. V.-T. Hoang, Q. Huang, M. Eic, T. O. Do, S. Kaliaguine, Langmuir 21, 2051–2057 (2005)
6. D. Zhao, J. Feng, Q. Huo, N. Melosh, G.H. Fredrickson, B.F. Chmelka, G.D. Stucky, Science 279, 548–552 (1998)
7. D. Zhao, Q. Huo, J. Feng, B.F. Chmelka, G.D.J. Stucky, Am. Chem. Soc. 120, 6024–6036 (1998)
8. D. Trong On, D. Desplantier-Giscard, D. Danumah, S. Kaliaguine, Appl. Catal. A 222, 299–357 (2001)
9. S. Kubo, K. Kosuge, Langmuir 23, 11761–11768 (2007)
10. B. Coasne, A. Galarneau, D.F. Renzo, R.J.M. Pellenq, Langmuir 22, 11097–11105 (2006)
11. M. Kruk, L. Cao, Langmuir 23, 7247–7254 (2007)
12. C.G. Goltner, M. Antonietti, Adv. Mater. 9, 431 (1997)

13. M. Antonietti, C. Goltner, Angew. Chem. Int. Ed. Engl. 36, 910 (1997)
14. G. Wanka, H. Hoffmann, W. Ulbricht, Macromolecules 27, 4145 (1994)
15. B. Chu, Z. Zhou, Surf. Sci. Ser. 60, 67 (1996)
16. A. Zukal, H. Siklova, J. Cejka, Langmuir 24, 9837–9842 (2008)
17. B. Newalkar, S. Komarneni, H. Katsuki, Chem. Commun. 23, 2389–2390 (2000)
18. S. Komarneni, R. Roy, Q.H. Li, Mater. Res. Bull. 27, 1393 (1992)
19. S. Komarneni, Q.H. Li, K.M. Stefansson, R. Roy, J. Mater. Res. 8, 3176 (1993)
20. S. Komarneni, Q.H. Li, R. Roy, J. Mater. Chem. 4, 1903 (1994)
21. S. Komarneni, R. Pidugu, Q.H. Li, R. Roy, J. Mater. Res. 10, 1687 (1995)
22. S. Komarneni, Q.H. Li, R. Roy, J. Mater. Res. 11, 1866 (1996)
23. S. Komarneni, V.C. Menon, Mater. Lett. 27, 313 (1996)
24. P. Chu, F.G. Dwyer, J.C. Vartuli, US Pat. 4,778,666 (1988)
25. U. Lohse, R. Bertram, K. Jancke, I. Kurzawski, B. Parlitz, E. Loeffler, E. Schreier, J. Chem. Soc. Faraday Trans. 91, 1163 (1995)
26. I. Girnus, K. Jancke, R. Vetter, J. Richter-Mendau, J. Caro, Zeolites 15, 33 (1995)
27. X. Meng, W. Xu, S. Tang, W. Pang, Chin. Chem. Lett. 3, 69 (1992)
28. A. Arafat, J.C. Jansen, A.R. Ebaid, H. Van Bekkum, Zeolites 13, 162 (1993)
29. C.G. Wu, T. Bein, Chem. Commun. 8, 925 (1996)
30. M. Park, S. Komarneni, Microporous Mesoporous Mater. 20, 39 (1998)
31. S. Cabrera, J.E. Haskouri, C. Guillem, J. Latorre, A. Beltran porter, D. Beltran porter, M.D. Marcos, P. Amoros, Solid State Sci. 2, 405 (2000)
32. P. Phinyawirat, R. Magaraphan, A.M. Jamieson, S. Wongkasemjit, Mater. Sci. Eng. A361, 147–154 (2003)
33. W. Chareenpinijkarn, M. Suwankruhasn, B. Kesapabutr, S. Wongkasemjit, A.M. Jamieson, Eur. Polym. J. 37, 1441–1448 (2001)
34. M. Sathupanya, E. Gulari, S. Wongkasemjit, J. Eur. Ceram. Soc. 22, 1293–1303 (2002)
35. M. Sathupanya, E. Gulari, S. Wongkasemjit, J. Eur. Ceram. Soc. 23, 2305–2314 (2003)
36. N. Phonthammachai, T. Chairassameewong, E. Gulari, A.M. Jamieson, S. Wongkasemjit, J. Met. Mater. Min. 12, 23 (2003)
37. P. Phinyawirat, A.M. Jamieson, S. Wongkasemjit, Microporous Mesoporous Mater. 77, 203–213 (2005)
38. N. Thanabodeekij, W. Tanglumlert, E. Gulari, S. Wongkasemjit, Appl. Organomet. Chem. 19, 1047–1054 (2005)
39. N. Thanabodeekij, S. Sadthayanon, E. Gulari, S. Wongkasemjit, Mater. Chem. Phys. 98, 131–137 (2006)
40. S. Mintova, J. Cejka, Stud. Surf. Sci. Catal. 168, 301–326 (2007)
41. J. Cejka, S. Mintova, Catal. Rev. 49, 457–509 (2007)
42. J. Perez-Ramirez, C.H. Christensen, K. Egeblad, C.H. Christensen, J.C. Groen, Chem. Soc. Rev. 37, 2530–2542 (2008)
43. P. Piboonchaisit, S. Wongkasemjit, R. Laine, J. Sci. Soc. Thailand 25, 113 (1999)
44. X. Zou, M. Sundberg, M. Larine, S. Hovmoller, Structure projection retrieval by image processing of HRTEM images taken under non-optimum defocus conditions, Ultramicroscopy 62, 103–121 (1996)
45. B. Su, X. Lu, Q. Lu, Langmuir 24, 9695–9699 (2008)
46. A. Okamoto, R. Nakamura, H. Osawa, K. Hashimoto, Langmuir 24, 7011–7017 (2008)
47. W. Tanglumlert, T. Imae, T.J. White, S. Wongkasemjit, J. Am. Ceram. Soc. 90, 3992–3997 (2007)

Room temperature synthesis of Ti-SBA-15 from silatrane and titanium-glycolate and its catalytic performance towards styrene epoxidation

Journal of Sol-Gel Science and Technology

ISSN 0928-0707
Volume 57
Number 2

J Sol-Gel Sci Technol (2010)
57:221-228
DOI 10.1007/s10971-010-2345-z

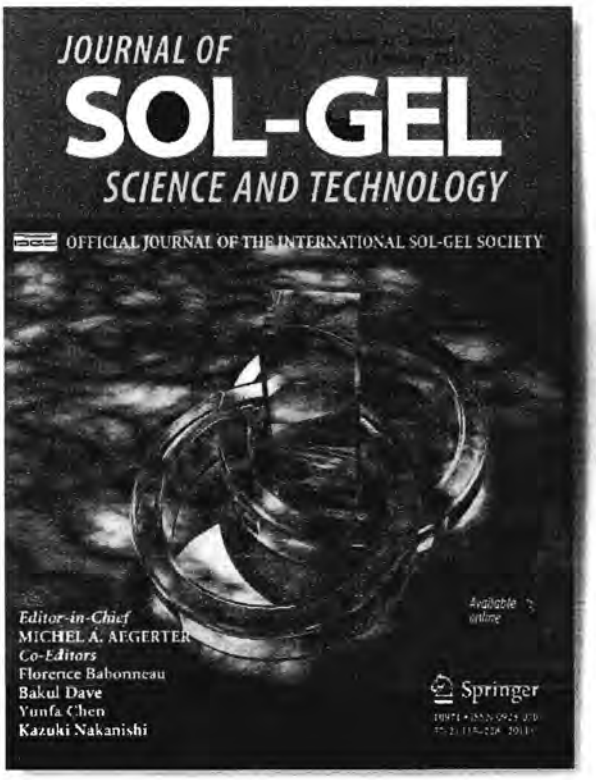

Springer

J Sol-Gel Sci Technol (2011) 57:221–228
DOI 10.1007/s10971-010-2345-z

ORIGINAL PAPER

Room temperature synthesis of Ti-SBA-15 from silatrane and titanium-glycolate and its catalytic performance towards styrene epoxidation

Busaraporn Samran · Supattra Aungkutranont · Timothy J. White · Sujitra Wongkasemjit

Received: 11 July 2010 / Accepted: 12 October 2010 / Published online: 21 October 2010

Abstract A novel room temperature sol–gel synthesis of Ti-SBA-15 is described using moisture stable silatrane and titanium glycolate precursors, and poly(ethylene oxide)-poly(propylene oxide)-poly(ethylene oxide) block copolymer ($EO_{20}PO_{70}EO_{20}$) as the structure directing agent. Catalyst performance was optimized by systematically investigating the influence of acidity, reaction time and temperature, and titanium loading. Small angle X-ray scattering (SAXS) and transmission electron microscopy (TEM) showed well-ordered 2D mesoporous hexagonal structures, while N_2 adsorption/desorption measurements yielded high surface areas (up to 670 m^2/g), with large pore diameters (5.79 nm) and volumes (0.83 cm^3/g). Diffuse reflectance UV–visible spectroscopy (DRUV) was found that tetravalent titanium as $Ti^{4+}O_4$ tetrahedra were incorporated in the framework through displacement of $Si^{4+}O_4$ after calcination (550°C/6 h) to loadings of 7 mol% Ti without perturbation of the ordered mesoporous structure, or decoration by extra-framework anatase containing $Ti^{4+}O_6$ octahedra. The catalytic activity and selectivity of styrene epoxidation using hydrogen peroxide (H_2O_2) showed that the conversion of styrene increases significantly at higher titanium contents. The only products of this reaction were styrene oxide and benzaldehyde, with selectivity of 34.2 and 65.8%, respectively, at a styrene conversion of 25.8% over the 7 mol% Ti-SBA-15 catalyst. Beyond this titanium loading, anatase is deposited on the framework and catalytic activity degrades. The performance of the new catalyst is also shown to be superior to conventional materials produced by incipient wetness impregnation where Ti resides on the surface of SBA-15, giving a styrene conversion of 11.9% under identical reaction conditions.

Keywords Ti-SBA-15 · Silatrane · Titanium-glycolate · Styrene epoxidation

1 Introduction

Since the discovery of the large and uniform hexagonal channel motifs, high specific surface area, and excellent hydrothermal stability of Santa Barbara Amorphous type material, SBA-15, silica molecular sieve by Zhao et al. [1, 2], using nonionic triblock copolymers as templates, much effort has been devoted to enhancing the syntheses and functionality of these materials because of their potential as catalysts, adsorbents for large organic molecules, and guest–host chemical supports [3, 4]. However, pure silica porous materials are poor catalysts due to weak acidity and redox potential [5, 6]. To overcome these limitations, heteroatoms are incorporated into the framework to create active sites, and many transition metals promote beneficial catalytic responses [7–10].

The introduction of Ti-substituted molecular sieves has added a new dimension to the application of silica

B. Samran · S. Aungkutranont · S. Wongkasemjit (✉)
The Petroleum and Petrochemical College and Center of Excellence for Petroleum, Petrochemicals, and Advanced Materials, Chulalongkorn University, Bangkok 10330, Thailand
e-mail: dsujitra@chula.ac.th

T. J. White
School of Materials Science and Engineering, Nanyang Technological University, Nanyang Avenue 639798, Singapore

T. J. White
Center for Advanced Microscopy, The Australian National University, Canberra 2601, Australia

based meso-frameworks for catalytic oxidation, and Ti-SBA-15 has proven to be a versatile catalyst for the selective oxidation with peroxide enhancement to produce fine chemicals and pharmaceuticals. To be effective, Ti should be incorporated crystallochemically in tetrahedral oxygen co-ordination (TiO_4) by isomorphic $Si^{4+} \leftrightarrow Ti^{4+}$ substitution, rather than as co-existing catalytically inactive anatase with $Ti^{4+}O_6$ octahedra [11]. Several attempts have been made to introduce titanium into the mesoporous silica framework of SBA-15 [12–18] by direct synthesis or post-synthesis treatment [9, 16, 19–23]. The principle limitation of the post-synthesis method is that metal oxides are deposited on external surfaces of the catalyst which blocks the channels and prevents the reactant molecules accessing many reactive sites in the matrix [23]. Zhang et al. [14] reported the successful incorporation of Ti into SBA-15 through a fluoride mediated reaction that accelerated the hydrolysis of a silica precursor. However, the expensive starting materials have limited its use. Newalkar et al. [16] reported the microwave-assisted hydrothermal synthesis of Ti-SBA-15 using tetraethyl orthosilicate (TEOS) and titanium tetrachloride ($TiCl_4$) as silica and titanium sources.

Wongkasemjit et al. [24–26] successfully prepared silatrane and titanium glycolate using inexpensive and widely available silica and titanium oxide as starting materials, respectively. The resulting moisture stable silatrane and titanium glycolate can be effectively used to synthesize many technological materials [27–31]. Commercially available silica and titanium sources are highly susceptible to hydrolysis, resulting in the rapid separation of amorphous silica that impedes mesopore formation. Therefore, it is advantageous to use precursors of reduced hydrolytic activity. Moreover, silatrane has also been proven successful for the synthesis of SBA-15 mesoporous silica at room temperature [32]. In the present study, this approach is extended to the synthesis of highly ordered Ti-SBA-15 from silatrane and titanium glycolate precursors, where the acidity, reaction temperature, reaction time, and Ti loading were optimized systematically. The catalysts were characterized using several complimentary techniques, including SAXS, DRUV, TEM, and N_2 adsorption. The catalytic activity of Ti-SBA-15 towards the epoxidation of styrene monomers with H_2O_2 employed as the oxidant was investigated as a function of temperature, time, and catalyst loading. To establish a baseline for comparison, titanium glycolate was impregnated on a SBA-15 framework by the incipient wetness impregnation method [33]. Products of the epoxidation reaction were analyzed using gas chromatography (GC). The conversion of styrene is calculated, based on the amount of styrene monomer used.

2 Experimental section

2.1 Materials

Fumed silica (SiO_2, 99.8%) (Sigma–Aldrich, St. Louis, MO), titanium dioxide (TiO_2) (Carlo Erba, Milan, Italy), triethanolamine (TEA) (Carlo Erba, Milan, Italy), tetraethylenetriamine (TETA) (Facai, Bangkok, Thailand), ethylene glycol (EG) (J.T. Baker, Philipsburg, NJ), acetronitrile (Labscan, Bangkok, Thailand), poly(ethylene oxide)-poly(propylene oxide)-poly(ethylene oxide) block copolymer ($EO_{20}PO_{70}EO_{20}$) (Sigma–Aldrich, Singapore), hydrochloric acid (HCl) (Labscan, Asia) were used without further purification or treatment.

2.2 Ti-SBA-15 sol–gel synthesis

Ti-SBA-15 materials were synthesized from silatrane and titanium-glycolate. The non-ionic triblock copolymer surfactant $EO_{20}PO_{70}EO_{20}$ was used as the structure-directing agent and 2M HCl was the acid catalyst. The preparation of Ti-SBA-15 with various n_{Ti}/n_{Si} molar ratios followed the method of Samran et al. [32]. A solution of $EO_{20}PO_{70}EO_{20}$:HCl:silatrane:H_2O = 2:60:4.25:12 (mass ratio) was prepared by dissolving 4 g of $EO_{20}PO_{70}EO_{20}$ polymer in 80 g of 2M HCl (part A) and 8.8 g of silatrane, synthesized according to ref. 25–26, in 20 g of H_2O (part B) with continuously stirring for 1 h to ensure complete dissolution. The solution of part B was then poured into part A. The required amount of titanium glycolate [24] was added into the homogenous solution with stirring. The resulting gel was aged at room temperature (RT) for 24 h and the product recovered by filtration, washed with deionized water, and dried overnight at ambient. Silicas were calcined at 550°C in air for 6 h using a tube furnace (Carbolite, CFS 1200, Hope Valley, U.K.) at a heating rate of 0.5°C/min to remove the residual organics. The catalysts were designated as (*x*) mol% Ti-SBA-15 where *x* denotes the percentage of the n_{Ti}/n_{Si} ratio. Titanium-free mesoporous SBA-15 was synthesized using the same procedure ($EO_{20}PO_{70}EO_{20}$:HCl:silatrane:H_2O = 2:60:4.25:12 (mass ratio)) in the absence of titanium glycolate. The reaction conditions for synthesis of Ti-SBA-15 were studied as a function of Ti loading, acidity, reaction time, and reaction temperature.

2.3 Ti-SBA-15 impregnation synthesis

Incipient wetness impregnation was used to deposit Ti metal on the SBA-15 support [38], using 7 and 10 mol% titanium glycolate. The precursor was dissolved in water and dropped onto the catalyst supports. Drying was carried out at 100°C for 12 h, followed by calcination (550°C/6 h)

in a Carbolite furnace (CFS 1200) at a heating rate of 0.5°C/min.

2.4 Characterization

SAXS patterns were obtained with a PANalytical PW3830 X-ray instrument using CuKα (λ_{av} = 0.154 nm) radiation generated at 50 kV and 40 mA, over the 2θ range 0.5–10°, step size of 0.01° and dwell time of 10 s per step. TEM was conducted using a JEOL JEM-2100F TEM instrument operated at an accelerating voltage of 200 kV with a large objective aperture. Nitrogen adsoption and desorption isotherms were measured at −196°C after outgassing at 250°C for 12 h under vacuum (Quantasorb JR, Mount Holly, NJ). The specific surface area was determined by the Brunauer–Emmett–Teller (BET) method. The pore size distributions were obtained from the adsorption and desorption branches of the nitrogen isotherms by the Barrett-Joyner-Halenda method. DRUV spectra were recorded from 190 to 600 nm with a Shimadzu UV-2550 spectrophotometer from catalyst powders loaded in a Teflon cell and using $BaSO_4$ as a reference.

2.5 Catalytic activity of Ti-SBA-15

The catalytic activity of Ti-SBA-15 towards epoxidation of styrene was established by combining 5 mmol of styrene, 5 mmol of 30% H_2O_2, 5 ml of acetronitrile and a required amount of Ti-SBA-15 (0.0500–0.2000 g) in a glass flask. The suspension was stirred and heated to a fixed time (1–6 h) and temperature (70–90°C) in an oil bath. Chemical analyses were carried out with a gas chromatograph (GC) equipped with a capillary column (DB-Wax, 30 m × 0.25 mm) and flame ionization detector (FID). The conversion of styrene was calculated based upon the amount of styrene monomer consumed.

3 Results and discussion

3.1 Ti-SBA-15 catalyst crystal chemistry

Zhao et al. [1] synthesized good quality SBA-15 of high surface area (690 m^2/g) using TEOS as the silica precursor that was aged (35°C/20 h) prior to hydrothermal reaction (100°C/48 h). Recently, Samran et al. [32] reported a novel method to prepare SBA-15 from silatrane at room temperature via a sol–gel process using a nonionic triblock copolymer as the template to avoid the need for hydrothermal treatment. Following this approach, high quality Ti-SBA-15, of large surface area (592–670 m^2/g), pore volume (0.83 cm^3/g) and pore size (5.7 nm), was readily synthesized. Generally, the SAXS pattern of SBA-15 shows scattering attributable to {10} and {30} planes of a 2D hexagonal meso-channel arrangement (Fig. 1). These characteristic lines were also observed in Ti-SBA-15. Moreover, the nature of Ti^{4+} as substitutional TiO_4 units or extra-framework TiO_6 polyhedra could be differentiated by DRUV. Catalysts showed strong absorption, around 220 nm, typical of the ligand-to-metal charge transfer transition in the tetrahedrally coordinated TiO_4 or $HOTiO_3$ species. This band arises from p ← d charge transfer between the Ti and O atoms associated with Ti–O–Si bonds and became more intense with increasing Ti content. An additional band at 330 nm for higher Ti contents is attributed to extra-framework titanium (probably anatase), suggesting there is an upper limit for Ti displacement of Si in the SBA-15 framework [34].

3.2 Effect of Ti loading

The SAXS patterns of calcined Ti-SBA-15 with 1–10 mol% Ti loading all show intense {10} ≡ {11} and {30} ≡ {33} reflections associated with *p6mm* plane symmetry [32] indicative of well ordered mesopores (Fig. 1a). As Ti loading increased SBA-15 was not perturbed, due to the mild synthesis conditions and extraordinarily high purity and moisture stability of the silatrane precursor. TEM of the Ti-SBA-15 (7 mol% Ti loading) directly confirmed the long range periodicity of the mesopores [2] (Fig. 2). N_2 adsorption/desorption isotherms and pore size distribution patterns provide quantitative assessments of the porosity (Fig. 3). All catalysts yielded a type IV isotherm (IUPAC classification), with a H1 type hysteresis loop characteristic of a large diameter mesoporous solid with narrow pore size distribution [2]. The well-defined step at a relatively high pressure of 0.5–0.7 corresponds to capillary condensation of N_2, within uniform pores (>5 nm diameter) and surface area (up to 670 m^2/g) (Table 1). The BET surface area and pore size slightly decrease with increasing Ti loading. DRUV spectra of Ti-SBA-15 all show an absorption band centered at ~220 nm, with the intensity increasing with Ti loading (Fig. 4a), that is attributed to charge transfer transition associated with isolated $Ti^{4+}O_4$ coordination [11, 14]. However, at the 10 mol% Ti loading, the 330 nm band appears from extra-framework anatase $Ti^{4+}O_6$ [16, 28].

3.3 Effect of acidity

The SAXS patterns of Ti-SBA-15 materials prepared at different acidity are shown in Fig. 1b, all exhibit a clear {10} reflection indicating uniform pore diameter, but the {30} reflection is broad when the acidity is reduced to 1M, suggesting that interpore order correlation is limited. Additionally, DRUV showed strong absorption at 220 nm

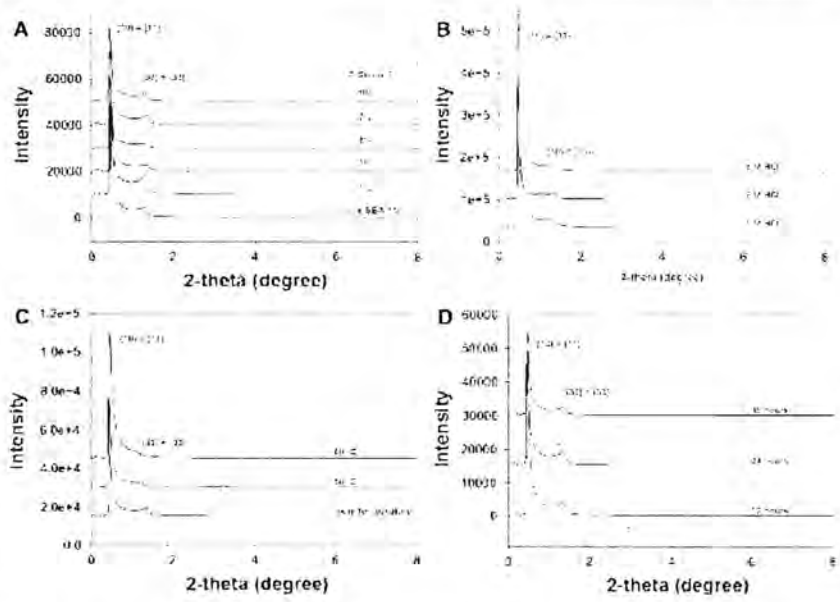

Fig. 1 SAXS patterns of a pure silica SBA-15 and Ti-incorporated samples of Ti-SBA-15 containing different amount of Ti loadings; b Ti-SBA-15 materials prepared at different acid concentrations; c Ti-SBA-15 synthesized at different temperatures; d Ti-SBA-15 synthesized at different aging times

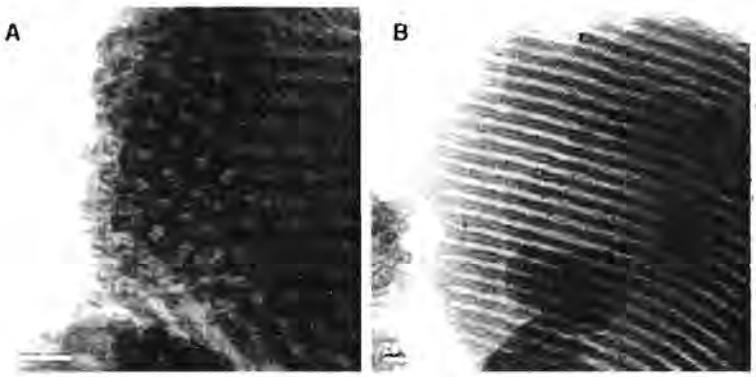

Fig. 2 TEM images of 7 mol% Ti-SBA-15, in which a in the direction perpendicular to the pore axis and b in the direction parallel to the pore axis

for the 1M HCl sample as direct evidence for Ti^{4+} incorporated into the mesoporous silica framework (Fig. 4b). It can be concluded that lower acidity favored framework incorporation of Ti which disrupts long range order in SBA-15 in agreement with Vinu et al. [12], who reported that lowering the acidity decreases the hydrolysis rate of the titanium precursors to match that of silica precursors. This may enhance the interaction between the Ti–OH and Si–OH species in the gel resulting in more complete Ti incorporation. At the highest acid concentration (3M HCl), DRUV yielded weak absorption at 220 nm, due to the ready dissociation of Ti–O–Si bonds [13]. While a change in acid concentration does not notably affect the surface area, pore volume and pore size (Table 2), the use of 2M HCl is considered optimal because it maintained the well ordered structure of the mesopores and showed high Ti incorporation.

3.4 Effect of temperature

Temperature affects liquid crystal formation [30]. In the present case, increasing the reaction temperature from ambient to 80°C for Ti-SBA-15 catalyst (10 mol% Ti loading/2M HCl/24 h) showed {10} periodicity remained intact while {30} was absent (Fig. 1c). BET confirmed the increase in pore size with reaction temperature (Table 3), while DRUV showed that at 80°C, $Ti^{4+}O_6$ disappeared because the Ti^{4+} species preferentially displaced Si^{4+} in

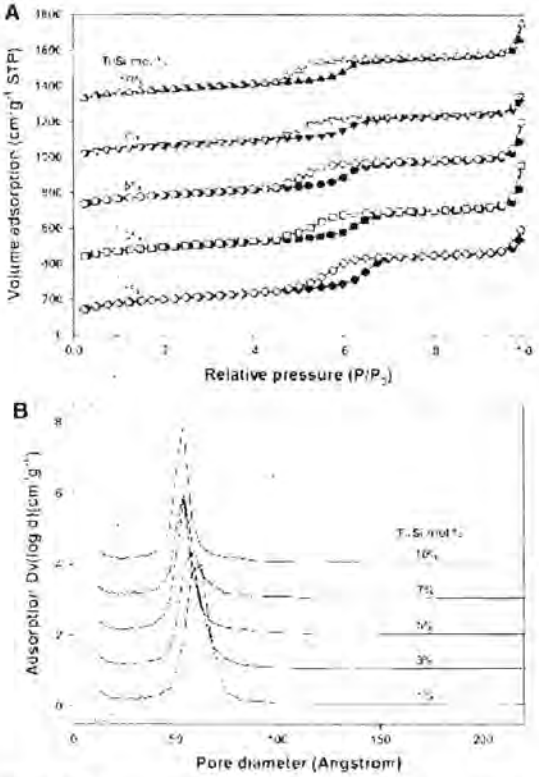

Fig. 3 N_2 adsorption/desorption isotherms a and pore size distributions b of Ti-SBA-15 containing different amount of Ti loadings

Table 1 BET and SAXS analyses of Ti-SBA-15 as a function of amount of Ti loading

Loaded Ti (%)	Surface area (m^2/g)	Pore volume (cm^3/g)	Channel diameter (nm)	
	BET	BET	BET	SAXS
1	670	0.83	5.79	6.8
3	643	0.81	5.77	6.7
5	618	0.76	5.40	6.5
7	592	0.67	5.39	6.5
10	597	0.71	5.37	6.4

the framework of SBA-15 (Fig. 3c). However, 2D order was compromised at the higher temperature, and therefore room temperature proved most suitable for the synthesis of Ti-SBA-15. Zhao et al. [2] reported that higher temperatures resulted in larger pore sizes possibly due to the PEO blocks becoming more hydrophobic that increased hydrophobic domain volumes, and lead to wider channels with accelerated Ti^{4+} incorporation into the SBA-15 framework but simultaneously limited long range order.

3.5 Effect of aging time

Aging time is an important parameter because in alkoxide-derived gels, the condensation reaction between surface functional groups continues beyond the gel point. During aging, there are changes in the textural and physical properties of the gel, and from 12 to 36 h (10 mol% Ti loading/2M HCl/RT) SAXS revealed that whilst the narrow {10} reflection is preserved, the {30} reflection broadens with aging time due to disruption of long-range hexagonal periodicity [30] (Fig. 4d). DRUV spectra indicate that with longer aging extra framework anatase $Ti^{4+}O_6$ appears (Fig. 4d), while N_2 adsorption isotherms found the surface area, pore volume and pore size all decreased (Table 4). It is believed that long reaction times, beyond equilibrium, cause the condensation reaction to reverse, resulting in mesopore deterioration [35].

3.6 Catalytic activity of Ti-SBA-15 towards styrene epoxidation

Styrene oxide and benzaldehyde were the principle products of styrene epoxidation with H_2O_2 over Ti-SBA-15. All titanium loaded catalysts demonstrated considerably higher styrene conversion than pure SBA-15 (Table 5). Raising the Ti content to 7 mol% increased the conversion of styrene remarkably (from 2.9 to 25.8%) with the selectivities for styrene oxide and benzaldehyde of 34.2 and 65.8%, respectively. Additionally, Ti-SBA-15 prepared by the sol–gel synthesis showed significantly higher conversion of styrene (25.8%) than an equivalent catalyst (in terms of Ti content) synthesized by the impregnation method (11.9%). When Ti content exceeds 7 mol% conversion efficiency decreases (from 25.8 to 12.4%), in agreement with DRUV that found the $Ti^{4+}O_4$ content was maximized in this catalyst beyond which $Ti^{4+}O_6$ extra-framework titanium appears as anatase which is less active. Combined with the diffraction and microscopy results, it is confirmed that Ti^{4+} incorporated within the SBA-15 framework is most active. This conclusion is consistent with Zhang et al. [14] and Ji et al. [36], who reported that the titanium species in the SBA-15 framework are the active sites for styrene oxidation reaction. Moreover, the selectivity of styrene oxide decreased while selectivity of benzaldehyde increased with titanium loading consistent with the study of Yu et al. [37] who reported that an increase of the Ti content in the mesoporous catalysts decreases epoxide selectivity and H_2O_2 efficiency due to a decrease of isolated Ti atoms in the SBA-framework.

Figure 5a shows that over 7 mol% Ti-SBA-15 styrene conversion increases with time whereas selectivity decreases, which may attributed to the secondary oxidation of styrene oxide [33]. The reaction is initially rapid due to the

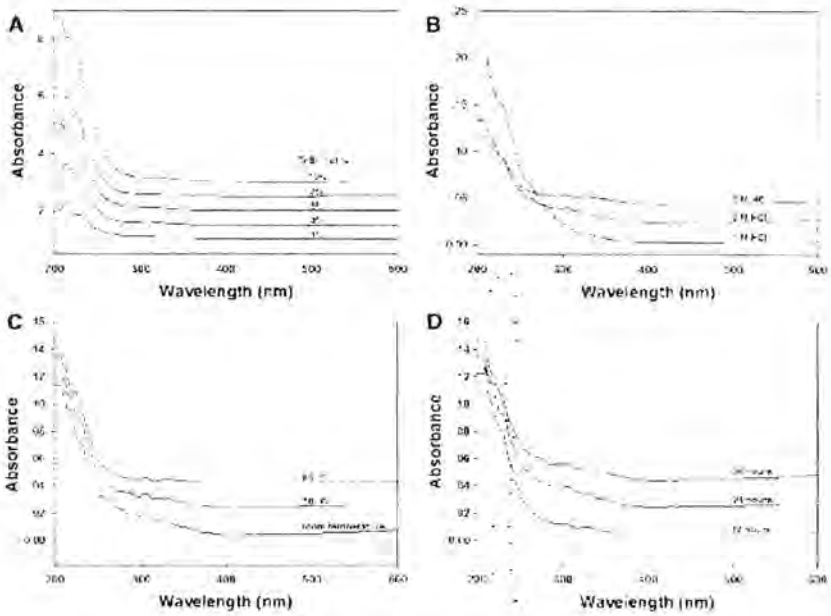

Fig. 4 Diffuse reflectance UV–visible spectra of the synthesized Ti-SBA-15: a at different amounts of Ti loadings; b at various acid concentrations; c at different temperatures; and d at different aging times

Table 2 BET and SAXS analyses of Ti-SBA-15 as a function of acidity

Acidity (M)	Surface area (m^2/g) BET	Pore volume (cm^3/g) BET	Channel diameter (nm) BET	SAXS
1	582	0.78	5.63	–
2	597	0.71	5.37	6.4
3	606	0.74	5.38	6.2

Table 3 BET and SAXS analyses of Ti-SBA-15 as a function of temperature

Temperature (°C)	Surface area (m^2/g)	Pore volume (cm^3/g)	Channel diameter (nm)	
	BET	BET	BET	SAXS
RT	597	0.71	5.37	6.4
50	596	0.72	5.68	–
80	626	0.95	6.60	–

Table 4 BET and SAXS analyses of Ti-SBA-15 as a function of aging time

Time (h)	Surface area (m^2/g) BET	Pore volume (cm^3/g) BET	Channel diameter (nm) BET	SAXS
12	637	0.79	5.68	6.4
24	597	0.71	5.37	6.4
36	609	0.71	5.39	–

Table 5 Comparison of catalysts for epoxidation of styrene

Catalyst (%)	Styrene conversion (%)	Selectivity (%)	
		Styrene oxide	Benzaldehyde
0% Ti (sol–gel)	2.9	46.6	53.4
3% Ti (sol–gel)	14.4	42.1	57.9
5% Ti (sol–gel)	13.9	36.8	63.2
7% Ti (sol–gel)	25.8	34.2	65.8
10% Ti (sol–gel)	12.4	30.1	69.9
7% Ti (impreg.)	11.9	45.7	54.3
10% Ti (impreg.)	10.2	29.2	70.8

abundance of H_2O_2 [36], reaches a maximum after 4 h, then remains constant for up to 6 h. The conversion of styrene slightly increased by raising the temperature from 70 to 90°C (Fig. 5b) consistent with the study of Laha et al. [38], but the selectivity of Ti-SBA-15 toward styrene oxide was highest at 80°C. The selectivity of benzaldehyde also increased with increasing the reaction temperature, meaning that the higher temperature favors further oxidation of styrene oxide [11]. The effect of catalyst concentration is shown in Fig. 5c, with styrene conversion increasing from 11.2 to 25.8% as the mass of catalyst was adjusted from 0.05 to 0.10 g, beyond which the rate was essentially constant. The initial improvement in performance with catalyst loading is due to an increase of active Ti sites in the system that facilitates styrene conversion [38].

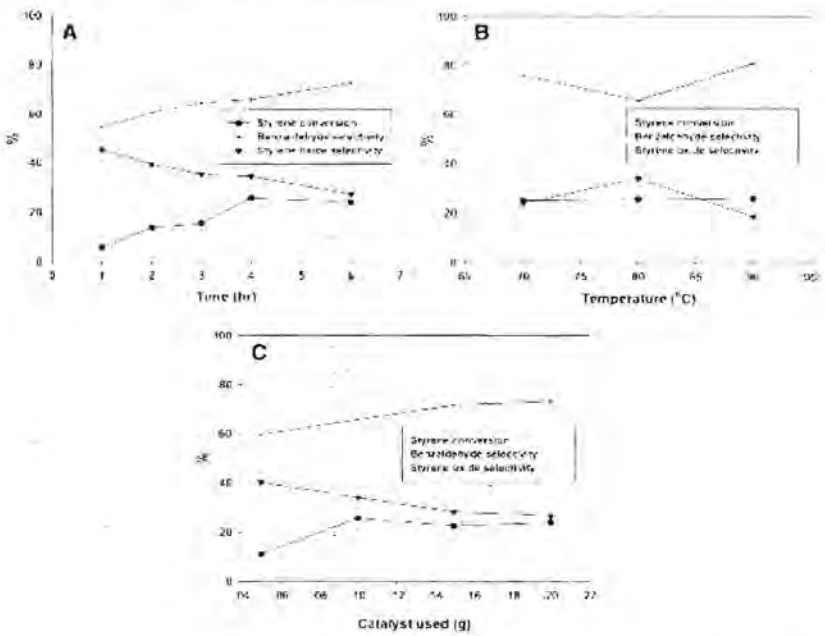

Fig. 5 a Effect of reaction time on the styrene oxidation using 0.1 g of catalyst, containing 7.0 mol% titanium content, at 80°C; b Effect of reaction temperature on the styrene oxidation using 0.1 g of catalyst, containing 7 mol% titanium content, for 4 h; c Effect of amount of catalyst, containing 7.0 mol% titanium content, at 80°C for 4 h

4 Conclusions

Ti-SBA-15 was successfully synthesized via a sol–gel process using silatrane as the silica precursor, titanium glycolate as a titanium source, and nonionic triblock copolymer as a template. The method is straightforward and can be conducted at room temperature without the need for hydrothermal treatment as conventionally required. Systematic variations of acidity, aging temperature, aging time, and Ti loading lead to an optimized Ti-SBA-15 product. Crystallochemical incorporation of titanium by $Ti^{4+}O_4$ substitution for $Si^{4+}O_4$ in the mesopores proves superior to impregnation or decoration with anatase ($Ti^{4+}O_6$). Tetrahedral Ti^{4+} coordination is maintained to a loading of 7 mol% titanium. Ti-SBA-15 materials show relatively high activity in the epoxidation reaction of styrene monomers due to the presence of $Ti^{4+}O_4$ in the SBA-15 framework. For the optimized catalyst (7 mol% Ti loading/2M HCl/24 h/RT), the epoxidation reaction of styrene was most effective at 80°C/4 h, using 0.05 g catalyst with the only products being styrene oxide and benzaldehyde. The selectivity of styrene oxide and benzaldehyde reached 34.2 and 65.8% at a styrene conversion of 25.8%. This research demonstrates that Ti-SBA-15 heterocatalyst can be synthesized by a low cost and energy efficient process that will allow scale-up for possible industrially application.

Acknowledgments This research work is financially supported by the Postgraduate Education and Research Program in Petroleum and Petrochemical Technology (ADB) Fund (Thailand), the Ratchadapisake Sompote Fund, Chulalongkorn University, and the Thailand Research Fund (TRF). The SAXS patterns were collected by Mr. An Tao and Ms. Li Henan at the School of Materials Science and Engineering, Nanyang Technological University.

References

1. Zhao D, Feng J, Huo Q, Melosh N, Frerickson GH, Chmelka BF, Stucky GD (1998) Science 279:548–552
2. Zhao D, Huo Q, Feng J, Chmelka BF, Stucky GD (1998) J Am Chem Soc 120:6024–6036
3. Sayari A (1996) Chem Mater 8:1840
4. Corma A (1997) Chem Rev 97:2373
5. Soler-Illia GJ De AA, Sanchez C, Lebeau B, Patarin J (2002) Chem Rev 102:4093
6. Taguchi A, Schuth F (2005) Micropor Mesopor Mater 77:1
7. He N, Bao S, Xu Q (1998) Appl Catal A 169:29
8. Corma A, Fornes V, Navarro MT, Perez-Pariente J (1994) J Catal 148:569
9. Vinu A, Murugesan V, Bohlmann W, Hartmann M (2004) J Phys Chem B 108:11496
10. Vinu A, Murugesan V, Tangermann O, Hartmann M (2004) Chem Mater 16:3056
11. Wu P, Tatsumi T (2002) Chem Mater 14:1657–1664
12. Vinu A, Srinivasu P, Miyahara M, Ariga K (2006) J Phys Chem B 110:801–806
13. Chen Y, Huang Y, Xiu J, Han X, Bao X (2004) Appl Catal A Gen 273:185

14. Zhang WH, Lu J, Han B, Li M, Xiu J, Ying P, Li C (2002) Chem Mater 14:3413
15. Wu S, Han Y, Zou YC, Song JW, Zhao L, Di Y, Liu SZ, Xiao FS (2004) Chem Mater 16:486
16. Newalkar BL, Olanrewaju J, Komarneni S (2001) Chem Mater 13:552
17. Berube F, Kleitz F, Kaliaguine S (2008) J Phys Chem C 112: 14403
18. Berube F, Kleitz F, Kaliaguine S (2009) J Mater Sci 44:6727
19. Luan ZH, Hartmann M, Zhao DY, Zhou WZ, Kevan L (1999) Chem Mater 11:1621
20. Luan ZH, Bae JY, Kevan L (2000) Chem Mater 12:3202
21. Morey MS, O'Brien S, Schwarz S, Stucky GD (2000) Chem Mater 12:898
22. Yue YH, Gedeon A, Bonardet JL, Melosh N, D'Espinose JB, Fraissard J (1999) Chem Commun 19:1967
23. Murugavel R, Roesky HW (1997) Angew Chem Int Ed Engl 36:477
24. Phonthammachai N, Chairassameewong T, Gulari E, Jamieson AM, Wongkasemjit S (2002) Met Mater Min 12:23–28
25. Phiriyawirut P, Magaraphan R, Jamieson AM, Wongkasemjit S (2003) Mater Sci Eng A 361:147–154
26. Charoenpinijkarn W, Suwankruhasn M, Kesapabutr B, Wongkasemjit S, Jamieson AM (2001) Eur Polymer J 37:1441–1448
27. Phonthammachai N, Chairassameewong T, Gulari E, Jamieson AM, Wongkasemjit S (2003) Micropor Mesopor Mater 66: 261–271
28. Tanglumlert W, Imae T, White TJ, Wongkasemjit S (2008) Mater Lett 62:4545–4548
29. Sathupanya M, Gulari E, Wongkasemjit S (2003) J Eur Ceram Soc 23:2305–2314
30. Phiriyawirut P, Jamieson AM, Wongkasemjit S (2005) Micropor Mesopor Mater 77:203–213
31. Thanabodeekij N, Sadthayanon S, Gulari E, Wongkasemjit S (2006) Mater Chem Phys 98:131–137
32. Samran B, White TJ, Wongkasemjit S (2010) J Porous Mater. doi:10.1007/s10934-010-9367-3
33. Tanglumlert W, Imae T, White TJ, Wongkasemjit S (2009) Cat Comm 10:1070–1073
34. Wang Y, Zhang Q, Shishido T, Takehira K (2002) J Catal 209:186–196
35. Yilmaz VT, Topcu Y, Karadag A (2002) Thermchimica Acta 383:129–133
36. Ji D, Zhao R, Lv G, Qian G, Yan L, Suo J (2005) Appl Catal A Gen 281:39–45
37. Yu J, Feng Z, Xu L, Li M, Xin Q, Liu Z, Li C (2001) Chem Mater 13:994
38. Laha SC, Kumar R (2001) J Catal 204:64–70